2011

# Design of an Implant for First Metatarsophalangeal Joint Hemiarthroplasty

Atul Kumar
*Cleveland State University*

# DESIGN OF AN IMPLANT FOR FIRST METATARSOPHALANGEAL JOINT HEMIARTHROPLASTY

Atul Kumar

Bachelor of Medicine and Bachelor of Surgery

Patna Medical College

February 2002

Masters in Medical Science and Technology

Indian Institute of Technology-Kharagpur

May 2004

Submitted in partial fulfillment of requirements for the degree

DOCTOR OF ENGINEERING IN APPLIED BIOMEDICAL ENGINEERING

at the

CLEVELAND STATE UNIVERSITY

June 2011

This Thesis has been approved for the Department of CHEMICAL AND BIOMEDICAL ENGINEERING and the College of Graduate Studies by

_____

Thesis/Dissertation Chairperson, Dr. Peter R. Cavanagh

_____

Department and Date

_____

Dr. George P. Chatzimavroudis

_____

Department and Date

_____

Dr. Randy M. Setser

_____

Department and Date

_____

Dr. Ahmet Erdemir

_____

Department and Date

_____

Dr. Crystal M. Weyman

_____

Department and Date

# ACKNOWLEDGEMENTS

I wish to express my sincere thanks to all those who have played a role in making this dissertation possible.

I would like to especially thank and express my gratitude to Dr. Peter R. Cavanagh for providing me with the opportunity to work on the research project presented in this dissertation. I also would like to thank him for all the invaluable advice, guidance, encouragement and support offered throughout the course of this research. I also would like to thank Dr. George P. Chatzimavroudis and Dr. Randy M Setser for the guidance they provided during my doctoral course work and their assistance in helping me find the perfect research laboratory for my dissertation work. I would also like to express my gratitude to Dr. Ahmet Erdemir for advice he provided that enabled me to greatly improve my computational skills throughout the course of this research. Special thanks go to Dr. Crystal Weyman and all of my dissertation committee members for serving on my committee and reviewing the manuscript of this thesis.

I would also like to express my thanks and appreciation to Dr. Yohannes Haile-Selassie and Lyman M. Jellema of the Cleveland Museum of Natural History who provided me with the opportunity to use the museums resources and helped with the data collection process. I would also like to thank and acknowledge the contributions of Dr. Donghoon Lee for assisting with the collection of imaging data for my dissertation work. Many thanks go to Ms Becky Laird and Ms Darlene Montgomery in Chemical and Biomedical Engineering Department at CSU for their support and administrative assistance that enabled me to concentrate on my research.

My thanks and gratitude also goes to Dr. Srikantan Nagarajan who motivated me to pursue a doctoral degree while I was doing Master's project under his guidance.

I would also like to recognize all my teachers from India and United States for helping to shape my career and preparing me to serve society.

Thanks also go to my friends from Seattle, Cleveland and India for providing me with great support and lasting good memories during the course of these last four years. Special thanks to Kerim, Srinivas, Thomas, Andrea and Ventakesh for all of the assistance they provided in helping me complete this research.

Lastly I acknowledge the love, affection, encouragement, inspiration and moral support given to me by my mother, brothers and all family members in all stages of my life.

DESIGN OF AN IMPLANT FOR FIRST METATARSOPHALANGEAL JOINT HEMIARTHROPLASTY

ATUL KUMAR

## ABSTRACT

Osteoarthritis (OA) is the most common form of arthritis and it affects 27 million US adults. OA disease involves all of the tissues of the diarthrodial joint and ultimately, may lead to softening, ulceration, loss of articular cartilage, sclerosis and polished appearance of the subchondral bone, osteophytes, and subchondral cysts.

The first metatarsophalangeal joint (MTPJ1) is affected in up to 42% cases of OA. Besides osteoarthritis, other conditions such as rheumatoid arthritis and gout also affect the MTPJ1. Involvement of MTPJ1 with these conditions invariably leads to deformed toe such as hallux valgus and hallux rigidus.

Over 150 surgical techniques exist for treatment of hallux deformity, which includes cheilectomy, arthrodesis, osteotomy, resection arthroplasty, and replacement of part or the entire articular surface with an implant. A hemi-implant, which partially replaces the 1$^{st}$ metatarsal head with minimal bone resection and without altering the sesamoid articulation has shown promising results and gives superior postoperative range of motion and pain reductions. But the geometry of such implants has not been explained in any literature and there are no details of the data used for designing such implants. An anatomically based approach to design the geometry of an MTPJ1 implant is needed in order to best fit the articulating surface of the adjacent phalanx. In the current study, a method was developed for designing a hemiarthroplasty implant for MTPJ1 based upon

the morphology of metatarsal. Ninety-seven metatarsal osteological specimens were scanned using a laser scanner to obtain 3D surface data. After aligning the surface data, the articular surface of each metatarsal head (MTH1) superior to the inter-condylar ridge were characterized by a section of an ellipsoid using non-linear unconstrained optimization (NLUO) and the section of the ellipsoid forms the surface of the implant. The implants based upon osteological specimens had a very good fit to metatarsal articulating surface with root mean square error of fit in the range of 0.29 and 0.42mm.

The cartilage region, in 14T MRI image from 1$^{st}$ metatarsal of two cadaver feet, was segmented semi-automatically, and a three-dimensional surface of the cartilage shell was created. The average thickness profile of the cartilage on articular part of MTH1 was obtained. For articulating surface of individual osteological surface data, a surface which simulates cartilage outline was created using the cartilage thickness profile. This cartilage outline surface was again characterized with the best fit ellipsoid using NLUO. The parameters of ellipsoid for the cartilage outline surface and the osteological surface were compared. Although the difference between the parameters for the ellipsoid obtained in these two conditions were not found to be significant ($p=0.05$), this result needs to be validated with more cartilage samples. In addition, scaling for size of the bones should be considered in calculation of the thickness of cartilage.

Thus, a new method to design the implant for MTH1 for arthroplasty was identified based upon bones from general population using numerical technique. This method can be extended in designing implants for other joints which need hemi-arthroplasty.

TABLE OF CONTENTS

LIST OF TABLES

LIST OF FIGURES

# CHAPTER I

# INTRODUCTION

## 1.1 Background and significance

The foot has two main functions, support and propulsion of the body. It combines the stability with the flexibility and its propulsive action is that of a flexible lever[1]. The joints at the bases of the toes of the foot are known as metatarsophalangeal joints (MTPJ), and among the five MTPJ, the first metatarsophalangeal joint (MTPJ1) is one of the most valuable joints for the functions of the foot Figure 1-1. The bones, which constitute this joint, are the first metatarsal, the first phalanx and two sesamoids. The first metatarsal articulates with the base of the first phalanx and two sesamoids. MTPJ1 is an ellipsoid-like joint between the rounded metatarsal head and the shallow cavity on the proximal phalangeal bases. Articular surface cover the distal and the plantar aspects of the metatarsal head and has two longitudinal grooves separated by a ridge; each groove articulates with a sesamoid bone embedded in the joint's capsule[2].

The total range of motion at the MTPJ1 in the sagittal plane is 111 degree which includes 76 degrees of dorsiflexion and 34 degrees of plantar flexion[3]. The abnormal

MTPJ1 has decreased range of motion[3]. Among the five MTPJs in foot, the greatest load in walking is on the MTPJ1, and it can be as high as 90% of body weight[4].

Osteoarthritis (OA), the most common form of arthritis, is a very devastating joint disease and affects 27 million US adults5[5]. Clinical outcomes for people with OA typically involve pain, limitation of daily living activities, and overall diminution of the quality of life[6].

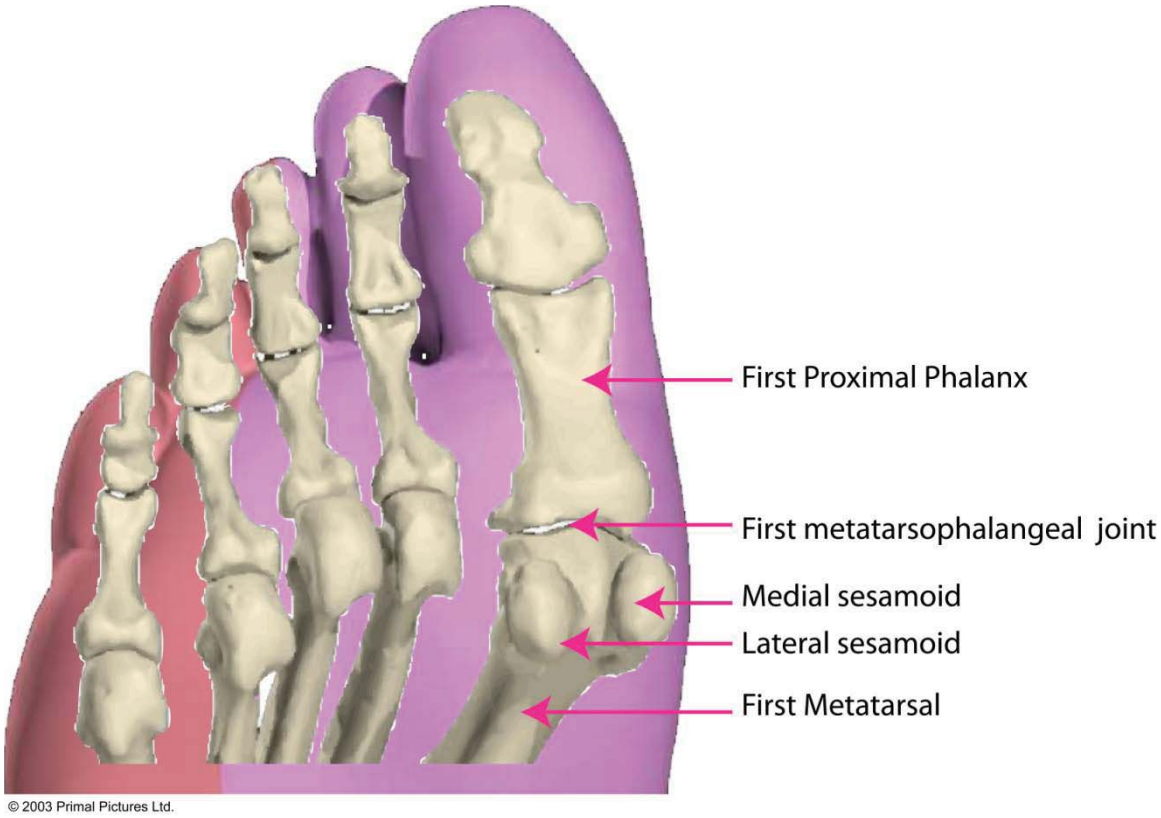


Figure 1-1: First metatarsophalangeal joint in foot with its bone

In Western populations, OA is one of the most frequent causes of pain, loss of function and disability in adults. In the US, it is second only to ischemic heart disease as a cause of work disability in men over 50 years of age[7]. Osteoarthritic diseases are a result of both mechanical and biological events that destabilize the normal coupling of degradation and synthesis of the articular cartilage chondrocytes (cells which constitute the cartilage), extracellular matrix and subchondral bone (the bone beneath the articular cartilage). It may be initiated by multiple factors including genetic, developmental, metabolic, and traumatic etiologies. OA disease involves all of the tissues of the diarthrodial joint. Ultimately, OA may lead to softening, ulceration, loss of articular

cartilage, sclerosis of the subchondral bone, osteophytes, and subchondral cysts. When clinically evident, OA diseases are characterized by joint pain, tenderness and limitation of movement[6].

The first metatarsophalangeal joint is affected in up to 42% cases of OA. In a joint-specific prevalence study in 3436 participants (69% female; 98% Caucasians; age between 40 to 94 years), the MTPJ1 was affected in 20% of OA patients which was evidenced by structural changes of osteoarthritis in dorso-plantar radiographic views of foot9. Menz[8] et al. using dorsi-plantar and lateral radiographic views of the foot found the prevalence of MTPJ1 OA to be 42.4% in 197 people (age between 62 to 94 years).

Besides osteoarthritis, other conditions such as rheumatoid arthritis and gout also affect the MTPJ1[9]. Rheumatoid arthritis[10] is characterized by persistent synovitis, systemic inflammation, and auto antibodies. 50% of the risk for development of rheumatoid arthritis is attributable to genetic factors and smoking is the main environmental risk. Uncontrolled active rheumatoid arthritis causes joint damage, disability and decreased quality of life. Rheumatoid arthritis affects 1.3 million adults in the US. In a follow up study of 848 patients who fulfilled the American College of Rheumatology (ACR) criteria for RA, Leeden12 et al. found involvement of MTPJ1 in 70% of patients at baseline and forefoot joint erosion in 60% of patients after eight years.

Gout affects 3.0 million adults in US5, and acute gouty arthritis typically presents with a sudden and severe exquisitely painful joint, most classically in the MTPJ1[11]. Involvement of MTPJ1 with these conditions invariably leads to a deformed toe[9].

Hallux valgus (Figure 1-2) and hallux rigidus (Figure 1-3) are two major deformities of the big toe. In a questionnaire-based study of 4249 adults aged > 30 years, the prevalence of hallux valgus was found to be 28.4%[9]. The questionnaire included self-assessed hallux valgus with a validated instrument, nodal osteoarthritis, and joint pain, history of rheumatoid arthritis and osteoarthritis of the big toe. In the same population, osteoarthritis and rheumatoid arthritis had an association with hallux valgus with odd ratios of 1.41 and 2.05[11]. In a study of 78 people by Bal[12] et al., with rheumatoid arthritis defined according to the American College of Rheumatology criteria, the frequency of hallux valgus deformity was 64.1%. Hallux rigidus is one of the most important predictors for functional capacity of foot. In a cross-sectional study of 784 subjects (age 74.5±6.0 years; 56.8% female, 44.5% African American, 41.7% white non-Hispanic, 13.8% Puerto Rican), the most common foot musculoskeletal disorder was found to be hallux valgus with a prevalence of 37.1% [13].

Over 150 surgical techniques exist for treatment of hallux deformity, which includes cheilectomy, arthrodesis, osteotomy, resection arthroplasty, and replacement of part or the entire articular surface with an implant. Arthrodesis is the surgical technique in which the MTPJ1 is fused, (Figure 1-4) which may lead to nonunion (10-15%) of the arthrodesis, malposition of the bones (4.5-28.5%), complications due to metal fixators (up to 46%), interphalangeal and metatarso-cuneiform arthritis and metatarsalgia (up to 20%)16. Cheilectomy is the surgery to remove bony lumps on the joint and is applied only for mild osteoarthritis of the MTPJ1 and in grade I and II hallux rigidus[14]. Osteotomies, where the bone is cut to change its alignment, can lead to shortening of the

1st metatarsal bone and abnormal plantar pressure distribution and pain in other metatarsal bones of foot[15].

Figure 1-2: Hallux valgus

Figure 1-3: Hallux rigidus

Source:
http://www.healthbase.com/resources/images/ortho/healthbase_medical_tourism_bunion_removal_surgery_bunionectomy_hallux_valgus.jpg
http://sanluispodiatrygroup.com/site_content/cms_content/library/images/00049/img_thumb_1551587416.jpg

Osteotomy cannot be used if the MTPJ1 has advanced osteoarthritis[16, 17]. Joint resection and inter-positional reconstruction, called resection arthroplasty, can lead to transfer metatarsalgia of the 2nd to 5th metatarsal head, weakness in plantar flexion, and shortening and elevation of the big toe[18].

Another modality for the correction of hallux deformity is the replacement of the MTPJ1 joint with a prosthesis, which is called arthroplasty. The replacement of the

metatarsal as well as phalangeal part of the joint with a two component implant is known as total arthroplasty and the replacement of either metatarsal or phalangeal part is known as hemiarthroplasty.

There are various designs of a two component implant including the Lawrence design, the Biomet implant, and the Futura® implant made from silicone (Figure 1-5a) or metal (Figure 1-6a,1-7a,1-8a)[19]. The silicone implants may cause silicone synovitis, regional lymphadenopathy, metatarsalgia, and stress fracture of the lateral metatarsals[19]. In a 5-year follow-up survivorship study of Bio-Action™ metal implants in 15 consecutive first metatarsophalangeal total joint replacements, 93.3% of the phalangeal components and 86.6% of metatarsal components showed signs of implant failure{Sinha, 2010 }. Another important consideration in using any total replacement implant is the difficulty of repair of a failed procedure[20].

To address some of the shortcomings of the resection procedures described above, metallic hemi-implants were developed21. Very few follow-up studies have been done on this type of implants. Salonga et al.[21] in a retrospective study of hemi-implants replacing the proximal end of phalanx (Figure 1-7a) with a Biopro® implant found that eight out of seventy-six (10.13%) cases had complications which included severe pain, sesamoiditis, extensor hallucis longus contracture, hallux subluxation and dislocation, and misaligned implants.

In advanced stages of hallux rigidus, the metatarsal head is severely denuded of its articular cartilage; however, the sesamoid articulations are usually spared except in the most extreme cases. A hemi-implant (Figure 1-8a), which partially replaces the 1st metatarsal head is used in these cases. This implant resurfaces the metatarsal head with

minimal bone resection and without altering the sesamoid articulation. One example of these implants, the HemiCAP® system for the MTPJ1, was approved by the FDA in 2004 and has shown promising results in patients with hallux rigidus, arthritic hallux valgus, failed previous osteotomies and cheilectomy, avascular necrosis of the metatarsal head, and failed fusion caused by increased pressure on the proximal phalanx[22]. To date, superior postoperative range of motion (increase by 65 degrees) and pain reduction (The mean American Orthopedic Foot and Ankle Society and 36-item Short-Form Health Survey Questionnaire scores of 82.1 and 96.1, respectively) have resulted from this implant[22].

Figure 1-4: Arthrodesis. Reprinted from "Comparison of Arthrodesis and Metallic Hemiarthroplasty of the Hallux Metatarsophalangeal Joint. Surgical Technique" by Raikin, S. M. and Ahmad, J, 2008, The Journal of Bone and Joint Surgery 90 (Suppl 2 Part 2): 171-180. Copyright 2008 by The Journal of Bone and Joint Surgery. Reprinted with permission.

a)

b)


Figure 1-5: a) Silicone implant. b) Silicone implant after arthroplasty of MTPJ1.
Source: http://www.joshuakaye.com/topics/halluxlimit.html

a)


b)

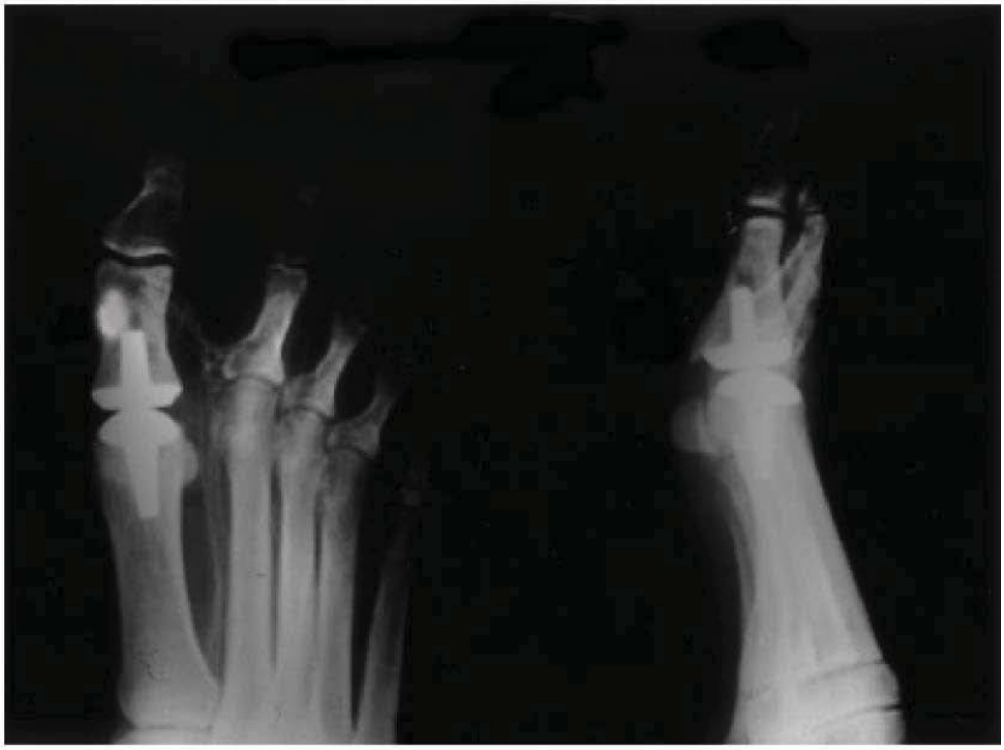

Figure 1-6: a) Two-component metal implant b) Two-component metal implant after total arthroplasty of MTPJ1. Reprinted from "Replacement arthroplasty for hallux rigidus. 21 patients with a 2-year follow-up." by Olms, K and Dietze, A, 1999, International orthopaedics 23 (4): 240-3. Copyright 1999 by Springer-Verlag 1999. Reprinted with permission.

a)


b)

Figure 1-7: a) Hemiarthroplasty implant (phalangeal). Reprinted from "A Retrospective Cohort Study of the BioPro(R) Hemiarthroplasty Prosthesis." by Salonga, Christine C; Novicki, David C; Pressman, Martin M and Malay, D Scot, 2010, The Journal of foot and ankle surgery: official publication of the American College of Foot and Ankle Surgeons, Apr 24. Copyright 2010 by the American College of Foot and Ankle Surgeons. Reprinted with permission. b) Implant resurfacing base of phalanx. Reprinted from "First metatarsophalangeal hemiarthroplasty for grade III and IV hallux rigidus," by Giza, Eric and Sullivan, Martin R, 2005, Techniques in Foot & Ankle Surgery: Volume 4 - Issue 1 - pp 10-17. Copyright 2005 by Lippincott Williams & Wilkins, Philadelphia.

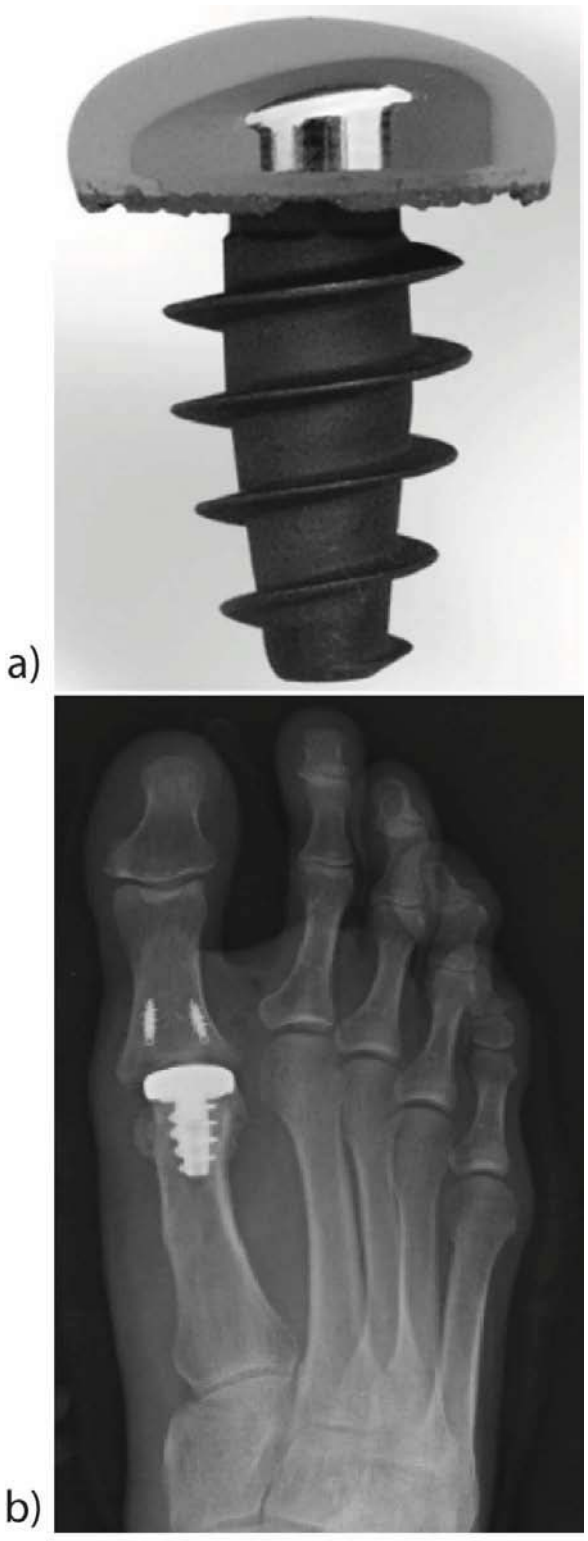


Figure 1-8: a) Hemi-arthroplasty implant (metatarsal). b) Implant resurfacing MTH1. Reprinted from "Resurfacing of the first metatarsal head in the treatment of hallux rigidus," by Carl T. Hasselman, 2008, Techniques in Foot & Ankle Surgery 7 (1): 31-40, Copyright 2005 by Lippincott Williams & Wilkins, Philadelphia.

An anatomically based approach to design geometry of an MTPJ1 implant is needed in order to best fit the articulating surface of the adjacent phalanx. There are no details in the literature concerning the geometry of the design of the hemiarthroplasty implants which replace the 1st metatarsal head. Most prior morphological studies of the first metatarsal bone have reported only caliper (linear) measurements[21, 22]. There has been no study of the curvature of the articulating surface of 1st metatarsal bone in three dimensions. The contribution of cartilage thickness on the articulating surface of MTH1 for the design of an implant has never been explored. In a few studies, microscopic evaluation[48] and creep indentation technique[50] have been used to study the distribution of cartilage thickness of the MTPJ1. To know the exact *in vivo* mapping of cartilage thickness on the articular surface of the MTH1, an imaging study is required. No imaging study exploring the cartilage thickness distribution of MTPJ1 and its contribution to the implant design has been done.

## 1.2 Objectives

The end goal of this investigation was to design a hemi-arthroplasty implant for the MTPJ1 based upon the morphology of metatarsal. The process for obtaining such a design is presented in this dissertation with the expectation that this will provide better kinematic outcomes for and satisfaction among patients. The study included the comparison of goodness of fit of implants to the metatarsal bone when the implant was designed with and without consideration of cartilage.

Achieving this goal required the acquisition of 3D surface data collection of metatarsal osteological specimens, imaging of metatarsal bone from cadaver bone, extraction of articular surface of MTH1 and finding a best fit to the articular surface of

MTH1. This process was divided into the following three specific aims:

SPECIFIC AIM 1: To characterize the bony geometry of the metatarsal head in specimens from the Hamann-Todd Osteological collection (http://www.cmnh.org/site/ResearchandCollections/PhysicalAnthropology/Collections/Hamann-ToddCollection.aspx ). Chapter 2 describes a method to accomplish this goal with multiple steps including acquisition of data from osteological specimens, identifying the articular surface of osteological specimens, classifying them into different size groups and finding a best fit ellipsoid for each of these groups.

SPECIFIC AIM 2: To examine the spatial relationship between the articular cartilage on the first metatarsal head and the underlying subchondral bone. Chapter 3 describes the method to examine this spatial relationship using new algorithms for segmenting the cartilage from MRI images of the MTH1, creating three-dimensional surfaces of cartilage and calculating the thickness profile for cartilage on the MTH1.

SPECIFIC AIM 3: To examine the effect of cartilage thickness on the design of an implant for a first metatarsophalangeal joint hemiarthroplasty. Chapter 4 compares the implant design developed with cartilage and without cartilage taken into consideration. Goodness of fit for both kinds of implant is compared.

# CHAPTER II

# DESIGN OF A 1ST METATARSOPHALANGEAL HEMIARTHROPLASTY IMPLANT BASED ON OSTEOLOGICAL SPECIMENS

[1,2]Atul Kumar, [3]Brian Donley, [1]Peter R. Cavanagh

[1]Department of Orthopaedics and Sports Medicine, University of Washington, Seattle, WA, USA
[2]Chemical and Biomedical Engineering Department, Cleveland State University, Cleveland, OH, USA
[3]Department of Biomedical Engineering, Cleveland Clinic, Cleveland, OH, USA

ABSTRACT

Prosthetic replacement of the articular surface of the first metatarsal head (MTH1) with the proximal phalanx (PP) is an accepted approach for the treatment of severe osteoarthritis of the first metatarso-phalangeal joint (MTPJ1). However, there are few studies describing the appropriate three dimensional geometry of such a replacement which must be congruent with the articular surface of the PP which is spared in most of the prosthetic replacement procedures of MTPJ1. In this study, 97 adult MTH1 bones from the Hamann-Todd collection at the Cleveland Museum of Natural History were scanned using a laser scanner with a resolution of 400 point per square inch. After a two-stage alignment process using landmark identification and an iterative closest point algorithm, the male and female specimens were divided into small, medium, large groups. A best fit ellipsoid was obtained using non-linear unconstrained optimization (NLUO) for the articular surfaces of the metatarsal heads for each size group. Identification of the corners of the MTH1 articular patches led directly to the final surfaces, on ellipsoids, suitable for the design of the hemi-arthroplasty. Average RMS errors between the articulating surfaces of the bone specimens and the optimal fit surfaces were between 0.29 and 0.42mm. Consideration of the thickness of cartilage overlying the MTH may further improve the fit.

## 2.1 Introduction

The first metatarso-phalangeal joint (MTPJ1) plays a crucial role in many human locomotor movements [4,23,24]. When conservative treatments of MTPJ1 pathology fail, a number of surgical options are available including arthrodesis [25,26], osteotomy[27,28 29], and replacement of part [30] -36 or all [31-33]-40 of the articular surface with an implant. In most MTPJ1 arthroplasty procedures, the distal articulating surface (the proximal 1st phalanx) is maintained and thus it is important that the geometry of any metatarsal head replacement be designed with close fidelity to the original metatarsal head. The alignment of the replacement must also be accurate to ensure optimal functioning. Although implant manufacturers often refer to their products as "anatomically designed" [34,35]-43 there is a paucity of data available on the design of MTPJ1 prosthetic components in the refereed literature. Numerical approaches to the derivation of implant surfaces have been previously described for the hip[36], knee[37], and elbow[38,39]. In this study, we present a quantitative approach to the design of replacements for the articular surface of the first metatarsal head (MTH1) based on an analysis of 3-D scans of osteological specimens.

## 2.2 Methods

Osteological specimens of the 1st metatarsal from the Hamann-Todd collection at the Cleveland Museum of Natural History were scanned using a NextEngine (NextEngine, Inc. Santa Monica, California) 3D desktop laser scanner with a precision of 400 data points per inch. A total of 97 adult bone sets were scanned (48 male and 49 female sets, age range: 30-50 yrs: mean age 39.5±5.69 yrs and 37.0±5.32 yrs for males and females respectively, body weight :59.06 ± 5.57 kg and 57.61 ± 7.21 kg for males

and females respectively. The relatively low body weights resulted from the nature of the Hamann-Todd collection which was assembled from the unclaimed dead of Cuyahoga County, OH between 1912 and 1938. Many of these individuals were emaciated after chronic illness. In addition, body weights were not taken in some cases until a month after death and thus an unknown amount of fluid could have evaporated or been lost in other ways. These limitations are not likely to affect the bony geometry of the specimens.

Metatarsal and phalanx bones were fixed to a turntable and scanned from at least 8 views. The resulting scans were then aligned and merged using standard NextEngine software to generate a single 3-D surface for each bone. Alignment to a common reference frame was achieved using a two stage process (Figure 2-1).

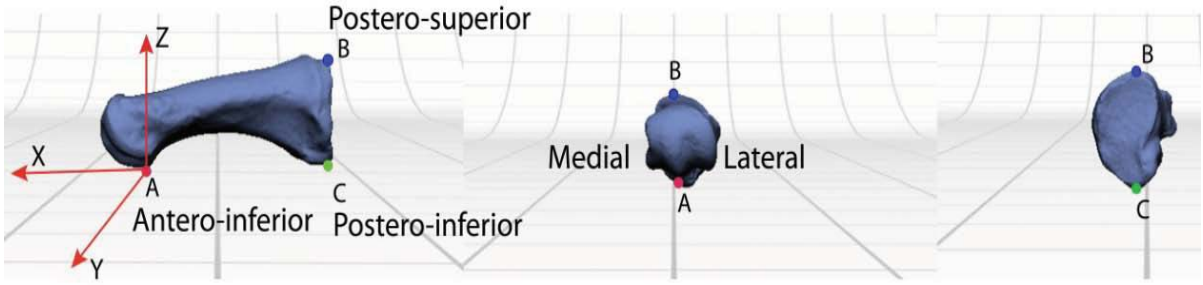


Figure 2-1: Lateral (A), anterior (B), and posterior (C) scans of a typical 1st metatarsal bone. Anatomical axes and landmarks used for initial alignment are shown

*Initial Alignment:* Three landmark points were identified on each specimen by viewing the 3-D image. These points, defined with respect to the anatomical position, were: Point A: the most antero-inferior point (on the inter-condylar ridge of the head); Point B: the most postero-superior proximal point (above the tarso-metatarsal joint); and Point C: the

most postero-inferior proximal point (below the tarso-metatarsal joint). The initial local reference frame shown in Figure 2-1 was then created for each bone where the x-axis was along CA, the y-axis was formed by the cross product of CA and BA. The z axis was then cross-product of the unit vectors along the x and y axes. When the alignment of different metatarsals expressed in this initial reference frame was compared, it was apparent that inaccuracy in the location of the three anatomical points and/or different amount of torsion of the shafts of the individual bones resulted in poor alignment of the articular surfaces (Figure 2-2). To minimize this variation so that the articular surfaces in various size groups could be compared, a secondary alignment was performed.

*Secondary Alignment:* Typical male and female metatarsal bones were chosen as templates for the secondary alignment using the following criteria: a high quality scan; broad undamaged articular surfaces; and a clearly identifiable crest between the trochlear surfaces for the sesamoids starting at around mid-height of the metatarsal head.

The initial local reference frames of the template bones were used to create an ellipsoid having its center at the origin and semi-axes parallel to axes of the reference frames. An unconstrained non-linear optimization process (FMINUNC in Matlab) in which the position of the center of the ellipsoid, the length of semi-axes, and the angles of rotations of the ellipsoid were varied led to an optimal ellipsoid fitted to each of the template bones. The final local reference frames for the template bones were then generated by transforming the initial local reference frame by the rotations and translations determined from the optimal fit ellipsoid. Male and female bones were analyzed separately.

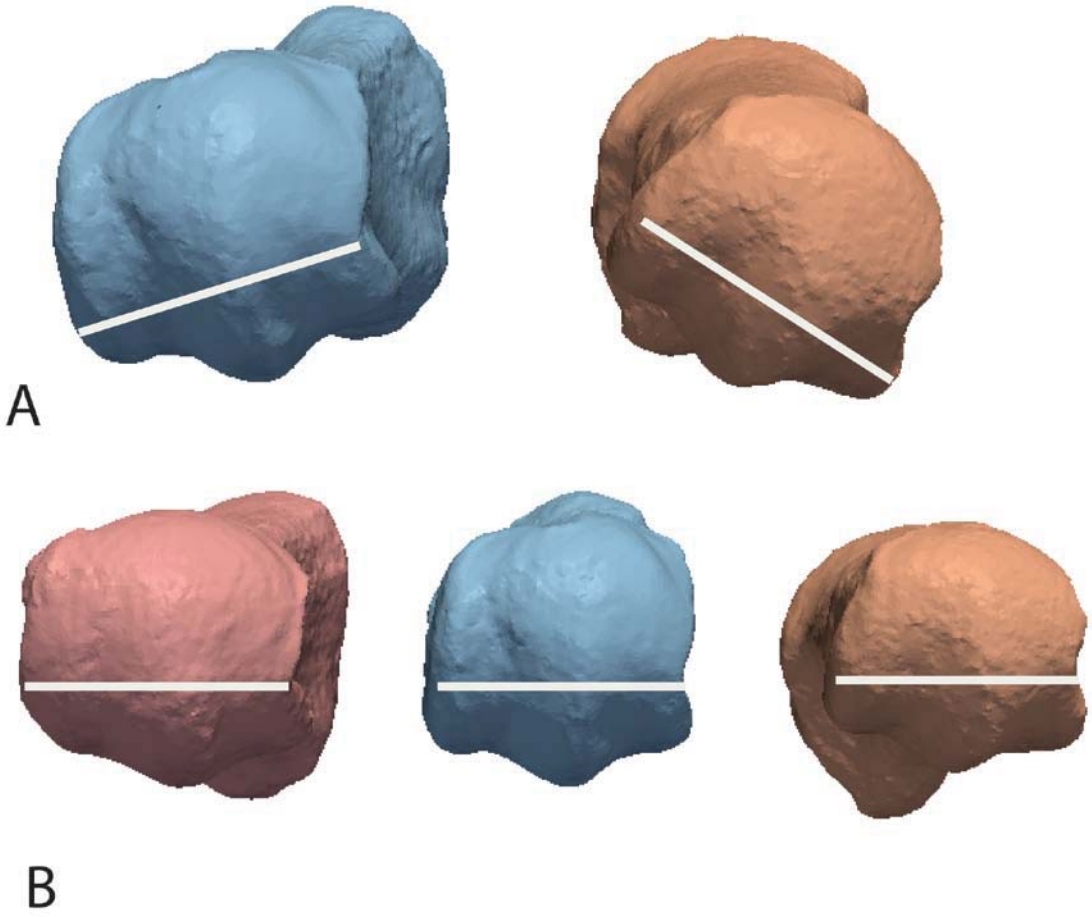


Figure 2-2: A. Specimens 0421 and 2242 in their initial reference frames viewed down the x-axis towards the origin. From the line drawn as a tangent to both condyles, the misalignment of the condylar surfaces after initial alignment is apparent. B. Template bone (left) and specimens 0421 and 2242 after secondary alignment with the template bone. The white line in an approximate tangent to medial and lateral condylar surfaces.

Individual target bones were then all aligned to the appropriate template bone (after first transforming the target bones from the other side of the body by a reflection in the X-Z plane of the initial reference frame). Bone length for all bones was obtained by calculating the largest distance between any two points on each bone and all points on the anterior 40% were isolated for secondary alignment. Unconstrained nonlinear optimization method was again used, but in this case with a minimization of the cost

function calculated from the sum of the squared distance between each point on the template bone and the closest point on the target bone[40]. All points on each entire target bone were then transformed according to the rotations and translations calculated from the optimization (Figure 2-2B and 2-3).

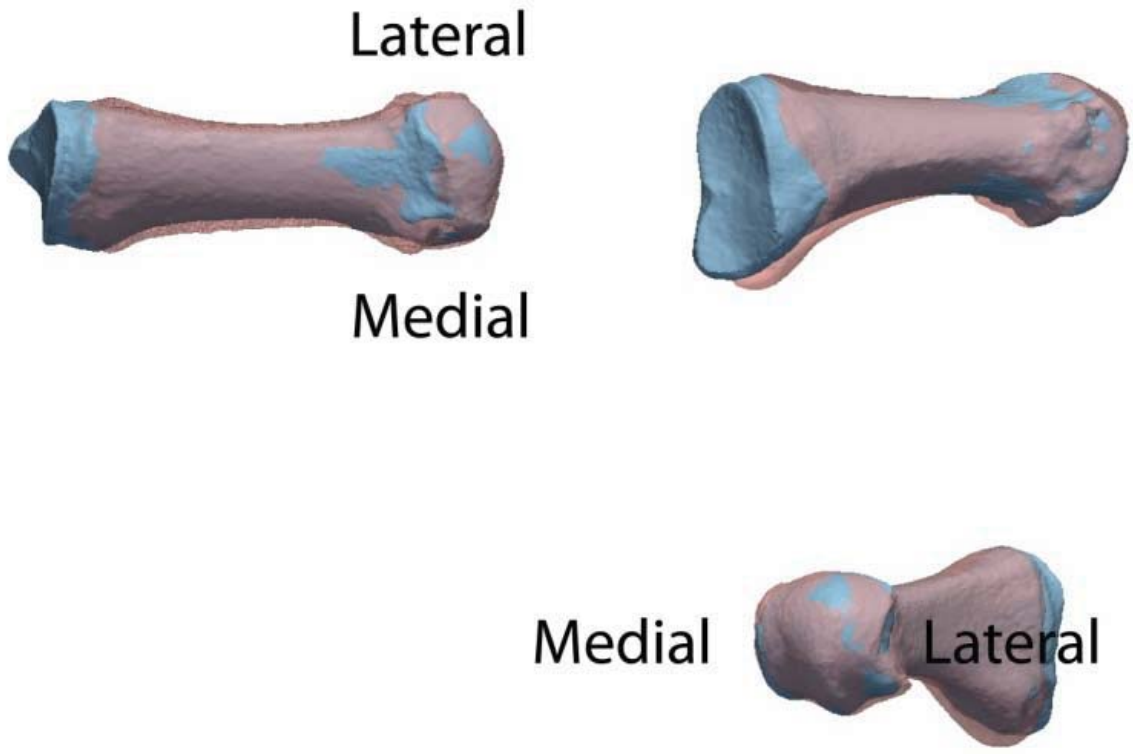


Figure 2-3: Alignment of target bone (blue) with template bone after secondary alignment.

*Finding the Articular Patch for the Phalanx and Sesamoids:*

The identification of the region of the metatarsal head surface that articulates with the proximal phalanx was accomplished by isolating the region of the articular patch superior to the inter-condylar crest. To accomplish this, the metatarsal head was identified by successive truncation of proximal regions. An axis was established

perpendicular to the XZ plane at the midpoint of the line between the most superior and inferior points on the metatarsal head (see Figure 2-4). Radial slices of the MTH were obtained around this axis. The cutting plane was rotating in increments of 1º, from -10º to 180º, about the Z-axis. Section width for each slice was defined between the minimum and maximum Y'' coordinates (Figure 2-5). Separate rules, described in Table 2-1, were necessary in different sectors of the MTH to segment the articular patch.

Table 2-1: Approach used to isolate the articular surface for both phalanx and sesamoids from the MTH1.

| Region | Aspect | Purpose | Action |
|---|---|---|---|
| + 10 deg to 180 | Medial and lateral | Trim the medial and lateral borders of the MTH which are not part of the articular surface | Trim symmetrically to 62% of current slice width |
| -10 deg to + 9 deg | Lateral | Trim the lateral border of the MTH | Trim lateral margin by 14% of width |
| At each 1 deg increment from -10 to + 9 deg | Medial | Include supero-lateral segment of articular surface | Remove (100%-5(n-1)) of entire slice where n=1,21 for slices -10 to +10. |

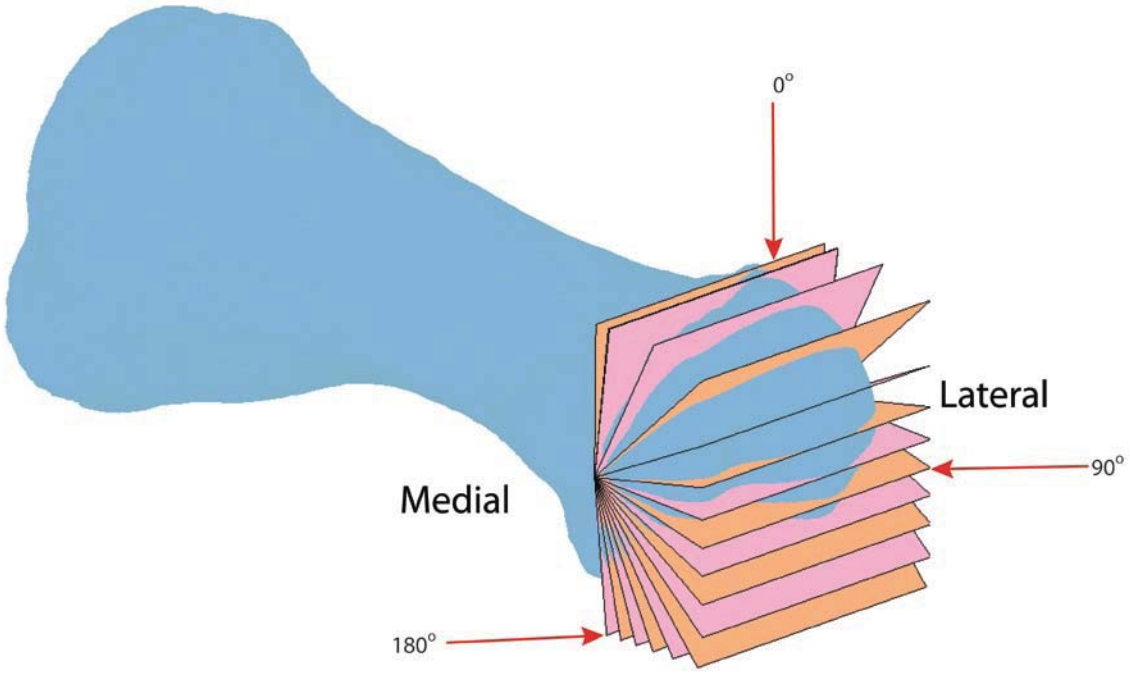


Figure 2-4: Cutting planes used to identify the articular surfaces on a typical bone (specimen 2242 used in Figure 2-2) generated by rotation about a line parallel to the Y axis in the final reference frame. See text for further details.

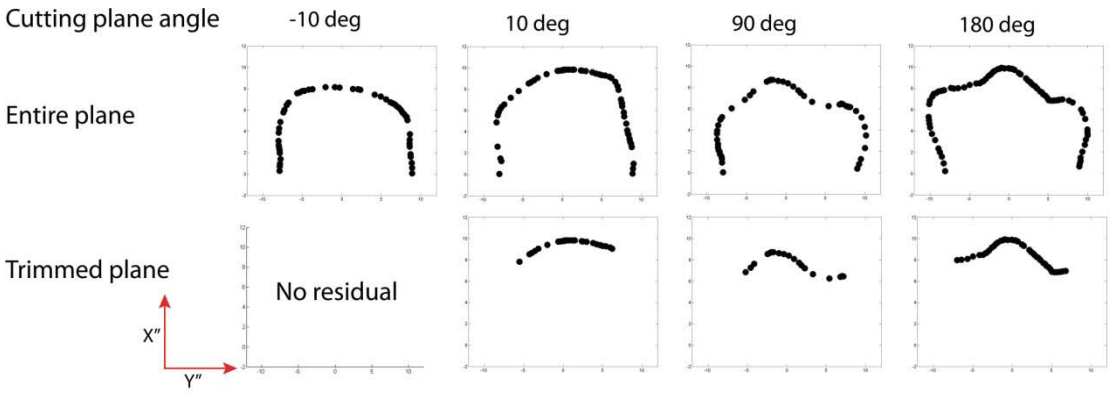


Figure 2-5: Individual sections of the MTH on the -10, 10, 90, and 180 degree cutting planes (above) and the articular surfaces identified by the cropping process (see text for details). There was no articular surface present on the -10 degree plane. Note the presence of the inter-condylar crest in the 90 and 180 degree sections

A quadratic curve was fitted to each slice and the root mean square (RMS) error of this curve fit in the middle one-third of the section was calculated. Critical residuals from 0.25 mm to 0.65mm were used iteratively on all slices to identify the inferior extent of the surface. At each critical value, the resulting articular patch was visually examined for the presence or absence of the crest. If no crest was present, the critical residual was incremented by 0.1mm and the process repeated. The median critical residual for all slices was 0.55mm in male and 0.45mm in female specimens (SD 0.13 both in male and female specimens). Because of rough articular surfaces, 10 cases required special treatment. Typical superior articular patches resulting from this process are shown in Figure 2-6.

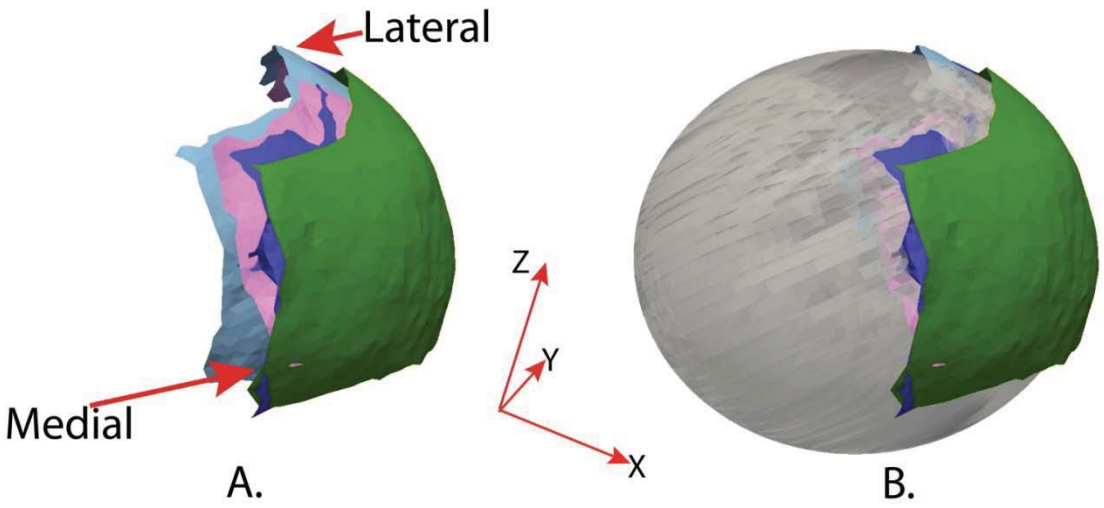


Figure 2-6: A. A set of superior articular patches from the female medium group. B. The same patches, shown in Figure 2-6A , with the best fit ellipsoid for the female medium group.

*Sorting into size-based groups based on metatarsal head dimensions:*

The method used to sort the bones into size groups was based upon the linear measurements on the MTH1 which approximately predicts the curvature of its articulating patches. Although more complex three dimensional methods are available, this simple method was used to allow clinicians to size an implant based on plain radiographs. The required measurements are shown in Figure 2-7.

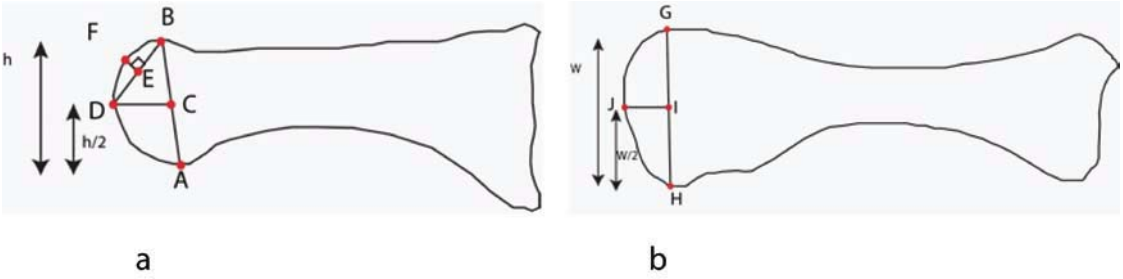


Figure 2-7: a. Sagittal view. b. Dorsi-Plantar view. A: Lowest point on MTH1; B: Highest point on MTH1; C: Mid-point of AB; D: Anterior most point at the mid-height of MTH1; E: Mid-point of BD; F: Point of intersection of perpendicular bisector of BD and arc formed by BD; h: Height of MTH. G: Most medial point on MTH1 ; H: Lateral point on MTH1; I: Mid-point of GH; J: Anterior most point at the middle of the width; W: Width of MTH

Based upon these measurements, best fit circles were obtained for arcs formed by MTH1 in sagittal view (between B and D) and in dorsi-plantar view (between G and H) using eq.1[49]. The average of these radii was taken as determinant of sizing as follows:

Average radius = — —— – ——

A normal distribution curve was fitted to the distribution of average radius in male and female group separately. The Shapiro-Wilk test of normality W statistics was 0.98 for distributions of both the male and female bones. The distributions were divided into three groups based upon z-score from the normal distribution (<-1z: Small; >+1z large; $\geq$-1 z $\leq$+1 medium) for males and females separately.

*Defining the Best-fit Articular Patch for each group*

Articulating patches obtained, as described above, from each metatarsal head expressed in the final local reference frame were compiled into a single data file. A best fit ellipsoid was obtained for this data set using an unconstrained nonlinear optimization method in Matlab to vary the nine degrees of freedom (3 semi-axis lengths, 3 orientations, and the three-dimensional location of the centroid). The shortest Euclidean distance from each point on the ellipsoid surface to the bone patch data was measured and minimization of the sum of these distances was used as the cost function for optimization (Figure 2-6B). The final step involved extraction of the region of the surface of the ellipsoid that contained all of the articular patches in each individual group. This was accomplished by identifying the median locations of the four corners of the set of articular surface patches and then radially projecting the mid-points for the following pairs corners on the ellipsoid : superior-lateral and inferior-lateral; superior-lateral and superior-medial; superior-medial and inferior-medial; and inferior-medial and inferior-lateral. A cutting plane was then created using an unconstrained optimization algorithm which minimized the sum of distances from these mid-points to the plane (Figure 2-8). To parameterize the cutting plane, a local reference frame with respect to each ellipsoid

was created such that the semi-axes of ellipsoid made the three major axes of the reference frame. An arbitrary point on the cutting plane was indentified and two direction vectors were calculated for the cutting plane at that point.

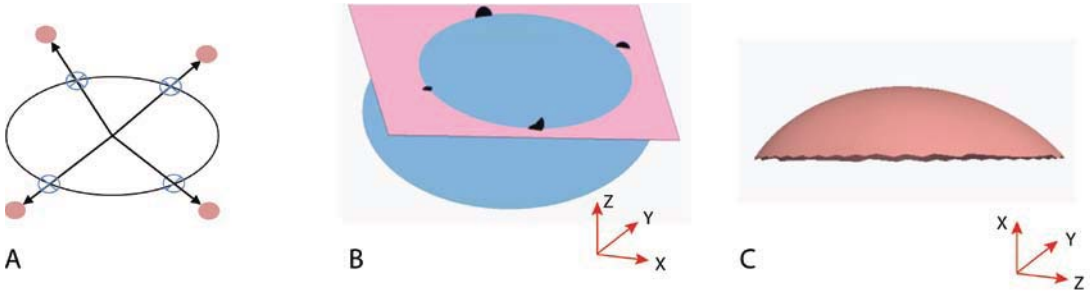


Figure 2-9: A. Median of mid-points (solid colored) between the four pair of corners projected on best fit ellipsoid surface. B. An optimal plane passing near to those four points on ellipsoid. C. Patch of ellipsoid extracted by the plane.

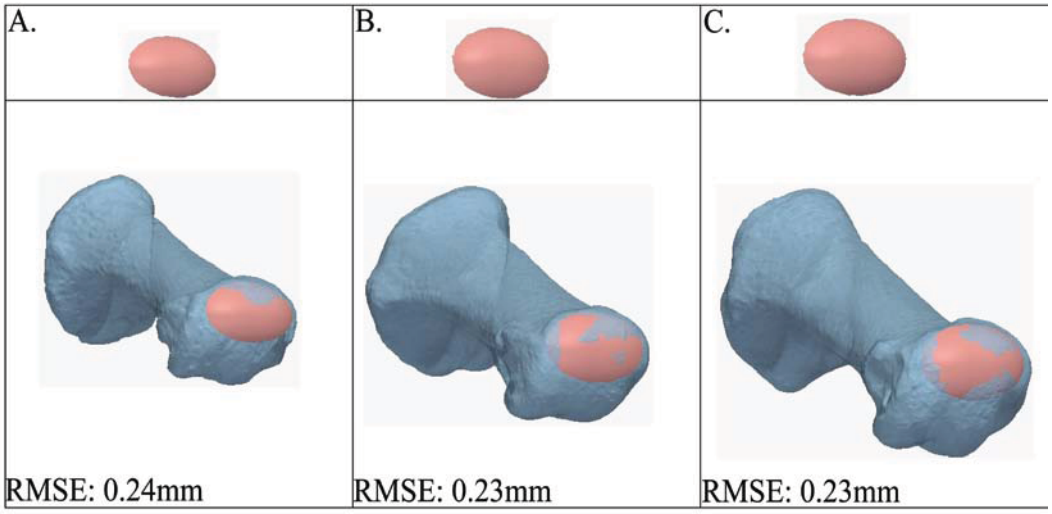


Figure 2-10: The women's small (A), medium(B) and large(C) implants shown in relation to specimens from respective group (specimen number 0128 (A), 1785(B), 2128(C)).(RMSE: Root mean square error).

## 2.3 Results

The class intervals used to classify the bones are presented in Table 2-2. These intervals were based upon the mean radii of the best fit circles to arcs formed by MTH1 in sagittal and dorsi-plantar views. One way analysis of variance and subsequent pairwise comparisons using Tukey tests (Matlab Statistical Toolbox) indicated that the mean radii for each group was significantly different from every other group ($p<0.05$) mean except those of medium female and small male, and large female and medium male groups.

The characteristics of the best fit ellipsoids for the articular surfaces for each of the six groups are shown in Table 2-3. These data represent the key outcomes of this study since, after appropriate cropping; they completely describe the geometry of the proposed hemi-arthroplasties. The orientations of the cutting planes for the ellipsoids are described with respect to the ellipsoidal local coordinate systems in Table 2-4. Examples of the final implant surfaces are shown both in isolation and in relation to a typical metatarsal bone for the female small, medium, and large groups in Figure 2-9. Average RMS errors between the articulating surfaces of the bone specimens and the optimal fit surfaces are presented in Table 2-5.

Table 2-2: Class intervals used to classify bones into small, medium, and large groups. The values are the mean radii of the two optimal-fit circles of the sagittal and dorsi-plantar planar projections of MTH1. ( Mean radius for male: 8.75±0.63mm and mean radius for female:8.03±0.53mm)

| | Small | Medium | Large |
|---|---|---|---|
| Male | <8.12 | 8.12- 9.38 | >9.38 |
| Female | <7.50 | 7.50 -8.56 | >8.56 |

Table 2-3: Dimensions and orientation (with respect to anatomical axes) of optimal-fit ellipsoids (Semiaxes and RMS error in mm; Yaw, Pitch and Roll in degrees.

| | Center X | Center Y | Center Z | Semiaxis X | Semiaxis Y | Semiaxis Z | Yaw | Pitch | Roll | RMS Error |
|---|---|---|---|---|---|---|---|---|---|---|
| MALE | | | | | | | | | | |
| Small (n=9) | 7 | -1.21 | 11.66 | 7.17 | 11.08 | 7.62 | 2.39 | -0.5 | 2.03 | 0.77 |
| Medium (n=32) | 7.33 | -1.18 | 11.1 | 7.62 | 11.51 | 8.83 | -3.7 | 0.33 | 3.03 | 0.69 |
| Large (n=8) | 6.5 | -1.54 | 9.41 | 7.97 | 13.44 | 10.95 | -2.5 | 1.89 | 6.55 | 0.77 |
| FEMALE | | | | | | | | | | |
| Small (n=6) | 2.87 | -2.42 | 13.2 | 7.44 | 10.16 | 6.51 | 5.12 | 5.52 | 5.69 | 0.39 |
| Medium (n=34) | -6.55 | -2.21 | 11.64 | 7.76 | 11.06 | 7.45 | 3.7 | 49.8 | 9.26 | 0.46 |
| Large (n=8) | 1.67 | -1.72 | 13.28 | 9.06 | 12.07 | 7.94 | 2.58 | 8.3 | 1.96 | 0.65 |

Table 2-4: Parameters of the cutting plane, which extracts the implant surface from ellipsoid, with respect to the ellipsoid having center at origin and semi-axes making the axes of reference frame. First and second direction vector represent the vectors for plane from one of the point on plane. X', Y' and Z' represent the coordinates in reference frame created with respect to ellipsoid.

| | Point on Plane | | | First direction vector | | | Second direction vector | | |
|---|---|---|---|---|---|---|---|---|---|
| | X' | Y' | Z' | X' | Y' | Z' | X' | Y' | Z' |
| MALE | | | | | | | | | |
| Small | 4.01 | 0.53 | 2.93 | 0.18 | -0.98 | -0.07 | 0.57 | 0.17 | -0.81 |
| Medium | 4.12 | 0 | 3.1 | -0.1 | -0.99 | 0.13 | 0.59 | -0.17 | -0.79 |
| Large | 5.51 | -0.2 | 4.53 | -0.1 | -0.99 | 0.08 | 0.63 | -0.13 | -0.77 |
| FEMALE | | | | | | | | | |
| Small | 3.67 | 0.56 | 3.45 | 0.47 | -0.8 | -0.37 | 0.51 | 0.58 | -0.63 |
| Medium | 0.42 | 0 | 5.19 | -0.09 | -0.1 | 0 | -1 | 0.09 | 0.08 |
| Large | 4.4 | 0.69 | 4.1 | 0.51 | -0.76 | -0.42 | 0.46 | 0.64 | -0.61 |

Table 2-5: Mean ± standard deviation of root mean square error between the ellipsoid patch and the MTH for individual each group

| | Small | Medium | Large |
|---|---|---|---|
| Male | 0.38± 0.05 | 0.42 ± 0.09 | 0.38 ± 0.11 |
| Female | 0.34 ± 0.06 | 0.29± 0.05 | 0.34± 0.07 |

## 2.4 Discussion

This study used a novel approach for designing an implant to resurface the primary articulating surface of MTH1 for MTPJ1 hemiarthroplasty. This approach uses MTH1 articular surface parameterization with an optimal ellipsoid fit. An ellipsoid was chosen because it has nine degrees of freedom and thus allows for more customization of the articular surface than, for example, a sphere which has only 4 degrees of freedom. An ellipsoid can be easily parameterized to define the implant surface.

MTPJ1 is a gliding hinge joint in which the axis of rotation moves dorsally as the proximal phalanx dorsiflexes beyond 30º to prevent dorsal jamming of the MTPJ1 articular surfaces. The kinematics of this movement is largely determined by the condylar shape of MTH1[19]. Thus in order to prevent the impingement of the articular surfaces the MTH1 implant must maintain the congruity of the native MTH1 condyles[41]. This is also important because the phalangeal articulation of MTPJ1 is spared in the hemi-arthroplasty procedure.

Examination of the orientations of the optimal fit ellipsoids for the different groups of bone dataset (Table 2-3) showed that the angles of pitch obtained for medium female group (49.80 degrees) was out-of-family compared to the other groups (average 6.91 degrees). The very similar lengths of semi-axes X and Z in the female medium group explain this pitch angle discrepancy. The similar semi-axes lengths make the ellipsoid's final position after optimization relatively insensitive to the angle of pitch.

The anatomical congruence of the ellipsoid based implants with the metatarsal head that they are intended to replace was excellent. The mean RMS error of fit of the implant to the six different size groups was between 0.29-0.42mm. Comparison of male and

female bones for the size of best fit ellipsoid showed sexual dimorphism suggesting that male and female versions of MTH1 implants may be required. The semi-axes of the ellipsoid fitted to male bones were invariably greater than those of the female bones which is consistent with previous studies[42,43], except our results showed male values for semi-axes X (parallel to the X-axis - see Figure 2-2B) were smaller than female values.

The size classification using the average of the radii of best fit circles to the anterior curves of MTH1 in the lateral and dorsi-plantar views was used because these measurements are easily accessible from planar and lateral radiographs and can thus be used to assist surgeons with pre-operative planning of sizing. This method is in contrast to previous studies that have used caliper measurements on the first metatarsal bone[43] without consideration of the curvature of the articular surface.

The present study has a number of limitations. Although a total of 97 specimens were examined, the numbers of specimens in some size and sex groups were relatively small and further work with a larger number of specimens is required to definitively identify sizing and sexual dimorphism. There is a possibility of subjective error in the alignment of the multiple scans for each specimen to create a single surface. During processing, a two staged alignment was needed to bring all bones to a common reference frame. The initial alignment based on subjectively chosen anatomical landmarks showed large variations and is not recommended as a primary method of alignment in future studies. However such alignment does provide good initial values for the secondary alignment using the iterative closest point algorithm (ICP) which requires a reasonable initial estimate to avoid local minima. In this study, we have focused on the metatarsal head articular surface, and have not considered either the articular surface of the proximal

phalanx or the articulation with the sesamoids. The rules used to extract articular surface (see Table 2-1) did not work for a few specimens and manual selection was required. In addition, no consideration was given to the articular cartilage covering over the metatarsal head. Although this has been previously shown to have a maximum thickness of 1mm[44] consideration of local variations in cartilage thickness may further improve the congruity of implant placed *in vivo.*

## 2.5 Conclusions

A new design approach to an implant for MTH1 hemiarthroplasty was identified based upon the three dimensional morphology of osteological specimens. After classification into sex and size-based groups, the resulting implant profile provided a very good fit to individual bones. This method can be extended to the design of implants for other joints which require hemiarthroplasty.

## 2.6 Acknowledgements

We appreciate the cooperation of Dr. Yohannes Haile-Selassie, Curator of Physical Anthropology at the Cleveland Museum of Natural History.

# CHAPTER III

# CARTILAGE THICKNESS MEASUREMENT OF FIRST METATARSAL HEAD USING 14T MRI

[1,2]Atul Kumar, [1]Peter R. Cavanagh

[1]Department of Orthopaedics and Sports Medicine, University of Washington, Seattle, WA, USA
[2]Chemical and Biomedical Engineering Department, Cleveland State University, Cleveland, OH, USA

## ABSTRACT

Hyaline articular cartilage is one of the most important structures of the first metatarsophalangeal joint (MTPJ1). Cartilage thickness mapping is required for accurate computational biomechanical assessment of the MTPJ1. Imaging techniques have been used to study cartilage thickness mapping of other joints like the knee, hip and wrist but no imaging study has been done to explore the MTPJ1. In this study, 2 adult MTPJ1s were harvested from cadavers and were scanned using a 14T MRI scanner. The cartilage region was segmented semi-automatically from the image. The segmentation method

used the Canny edge detection algorithm and an intensity based ‘edge growing algorithm’. The segmented cartilage from the image was stacked to form 3D cartilage shells. The point-to-point distance between the outer and inner shells of cartilage was measured to obtain cartilage thickness mapping of the MTH1. The MTH1 articular surface was divided into 6 regions and the thickness mappings of all the regions were compared. The overall mean thicknesses of cartilage in different regions were found to be 0.59 to 0.79 mm.

## 3.1 Introduction

Hyaline articular cartilage is one of the most important structures in a synovial joint. It protects the bone articular surfaces from abrasion and provides a smooth lubricated surface for joint movement[45]. To characterize the mechanical properties of a diarthrodial joint and to understand its morphology, the articular cartilage thickness measurement and the variation of thickness across the surface of the joint are required [46].

The thickness of the hyaline cartilage of a synovial joint varies from region to region of the articular surface[47]. The articular cartilage usually mimics the contours of the subchondral bone to which it is attached[48], and the thickness of articular cartilage seems to be related to the congruence of a joint. Thin cartilage is found in congruent joints, such as the ankle, whereas thick cartilage is found in incongruent joints, such as the knee [49].

Various methods for the measurement of thickness include optical [49] [50] and ultrasonic techniques[51] [52], , laser scanning morphometry[53], histomorphic techniques[44] [54], CT[55], MRI[56] and laser scanning[57]. Imaging techniques such as CT, MRI and ultrasonography have been used with other joints such as the knee[58,59], hip[60,61] and wrist[62]. To identify the cartilage region in the images, most of these methods have used manual segmentation of cartilage by a radiologist or trained researcher which makes this process demanding in terms of labor and time. Manual segmentation is also susceptible to subjective error during selection of a region of interest.

The first metatarsophalangeal joint (MTPJ1) plays a crucial role in many human locomotor movements [63,23,24]. Osteoarthritis, a degenerative disease of cartilage, involves the MTPJ1 in up to 42% cases[8]. To the best of our knowledge no imaging studies have

been done to explore the cartilage thickness of the MTPJ1. In a few studies microscopic evaluations [44] and creep indentation techniques[46] have been used to study the cartilage thickness of the MTPJ1. Muehlman[44] et al. reported a correlation between the cartilage thickness distribution and weight bearing distribution on the head of the 1st metatarsal bone. Athanaiou[46] et al. study suggest the cartilage thickness of MTPJ1 is indicative of the functional environment of MTPJ1.

To measure the *in vivo* thickness of the cartilage in a reproducible manner, an imaging study of the cartilage is required. The imaging method capable of directly visualizing articular cartilage is magnetic resonance imaging[58] or contrast enhanced CT [64]. The objective of our current work is to

- Determine the thickness of cartilage in different regions of the first metatarsal head (MTH1) using 14T MRI images.
- Describe a new method which uses image processing and computational geometry for segmentation of cartilage in the MRI image of the MTH1.

Figure 3-1: 14T MRI scanner

## 3.2 Method

### 3.2.1 Data Acquisition

MRI images of MTPJ1 specimens from two cadavers (75 years female and 77 years male) were acquired from a 14T MRI scanner (Bruker, Karlsruhe, Germany) (Figure 3-1) using a turbo spin echo pulse sequence (Appendix B) with voxel size of 0.05 x 0.05 x 0.10 $mm^3$ (for specimen from 75 year female) and 0.04 x 0.04 x 0.04 $mm^3$ (for specimen from 77 year female). Field of view was 25 x 25 x 25$mm^3$ (for specimen from 75 year female) and 20 x 20 x 20$mm^3$ (for specimen from 77 year female). Exclusion criteria for the specimen were as follows: fracture, previous toe surgery, and degenerative disease which were defined as the presence of osteophytes. The transverse view of the grayscale image of each MTH1 was used for further analysis (Figure 3-2a.).

### 3.2.2 Cartilage thickness mapping

Using concepts of image processing and computational geometry the cartilage thickness mapping of the MTH1 was done in MATLAB (MathWorks Inc., Natick, MA). This was accomplished in multiple stages including; extraction of outer border of cartilage from grayscale image, segmentation of complete cartilage region in the image, smoothing of the segmented cartilage region, 3D reconstruction of cartilage, and cartilage thickness measurements. Various intensity based techniques for image segmentation, such as thresholding and region growing[65], were tried before the cartilage segmentation method developed by the author was implemented.

#### 3.2.2.1 Cartilage outer border extraction

The various steps for extraction of the outer border of the cartilage were performed in a MATLAB based GUI. For each slice of the grayscale image of MTH1, the edges of the cartilage image were detected with a Canny edge detection algorithm[66] (Figure 3-2) (Appendix D). The algorithm used a Gaussian filter, with standard deviations of 2 and 3, for noise reduction in the image. Different values of standard deviations were needed for the two different image datasets.

A fused image of all the edges in the grayscale image together with the original image was created (Figure 3-3). The cartilage region in the image shows two borders: an outer border formed by the edges on the interface of the cartilage and the soft tissue or water surrounding the cartilage; and an inner border formed by the interface between cartilage and subchondral bone. The outer border consisted of large continuous fragments of edges, while the inner border consisted of small fragments of edges, so the outer border required less manual intervention.

The edges which touched the outer border of the cartilage and did not lie completely on the border were trimmed manually. The rest of the edges were trimmed manually, saving the outer border of the cartilage, to make the further steps run faster. Small gaps (Figure 3-4) in the outer border of cartilage, due to the damaged surface of the cartilage as an effect of aging, were interpolated with a quadratic interpolation function. The interpolation function used was based on curve fitting to the edge segments adjacent to the gap. These edge segments were selected by manually choosing two end pixels, and all the pixels between end pixels were found using an 'edge walking algorithm' (explained below).

After interpolation, the outer border of the cartilage was extracted from the fused image using an 'edge walking algorithm' (explained below). In this process two pixels are chosen manually on the outer border and the all the pixels between those two points

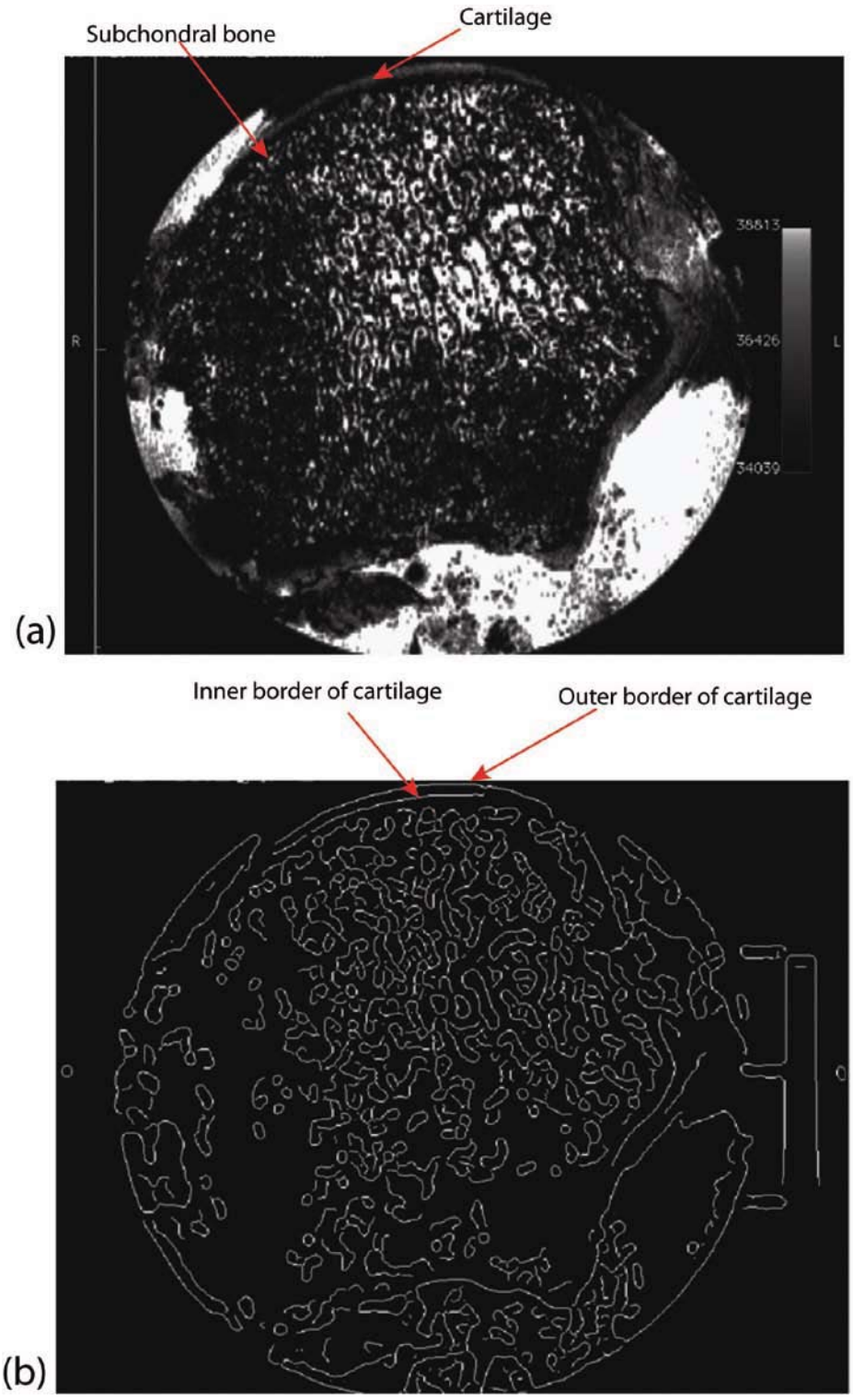


Figure 3-2: (a) Transverse section image of 1st metatarsal head with 14T MRI. (b) Edges detected in the image shown in Figure 3-2(a) with canny edge detection algorithm

on the border are extracted. This process was repeated until the complete outer border was extracted (Figure 3-5).

Edge walking algorithm: Based upon the concept of topological walk[67] an edge walking algorithm in two dimensions was implemented by the author. In this algorithm, pixels in the image are considered as a point cluster in 2D space. The algorithm finds the geodesic path from the given starting point towards the given finish point such that the path will

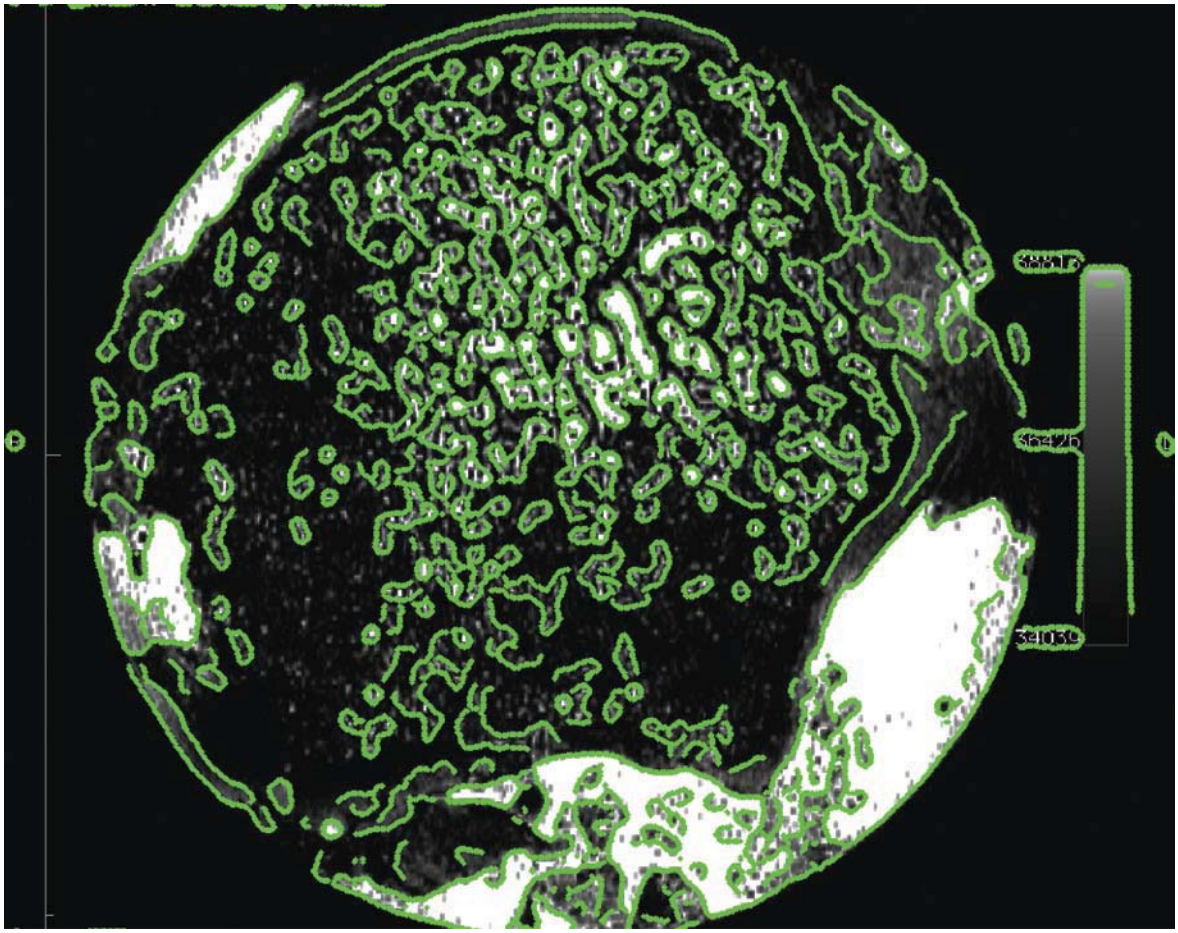

Figure 3-3: Fusion image of the grayscale image and the edges found in the grayscale image with canny edge detection.

include the successive nearest points. First, the algorithm finds the connectivity of the points in its cluster using Delaunay triangulation [68] (Appendix C) and finds the first two nearest connected neighbors to the starting point. From these two points, the one that is closer to the finish point is included in the geodesic path and this point becomes the starting point for next iteration. This process runs iteratively until the finish point is reached and included in the geodesic path.

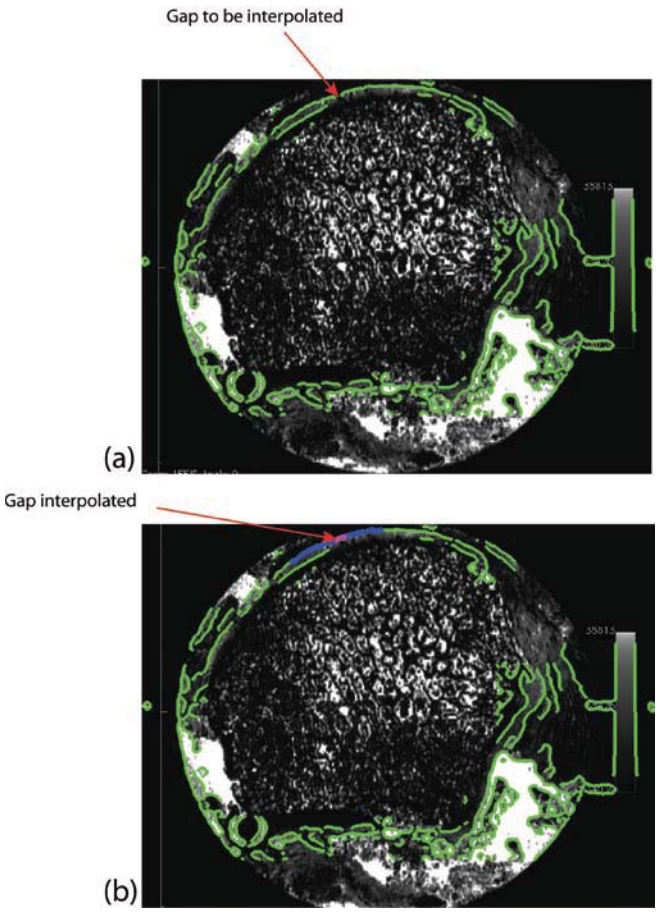


Figure 3-4: (a) Upper border with gap. (b) Interpolated gap (red) with the two segments (blue) of edge used for quadratic interpolation

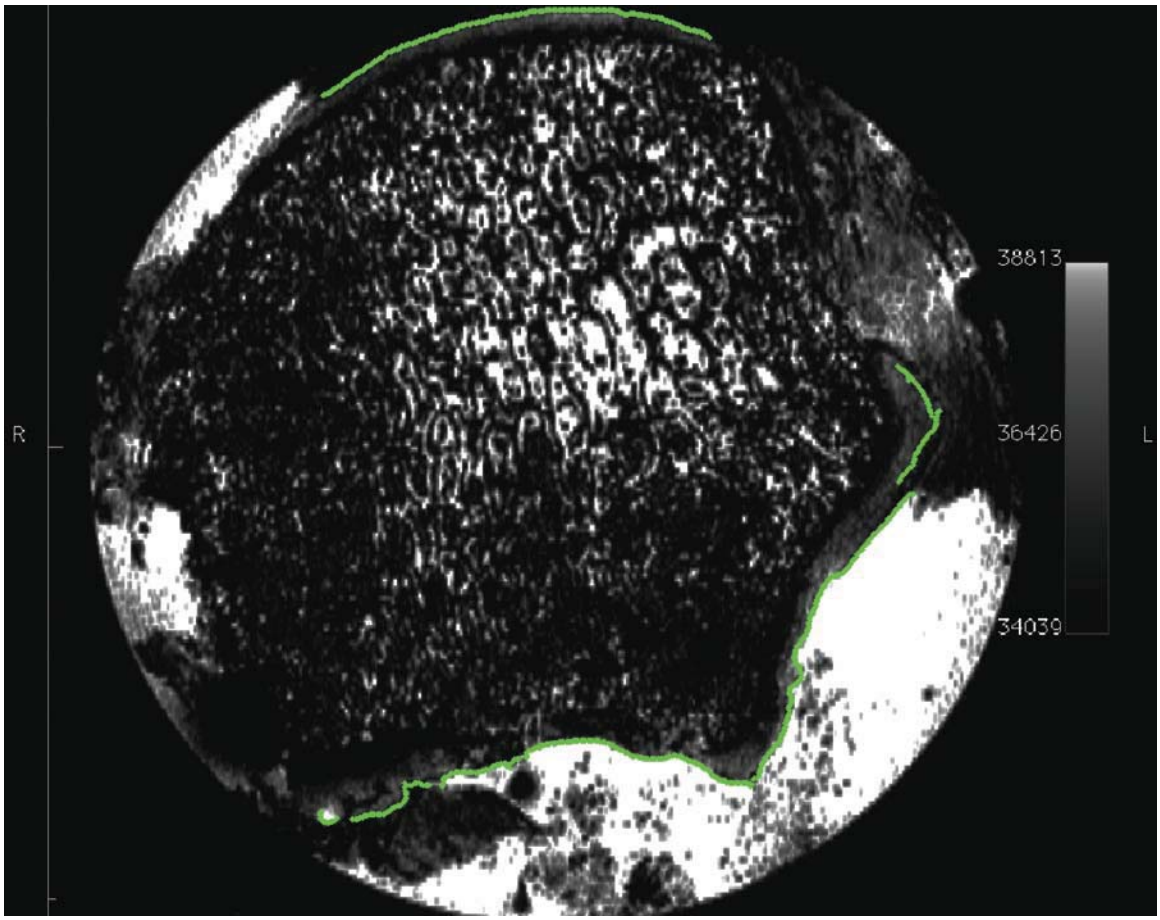


Figure 3-5: Transverse section of MTH1 with outer border (green) of cartilage.

### 3.2.2.2 Cartilage region extraction

Edge growing algorithm: Based upon the concept of seeded region growing[69] an 'edge growing algorithm' was implemented by the author. In this algorithm, first a best fit circle to the outer border is calculated using a non-linear unconstrained optimization method. For each pixel (called a "seed point") of the outer border, the nearest neighbor pixel towards the center of the circle is examined for its intensity value. The nearest

neighbor pixel which has intensity within a range of threshold intensity values (5 to 220) is included in the region of cartilage and this neighboring pixel becomes the seed point for next iteration. This process goes on iteratively until a seed point with the lowest value of intensity threshold is detected and the next nearest neighbor of this seed point has the intensity greater than that of seed point. The last seed point forms the pixel for inner border of cartilage. The number of pixels between the initial seed point and the last pixel included in the region is called 'depth' of the cartilage for that initial seed point. A collection of last pixels forms the inner border of cartilage in the image and the pixels between the inner and outer borders represent the cartilage region. In this manner, the cartilage area and its inner border were identified for each slice (Figure 3-6).

As seen in Figure 3-6 the inner border of the cartilage was rough and required smoothing which was accomplished with a customized mean filter.

Mean filter: For each pixel (target point) of outer border, a window of size up to 20% of the number of pixels in the outer border is created. The window contains the target point and its neighboring pixels on the outer border. Then a mean of 'depth' for all pixels in this window is calculated. The depth of the target point is replaced with this mean value, and based upon this depth; a new inner pixel for the inner border is calculated. This process runs iteratively for all the points in the outer border and a smoother inner border of the cartilage surface is obtained.

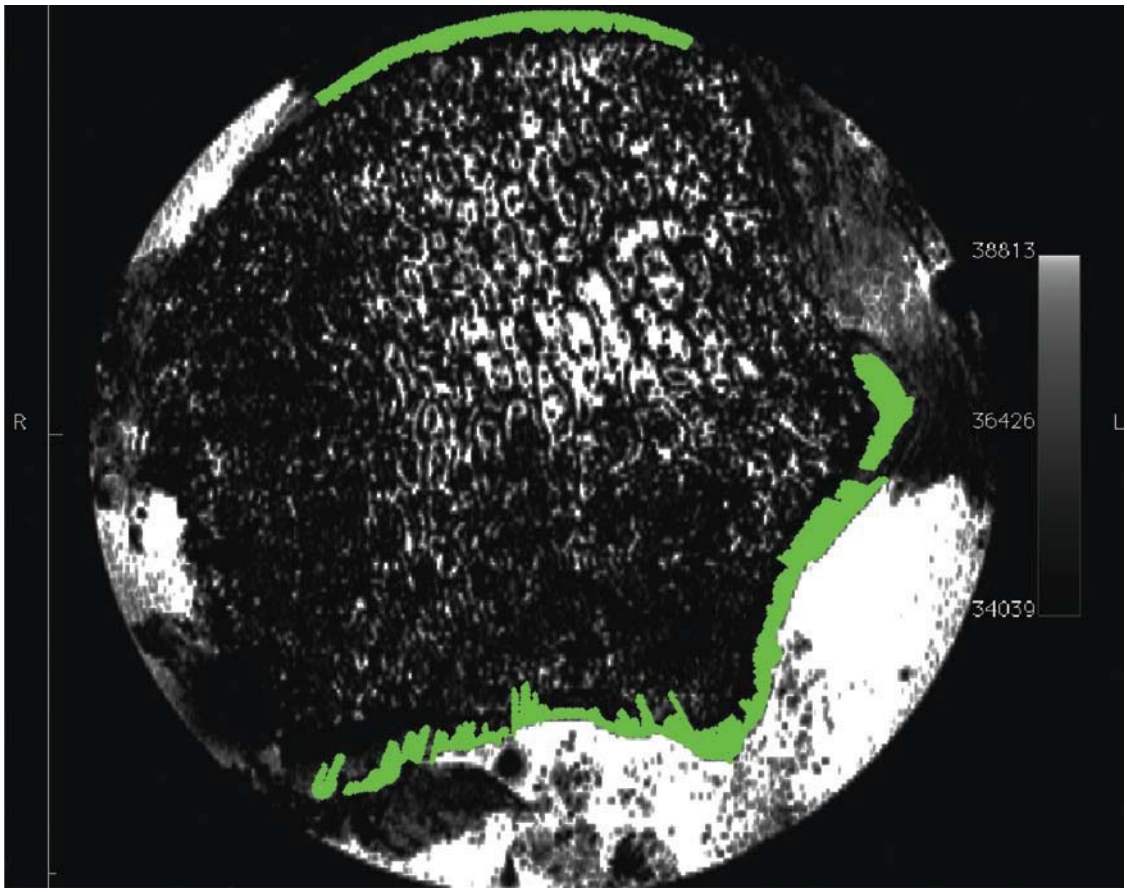


Figure 3-6: Cartilage segmentation with an ‘edge growing algorithm’.

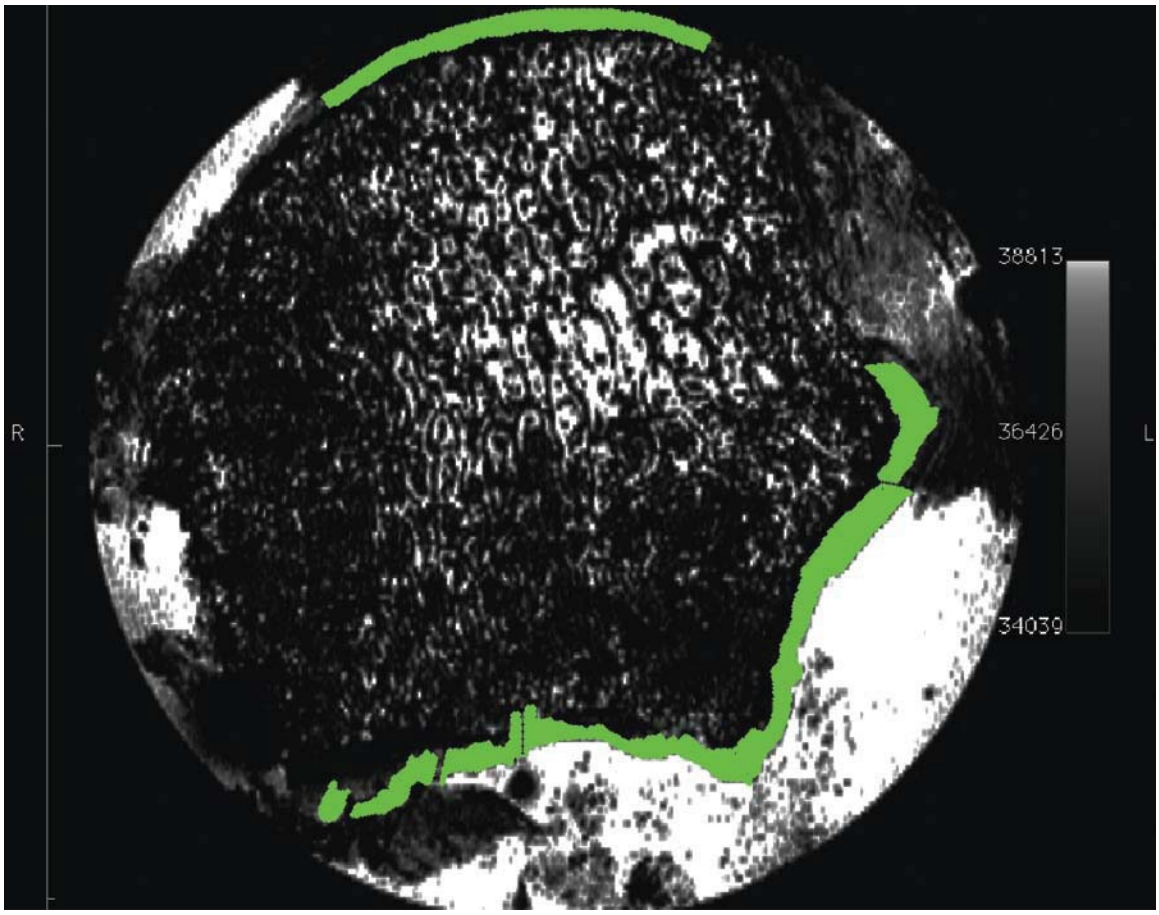


Figure 3-7: Cartilage region after mean filtering

### 3.2.2.2 Creating cartilage articular surface

The inner and the outer border of the cartilage from all the slices of the MTH1 image were stacked to form a three-dimensional inner shell and outer shell of cartilage, respectively. These shells were clusters of points which represented pixels of the image at the outer and inner borders of the cartilage. The upper part of the articular surface which articulates with the base of the 1$^{st}$ phalanx was extracted manually in Paraview 3.10 (Kitware, Inc. New York). A Taubin[70] smoothing filter (λ: 0.5 and μ: -0.53) was used for these 3-D shells to smooth their surfaces, and final surfaces for use in thickness

measurement was obtained (Figure 3-8 and 3-9). The outer shell of the cartilage layer in each specimen was aligned to the osteological articular surface of one of the template metatarsals, used in Chapter 2, using iterative closest point algorithm[40] (ICP). The rotations and translations obtained by ICP for the outer shell were then applied to transform the inner shell of cartilage.

### 3.2.2.3 Dividing the cartilage articular surface into six regions

A best fit sphere for the outer shell was obtained using an unconstrained optimization method. The outer shell of the cartilage was divided into six regions as shown in Figure 3-11. These six regions were based upon the previous study by Muehlman[44] in which the cartilage thickness was measured in different load bearing regions of MTH1. To divide the articular surface into six regions, the articular surface was projected into YZ plane and a rectangle in YZ plane with the dimension of the articular surface extension in YZ plane was created. This rectangle covered the projected articular surface points (for reference frame see Figure 2-2). This rectangle was then divided into six regions by a 3x3 grid. The points of the projected articular surface belonging to different regions were identified and then their corresponding points in the 3-D articular surface were identified. Similarly, the inner shell of the cartilage was also divided into six regions.

### 3.2.2.3 Calculating the cartilage thickness

For each region on the cartilage articular surface, rays were drawn from the center (O) of the best fit sphere (obtained in section 3.2.2.4) to each point (A) on the outer shell of cartilage. For each ray, the nearest point (B) on the inner shell of the cartilage was

identified and the distance between this nearest point (A) and the ray's point on the inner shell (B) was calculated as thickness of cartilage for that point (A) (Figure 3-10).

## 3.3 Results

The cartilage thickness mapping of MTH1 articular region was done at 6 regions on the surface of the articular cartilage shown in Figure 3-11. Median and median absolute deviation (MAD) of the cartilage thickness mapping in different regions for two specimens were calculated and are represented in Figure 3-12. The average of these median thicknesses from all the regions was 0.73±0.07 mm. The thickest cartilage was observed in region D (0.79 mm) and thinnest was observed in region E (0.59 mm). Table 3.1 shows the mean thickness of cartilage for each of six regions on the MTH1.

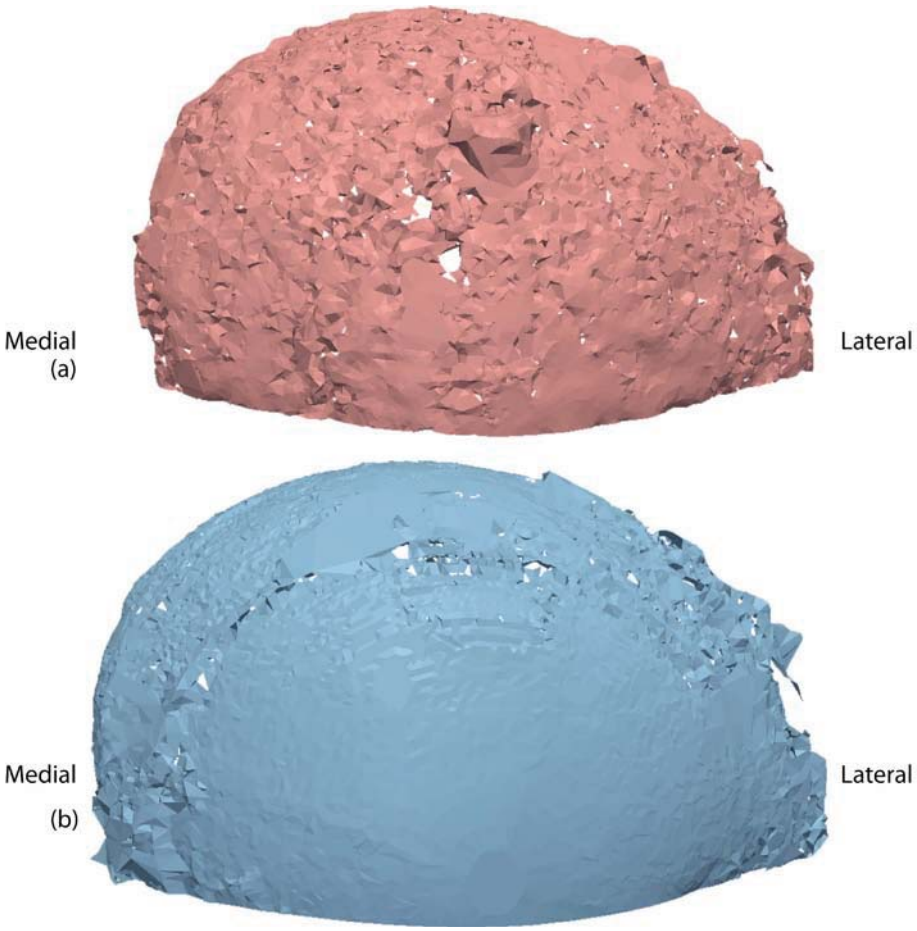


Figure 3-8: (a) anterior view of inner surface of cartilage shell. (b) anterior view of outer surface of cartilage shell. Note the smoothness of the outer shell compared to the inner shell

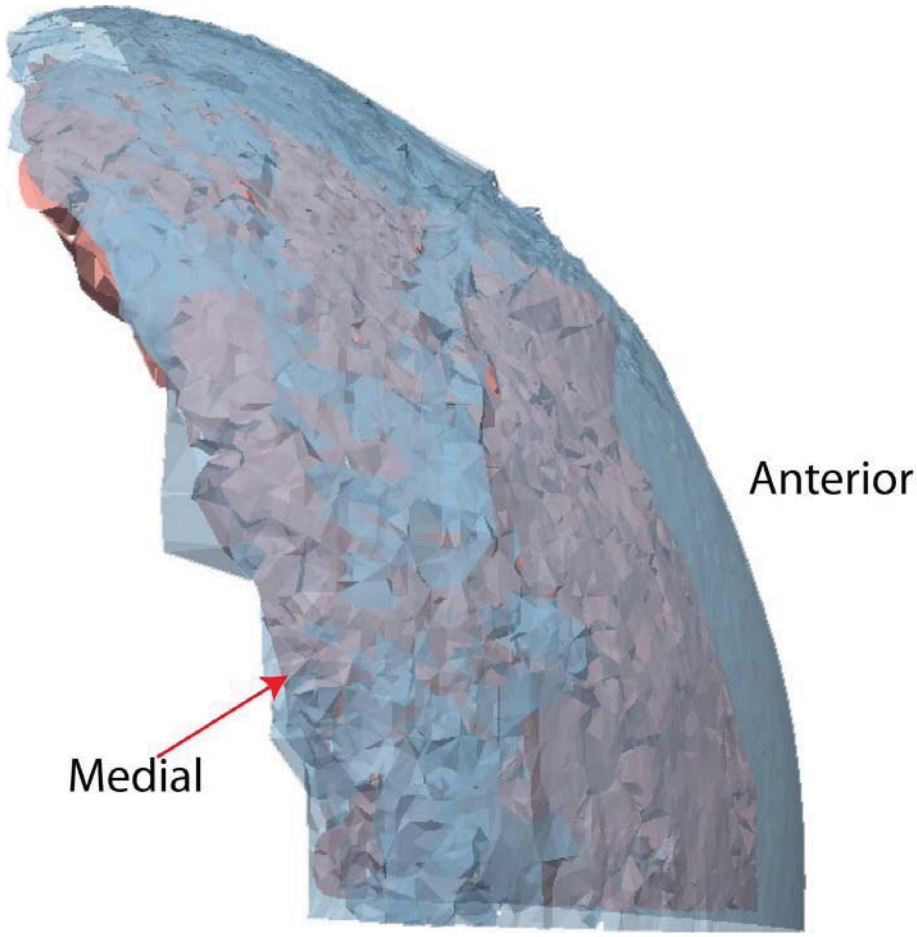


Figure 3-9: Inner and Outer cartilage shell

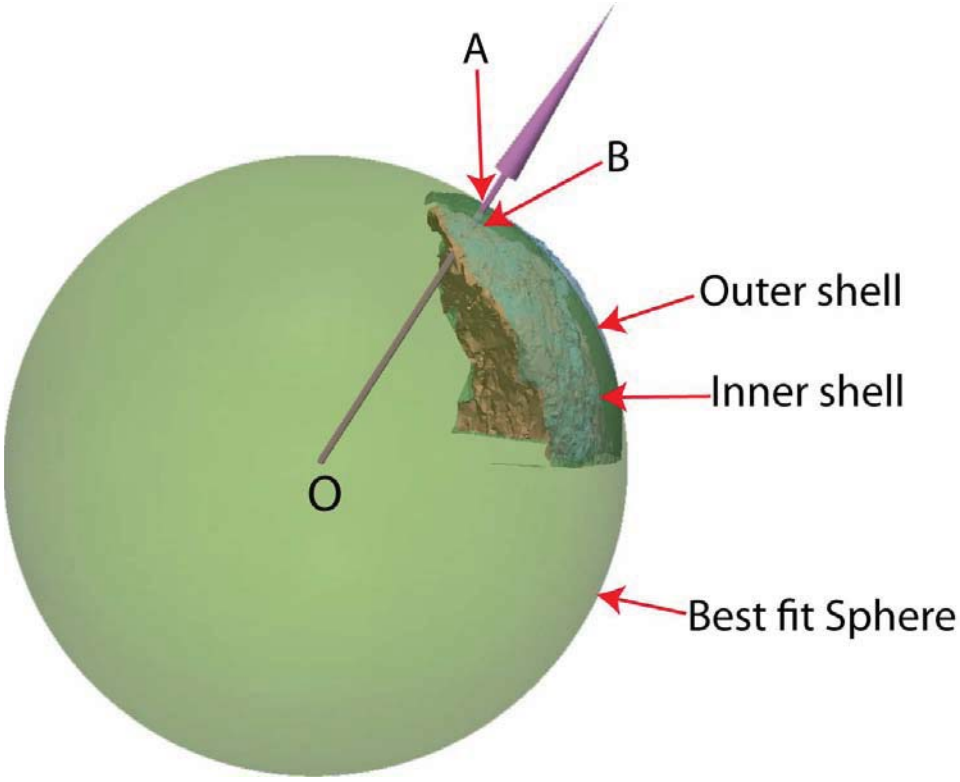


Figure 3-10: Ray from center (O) of the best fit sphere to a point (A) on outer shell of cartilage. B is the point on inner shell nearest to the ray OA.

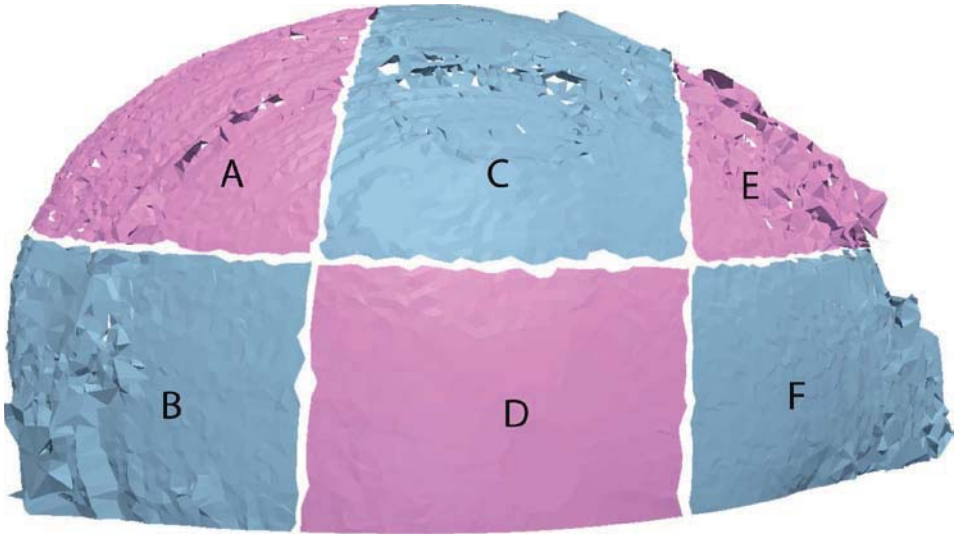


Figure 3-11: Articular surface of MTH1 divided into 6 regions A to F for cartilage thickness analysis.

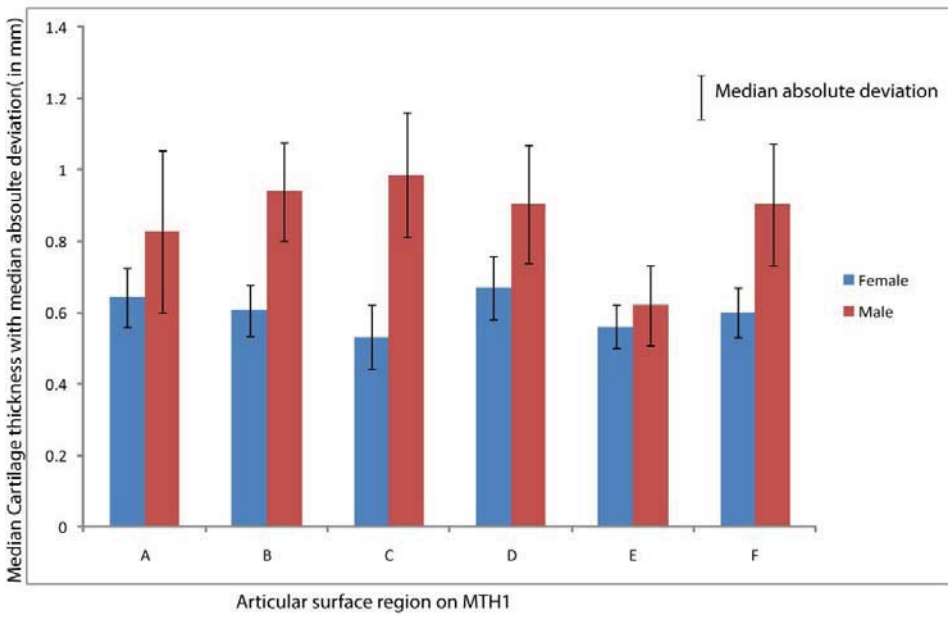


Figure 3-12: Bar chart for the median and median absolute deviation of thickness of cartilage on 6 regions of MTH1 for two specimens

Table 3-1: Mean (± standard deviation) thickness of the cartilage in six regions of the MTH1 upper articular surface.

| Region | A | B | C | D | E | F |
|---|---|---|---|---|---|---|
| Thickness(in mm) | 0.74±0.13 | 0.77±0.24 | 0.76±0.32 | 0.79±0.17 | 0.59±0.04 | 0.75±0.21 |

## 3.4 Discussion

A new method based upon 14T MRI imaging of MTH1 is presented to measure the distribution of cartilage thickness on MTH1. Cartilage was represented as a shell consisting of a point cluster in 3D space with inner and outer surfaces. The cartilage shell was divided into 6 regions and the distribution of the thickness at different regions was

compared. This technique enabled us to study thin (< 1mm) highly curved cartilage layers.

Few studies have reported the cartilage thickness distribution of the MTH1. Liu et al. [46] reported the MTH1 articular cartilage thickness in cadaveric specimen obtained with a creep indentation technique [46]. Muehlman et al. [44] also performed a cadaveric study in which samples were taken from 9 sites on the MTH1 and articular cartilage thickness was measured using microscopic evaluation.

Previous studies of cartilage thickness mapping used a large amount of manual measurement which is demanding in terms of labor and time. Previous studies were also destructive to the MTH1. In our present study, these difficulties were overcome using a unique semi-automated method of measuring articular cartilage thickness and of mapping the thickness. The median cartilage thickness varied from 0.59 to 0.79 mm in six regions of the MTH1. The following mean value for MTH1 cartilage thickness has been reported previously: 0.56 to 1.11 mm by Liu[46] using biphasic creep indentation technique and 0.75 to 1.35 mm by Muehlman[44] using microscopic evaluation. The thickness of cartilage measured in our study lies within the range of the thicknesses obtained in previous studies. The region D on MTH1 which showed the thickest cartilage, also agree with the study of Muehlman.

MRI has been explored to measure the cartilage thickness of different joints such as the knee [59], and hip [55,61], but it has not previously been explored to measure the MTH1 cartilage thickness. To the best of our knowledge, no published studies regarding evaluation of articular cartilage thickness have used 14T MRI. 14T MRI acquires a very

high resolution image, and in this study a resolution of up to 0.04mm per pixel was achieved. This technique can be ideal for measuring cartilage thickness in sub-millimeter range.

There are a number of potential limitations in the present study. First, to establish a reliable average thickness of cartilage of general population, a greater number of samples are required. Second, because of very low difference between the grayscale values of the cartilage and the subchondral bone, it was very difficult to obtain a smooth inner shell of cartilage. Smoothing of the data of inner shell was performed and this may have led to loss of data of the cartilage shell and subsequent errors in the estimation of cartilage thickness. Third, since this method is a threshold-based technique, the thickness of the cartilage obtained may vary with the threshold of intensity selected for identifying the cartilage region. The sensitivity of the method with the change in the threshold will be studied in future work.

There are several potential advantages of this new technique for thickness mapping. First, the consideration of cartilage thickness mapping will give a better estimation of the contour of the MTH1 which may help in better designing MTH1 implants used for arthroplasty of the MTPJ1. Second, in the computational biomechanical assessment of the MTPJ1 using a finite element model, the incorporation of an inhomogeneous cartilage thickness distribution may result in more precise estimated of the actual stress distribution around the articular cartilage [71] [72]. Third, the technique developed for segmentation of cartilage from MRI images can be applied to segment the cartilage from MRI of other joints such as the knee, ankle or wrist. The conventional intensity-based image segmentation methods, such as thresholding and region growing,

could not segment the cartilage region from the image, so this customized semi-automated cartilage was implemented by the author. Fourth, 14T MRI can be explored to study the cartilage thickness mapping on other bones such as the rest of the metatarsal bones [73] and wrist[74] which also likely have sub-millimeter cartilage thicknesses. Fifth, the complete technique can be used for measurement of the volume of cartilage on the joints. The volume of cartilage is known to correlate with the radiographic grade of osteoarthritis [75] .

## 3.5 Conclusion and Future work

A semi-automated method for cartilage segmentation and a method for cartilage thickness mapping have been presented. Although the results need further validation with a greater number of specimens, the method is suitable for application to other joints for the measurement of cartilage thickness. The point-to-point correspondence of the subchondral bone surface and the cartilage thickness mapping will be done so that the thickness mapping can be placed properly on the MTH1 to create an appropriate model of bone. The effect of placing a cartilage thickness map on the geometry of the implant used for the MTPJ1 arthroplasty will be studied.

## 3.6 Acknowledgments

We appreciate the cooperation of Donghoon Lee from Department of Radiology at University of Washington; and Institute of Simulation and Inter-professional Studies, University of Washington, Seattle.

# CHAPTER IV

# EFFECT OF CARTILAGE THICKNESS ON DESIGN OF AN IMPLANT FOR FIRST METATARSOPHALANGEAL JOINT HEMIARTHROPLASTY

[1,2]Atul Kumar, [1]Peter R. Cavanagh

[1]Department of Orthopaedics and Sports Medicine, University of Washington, Seattle, WA, USA
[2]Chemical and Biomedical Engineering Department, Cleveland State University, Cleveland, OH, USA

## ABSTRACT

In the normal first metatarsophalangeal joint (MTPJ1), the first metatarsal head (MTH1) has articular cartilage which forms the MTPJ1 with the proximal phalanx. The implant for a MTPJ1 hemi-arthroplasty should be congruent to the contour of the articular cartilage for better fitting to the phalanx. The current study investigates the effect on the geometry of the implant for MTPJ1 hemi-arthroplasty when the thickness of cartilage on the MTH1 is considered. The three-dimensional surfaces of 97 metatarsal

osteological specimens were obtained with a laser scanner. The segment of the MTH1 articular surface which articulates with proximal phalanx was divided into six regions. The thickness profile of the cartilage covering the subchondral bone of MTH1 was obtained from two cadaver feet using MRI imaging and numerical analysis. This thickness profile was placed over the articular surface of the each of the osteological specimens to create a cartilage surface for each specimen. The created cartilage surface and the articular surface on the osteological specimen of MTH1 were divided into three size groups, for male and female separately and a best fit ellipsoid for each of the groups was obtained. The ellipsoid parameters obtained for the articular surface of MTH1, with and without cartilage were compared. A paired t-test showed no significant difference between the parameters of ellipsoid in the two conditions ($p = 0.05$).

## 4.1 Introduction

In the normal first metatarsophalangeal joint, the first metatarsal head (MTH1) has articular cartilage which forms the MTPJ1 with the adjoining structures. An implant placed over MTH1 for hemiarthroplasty should therefore be congruent with the contour of the cartilage. In the previous chapter the shape of the implant based upon the contour of the subchondral bone (MTH1 of osteological specimens) was developed and the thickness of cartilage on MTH1 was measured using 14T MRI. The current study investigates the effect of cartilage thickness on the shape of the implant for MTPJ1 hemiarthroplasty. For other joints such as the spine[71], it has been shown that cartilage thickness distribution affects the results from computational models. The design of implants for joints such as the humerus[76] has also been based upon the geometry of articular cartilage. To the best of our knowledge, the effect of cartilage thickness on the design of an implant has not been explored for MTPJ1. This study will help in deciding if consideration of the cartilage thickness is significant in designing the hemi-arthroplasty implant.

## 4.2 Method

The metatarsal osteological specimens used in Chapter 2 and the MTH1 MRI scans used in Chapter 3 are further used in this chapter. A total of 97 three-dimensional surfaces of the osteological specimens of the first metatarsal were used in the analysis (48 male and 49 female sets, age range: 30-50 yrs: mean age 39.5±5.69 yrs and 37.0±5.32 yrs for males and females respectively, body weight: 130.2 ± 12.29 lb and 127.0± 15.89 lb for males and females respectively). MRI images of MTPJ1 specimen from two cadavers (75 year-old female and 77 year-old male) were acquired with 14T MRI scanner (Bruker,

Karlsruhe, Germany) (Figure 3-1) using turbo spin echo pulse sequence (Appendix B) and a voxel size of 0.05 x 0.05 x 0.10 $mm^3$ (for the specimen from 75 year female) and 0.04 x 0.04 x 0.04 $mm^3$ (for the specimen from 77 year male). Field of view was 25x 25 x 25$mm^3$ (for the specimen from a 75 year female) and 20 x 20 x 20 $mm^3$ (for the specimen from a 77 year female).

Surface data of thee metatarsal osteological specimen were aligned to a common reference frame using a two-stage process, initial alignment and secondary alignment, as it was done in Chapter 2 (see page 17-20). Results of the initial alignment and the secondary alignment are shown in Figure 4-1 and 4-2, respectively. The osteological dataset was divided into three size groups of small, medium and large as was done in Chapter 2 (see page 26), for males and females separately.

The articular surface on the MTH1 which articulates with the phalanx was extracted using the rotating plane and curve fitting technique described in Chapter 2 (see page 20-24). The results of the surfaces are shown in Figure 4-3A. For each individual articular surface, a best fit sphere was obtained using an unconstrained nonlinear optimization method in Matlab to vary the four degrees of freedom (radius of the sphere, and the three-dimensional location of the centroid). The shortest Euclidean distance from each point on the sphere surface to the articular surface was measured and minimization of the sum of these distances was used as the cost function for optimization.

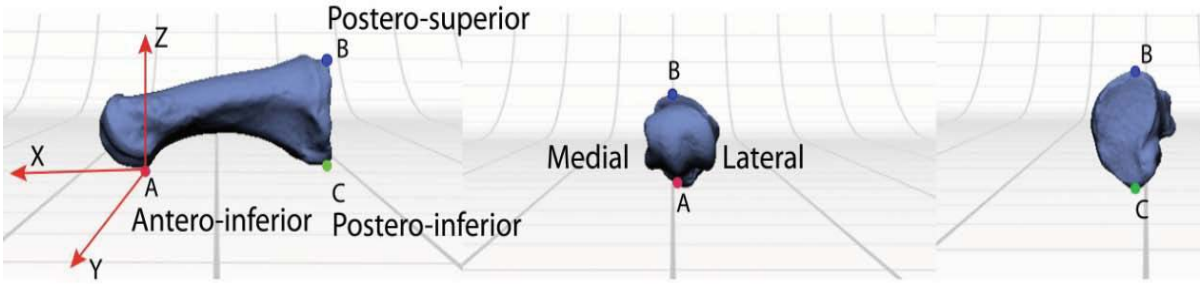


Figure 4-1 : Lateral (A), anterior (B), and posterior (C) scans of a typical 1st metatarsal bone. Anatomical axes and landmarks used for initial alignment are shown

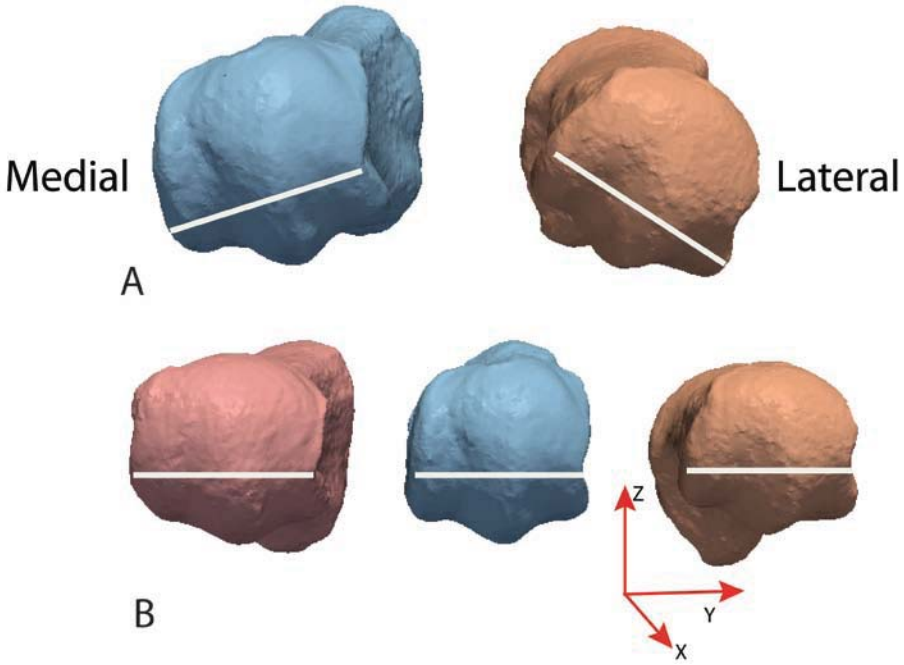


Figure 4-2: Alignment of target bone (blue) with template bone after secondary alignment.

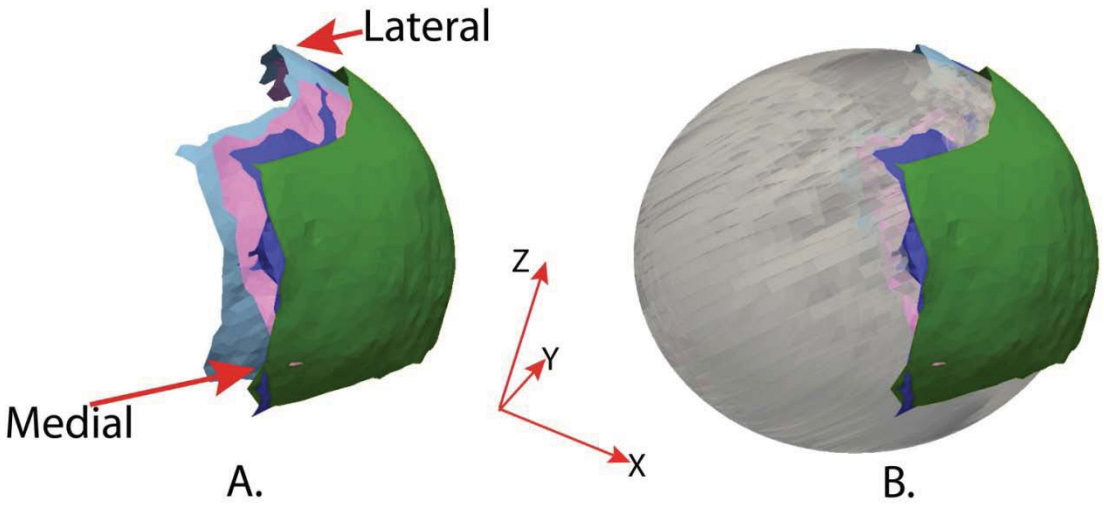


Figure 4-3: A. A set of superior articular patches from the female medium group. B. The same patches, shown in Figure 2-6A , with the best fit ellipsoid for the female medium group.

### 4.2.1 Dividing the osteological articular surface into six regions

Each of the 97 osteological articular surfaces was divided into six regions as shown in Figure 4-2. To divide the articular surface into six regions, the surface was projected into the YZ plane and a rectangle in this plane was created with the dimensions of the bounding box to the surface (for reference frame see Figure 4-2). This rectangle was then divided into six regions by a 3x3 grid. The points of the projected articular surface belonging to different regions were identified and then their corresponding points in the 3D articular surface were also identified Figure 4-4 and 4-5.

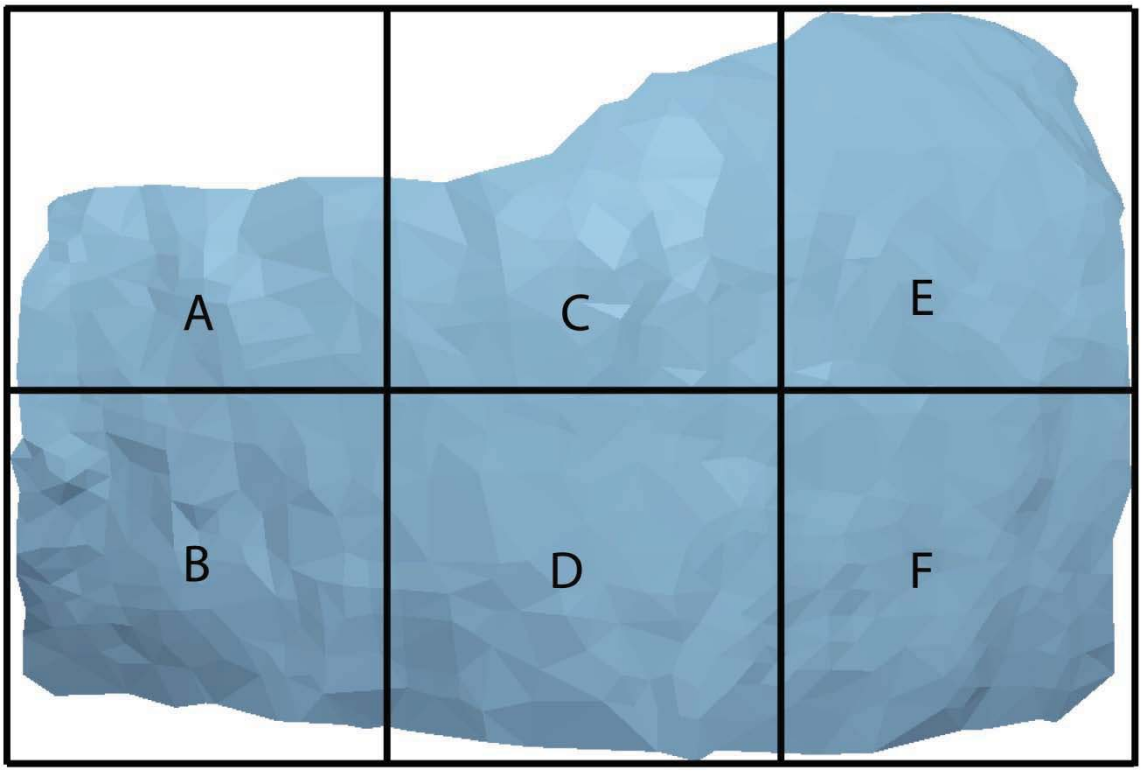


Figure 4-4: Grid to divide the articular surface into six regions.

### 4.2.2 Creating a cartilage surface for osteological specimens

For each region of an osteological articular surface, unit vectors in the direction of the center of a best fit sphere to every point on the region were calculated and the tail of unit vectors were placed over their respective points on the osteological articular surface. The average thickness of cartilage for each of the region was obtained as described in Chapter 3. The unit vectors, placed on the osteological articular surface, were multiplied by the average cartilage thickness of the respective region. The cluster of points formed by the head of the resultant vectors created a surface which simulates the outline of cartilage on the osteological articular surface. A Laplacian flow filter[77] was used for smoothing the cartilage outline surface to remove the sharp change in the topography of

the cartilage outline at the transitional point of two different regions on the articular surface (Figure 4-5).

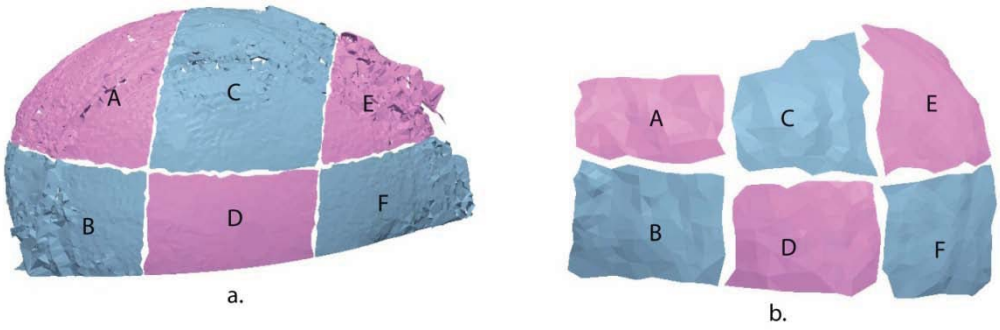


Figure 4-6: A. Six regions on the cartilage outer shell surface. B. Six regions on the articular surface of 0228 osteological specimen surface.

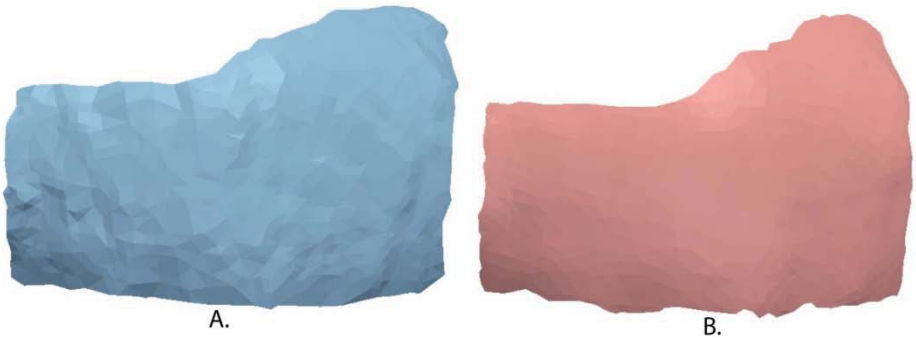


Figure 4-7: A. Articular surface of osteological specimen number 0228 B. Articular surface of cartilage shell created for osteological specimen 0228

The cartilage articulating surfaces were divided into three size groups, for male and female separately, using the classification of bones done in Chapter 2. The cartilage surfaces obtained for each size group were compiled into a single data file. A best fit

ellipsoid was then obtained for these data points using non-linear unconstrained optimization as it was done in Chapter 2 (see page 26). .

## 4.3 Results:

The parameters for the ellipsoid were obtained for the articular patch with cartilage (Table 4-1). The comparison of their semi-axes with the ellipsoids obtained without cartilage, are presented in the Figure (4-7a -4-7c).

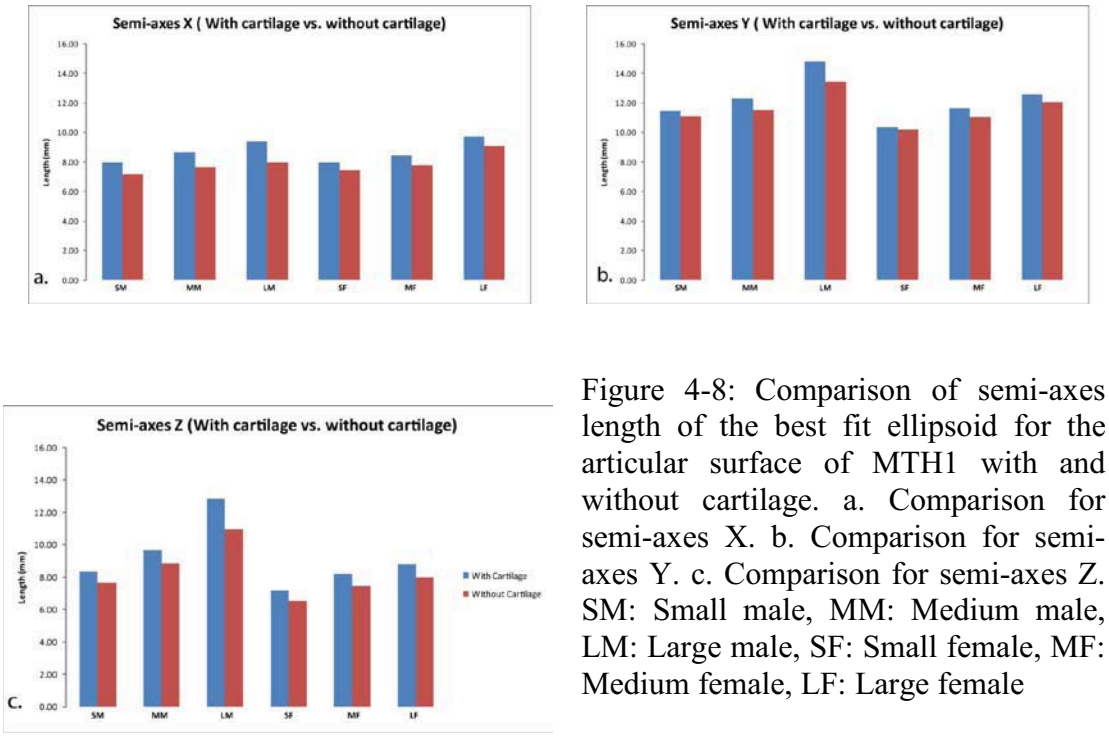


Figure 4-8: Comparison of semi-axes length of the best fit ellipsoid for the articular surface of MTH1 with and without cartilage. a. Comparison for semi-axes X. b. Comparison for semi-axes Y. c. Comparison for semi-axes Z. SM: Small male, MM: Medium male, LM: Large male, SF: Small female, MF: Medium female, LF: Large female

Table 4-1: Ellipsoid parameters for the MTH1 articular surface with and without consideration of cartilage.

W: With cartilage, WO: Without cartilage, X: Semi-axis X, Y: Semi-axis Y, Z: Semi-axis Z, Error: Root mean square error (X,Y,Z and Error are in millimeter); Yaw, Pitch and Roll are in degrees.

| | X | | Y | | Z | | Yaw | | Pitch | | Roll | | Error | |
|---|---|---|---|---|---|---|---|---|---|---|---|---|---|---|
| | W | WO | W | WO | W | WO | W | WO | W | WO | W | WO | W | WO |
| MALE | | | | | | | | | | | | | | |
| Small (n=9) | 7.94 | 7.17 | 11.47 | 11.08 | 8.32 | 7.62 | 2.48 | 2.39 | 0.27 | -0.5 | 1.55 | 2.03 | 0.77 | 0.77 |
| Medium (n=32) | 8.64 | 7.62 | 12.27 | 11.51 | 9.64 | 8.83 | 0.4 | -3.7 | 0.01 | 0.33 | 0.42 | 3.03 | 0.7 | 0.69 |
| Large (n=8) | 9.38 | 7.97 | 14.83 | 13.44 | 12.81 | 10.95 | -1.04 | -2.5 | 8.96 | 1.89 | 2.23 | 6.55 | 0.8 | 0.77 |
| FEMALE | | | | | | | | | | | | | | |
| Small (n=6) | 7.95 | 7.44 | 10.37 | 10.16 | 7.19 | 6.51 | 2.4 | 5.12 | -0.43 | 5.52 | 1.63 | 5.69 | 0.39 | 0.39 |
| Medium (n=34) | 8.41 | 7.76 | 11.63 | 11.06 | 8.18 | 7.45 | 1.54 | 3.7 | 50.87 | 49.8 | 12.75 | 9.26 | 0.47 | 0.46 |
| | 9.72 | 9.06 | 12.55 | 12.07 | 8.8 | 7.94 | -0.43 | 2.58 | 2.36 | 8.3 | -0.18 | 1.96 | 0.65 | 0.65 |

Paired t-test for the measurement of these axes length did not show significant difference between the semi-axes of ellipsoids obtained for articular surface with cartilage and without cartilage ($p=0.05$).

## 4.4 Discussion

In this study, the effect of cartilage thickness on the design of the MTH1 arthroplasty implant was investigated. The cartilage shells were obtained as 3-D point surfaces. The thickness at each point of the surface of the outer shell and the distance vectors (thickness vectors) from each point on the outer shell to the inner shell were obtained from previous studies. These thickness vectors were placed over the MTH1 osteological specimen articular surfaces to create a cartilage surface outline. The surfaces of cartilage outline were grouped into different sizes. Best fit ellipsoids were obtained for each group and the ellipsoid parameters were compared with the result of ellipsoids obtained for articular surfaces of the osteological specimens. Although, there was no significant difference between the ellipsoid parameters ($p>0.05$) this result is not conclusive because only two specimens were studied and the cartilage thickness was not scaled for metatarsal bones of different sizes. This result needs to be investigated further.

The success of an implant highly depends upon the congruity of MTH1 to the base of 1$^{st}$ phalanx. In a normal state, it is the cartilage on MTH1 which forms the articulating surface for the base of 1$^{st}$ phalanx. So, an implant based upon the geometry of the cartilage would likely be more congruent to the base of 1$^{st}$ phalanx. Since the cartilage thickness on MTH1 is in sub-millimeter range, the curvature of the MTH1 osteological specimen may not change significantly when the cartilage thickness profile is considered in designing the implant.

For other joints such as the spine[71], it has been shown that cartilage thickness distribution does affect the computational model, where the mean thickness of cartilage was between 0.49 to 0.61 mm on different cervical vertebrae. There have been studies which design the implants for joints such as the humerus[76] based upon the geometry of cartilage. To our knowledge, there has been no study which investigated the effect on the geometry of implant design due to thickness of cartilage.

There are potential limitations in the present study. First, to establish a reliable average thickness of cartilage of the general population, more samples are required. Second, the cartilage inner shell used in this work, for obtaining the cartilage thickness profile, was not very smooth because of unclear demarcation between the cartilage and the subchondral bone, and the noise in the MRI images. Third, to fit the MTH1 inside the MRI scanner, the articular surface was trimmed, so the complete cartilage thickness profile was not available.

The method used in the current study can be used to study any other joints which need hemi-arthroplasty to find the changes in the design of implant due to cartilage.

## 4.5 Conclusion and future work:

The current study investigated the effect of cartilage thickness on the design of a first metatarsophalangeal joint hemiarthroplasty implant. The method of investigation helps in understanding the design of the implant. A study with more cartilage thickness data is needed before a final implant design is proposed.

## 4.6 Acknowledgment

We appreciate the cooperation of Dr. Yohannes Haile-Selassie, Curator of

Physical Anthropology at the Cleveland Museum of Natural History; Institute of Simulation and Interprofessional Studies; and Donghoon Lee from Department of Radiology, at University of Washington, Seattle.

# CHAPTER V

# DISCUSSION AND CONCLUSION

## 5.1 Summary

The current study investigated the surface characteristics, the cartilage thickness, and the design of an implant for the MTH1. The method included the use of a laser scanner, 14 Tesla MRI image, and the concept of optimization, computational geometry and image processing.

In the first part of the study, an implant was designed based upon the morphology of MTH1 from the surface of osteological specimens of the first metatarsal. The process for designing the MTH1 hemiarthroplasty implant uses MTH1 articular surface parameterization with an optimal fit ellipsoid. The anatomical congruence of the ellipsoid based implants to the MTH1 was excellent with the mean RMS error of fit was between 0.29-0.42mm. An ellipsoid was chosen for this study because it has nine degrees of

freedom and thus allows for more customization of the articular surface. Besides, an ellipsoid can be easily parameterized to define the implant surface.

In the current study 14T MRI images were used for calculating the MTH1 articular cartilage thickness profile. The cartilage layer was represented as a shell with outer and inner cartilage outlines which consisted of a point cluster in 3-D space. The thickness of cartilage calculated in our study lies within the range of the thickness obtained in previous studies using different methods. The region on MTH1 which showed the thickest cartilage, also matches with a previous study of the thickness measurement of cartilage.

In the last part of the study, the effect of cartilage thickness on the design of an MTH1 arthroplasty implant was investigated. Best fit ellipsoid parameters for the articular surface of the MTH1, with and without consideration of MTH1 cartilage, were obtained. Although, there was no significant difference between the ellipsoid parameters, this result is not conclusive because of only two specimens were studied and the cartilage thickness was not scaled for metatarsal bones of different sizes. This result need to be investigated further.

## 5.2 Contributions

Three dimensional surface data of the first metatarsal osteological specimens and the MRI image of the MTH1 with 14T MRI provide a detailed view of the geometry of MTH1. The set of 48 female and 49 male first metatarsal osteological surface data obtained has the potential to provide insight into the surface characteristics of the first metatarsal and was used in this study for the characterization of the articular surface of MTH1.

A new method for automatic extraction of the articular surface from the entire distal surface of bone was applied for obtaining the articular surface of MTH1. This can be applied with appropriate modification to other bones such as the lesser metatarsal bones and the proximal surface of the humerus for the automatic extraction of articulating surfaces.

A new method for the sizing of the MTH1 bones was developed. This classification method used measurements which can be taken clinically on the lateral and dorsi-plantar view of MTH1 x-ray images. These measurements predict the curvature of the articular surface of MTH1 and predict the size of implant which should be used in individual patients. This method of classification may have wide applications for other joints like other metatarsophalangeal joints, the metacarpophalangeal joints, and the shoulder.

The measurement of thickness of cartilage of MTH1 involved segmentation of the cartilage from MRI images. This segmentation method involved the application of two algorithms which have not been used previously in the MTPJ1 context; 'edge walking' and 'edge growing' algorithms. The edge walking algorithm can be used to select the required edge in a binary edge image of any grayscale image. The edge growing algorithm was able to segment a cartilage region in the MRI image where simple region growing and thresholding methods failed. Region growing and thresholding did not work because of the very low difference in intensity between the region of interest and that of its surrounding region in the image. This edge growing algorithm can be applied to segment a region of interest in images similar to the cartilage image used in the current study. The overall technique developed for segmentation of cartilage from MRI images

can be applied to segment the cartilage from an MRI of other joints such as the knee, ankle or wrist.

This was the first study to make measurements from high resolution MRI for cartilage thickness of the MTH1. The previous methods used for such measurements were subject to error and lack of reproducibility, and these problems have been addressed with the semi-automated method for thickness measurement in the current study.

The 14T MRI was used for image acquisition which provides a resolution of 0.04-0.05mm per pixel. This technique is ideal for measuring cartilage thickness in the sub-millimeter range of other bones such as the lesser metatarsal bones [73] and the bones of the wrist and hand[74] .

## 5.3 Limitations and Suggestions for Future Work

Although the total number of first metatarsal osteological specimens examined was 97 specimens, the numbers of specimens in some size groups were relatively small. Further work with a larger number of specimens is required for definitive comparison of structural characteristics of the male and female first metatarsal. There is a possibility of subjective error in the alignment of the multiple scans while creating a single surface of the first metatarsal obtained from laser scanner from different angles of view. The rules used to extract articular surface of MTH1 did not work for a few specimens and manual selection was required. More robust rules for the extraction of those surfaces are required.

Only two specimens were used in the current study of cartilage thickness. To establish a more representative thickness profile of cartilage in the general population, a greater number of samples are obviously required. In the method of identifying the

cartilage region and creating the cartilage shell, smoothing of the data was done which may lead to loss of data of the cartilage shell and affect the measurement of thickness profile. The cartilage segmentation method was a threshold-based technique so the thickness of the cartilage obtained may vary with the threshold of intensity selected for identifying the cartilage region. The sensitivity of the method with the change in the threshold should be subjected to more study in the future.

Another possible approach is the creation of a statistical shape model using principal component analysis (PCA). PCA of the metatarsals could allow a more detailed study of the sexual dimorphism of the first metatarsal. This study will help in deciding if the sexual dimorphism is significant for the first metatarsal and how it can affect the design of an implant.

The implant created with the current work should be functionally evaluated using the finite element method and robotics study[78]. The virtual surgery toolbox, developed by Tadepali et al.[79] could be used to replace the articular surface of MTH1 with the implant surface and then the MTH1 could be included in a finite element model of first ray such as that developed by Budhabhatti et al[80]. This finite element model would allow an examination of the range of motion of MTPJ1 and failure criteria of the implant surface. This study could be supported by an investigation of MTPJ1 joint kinematics after hemi-arthroplasty of a cadaver foot, with the help of robot. The kinematics and failure criteria analysis of the implant designed in this study could be compared with other implants currently available for MTPJ1 hemiarthroplasty.

## 5.4 Conclusion

The method developed here creates an implant based upon the morphology of MTH1 which has excellent fit to the native MTH1. An implant which is anatomically more congruent to the MTH1 will give a better fit to the articulating phalanx with improved kinematics of MTPJ1 after hemiarthroplasty. This method can also be applied to study the surface characteristics of other joints which need hemiarthroplasty such as the shoulder and knee.

To our knowledge, the current study is the first to identify a quantitative approach to the design of a MTPJ1 hemi-arthroplasty implant. Although, the sample size of data was not sufficiently large to generalize the design for the general population, it defines the method which can be used for a more extensive study in the future.

# Appendix A: Three dimensional surface data acquisition with laser scanner

*Instrument set up for laser scanning*: The metatarsal and phalanx osteological specimens were scanned with Next Engine (Santa Monica, CA) laser scanner to obtain the three-dimensional surface data of osteological specimens. The following steps were followed to obtain the surface data.

1. The scanner (shown in Figure A-1) was connected to the computer and ScanStudio™ (Santa Monica, CA) software was started in the computer.
2. Pencil markings were placed on the surface of osteological specimens (shown in Figure A-2)
3. Osteological specimen was placed, with the help of a stand, on the rotating platform attached with the scanner.
4. Parameters for scanning were set in the scan studio software (Figure A-3). These parameters included total angle of rotation of the platform, required density of points on the surface data, brightness of the object and the distance between the platform and the scanner.
5. Scanning was started and the specimen gets scanned from different angles to obtain surface data from different views.
6. Surfaces from different views were aligned with the help of markings on the specimen and a 3D surface of the specimen was created in ScanStudio™.

7. All the surfaces were fused to obtain a single surface of the specimen. A typical final surface is shown in Figure A-2 and A-4.

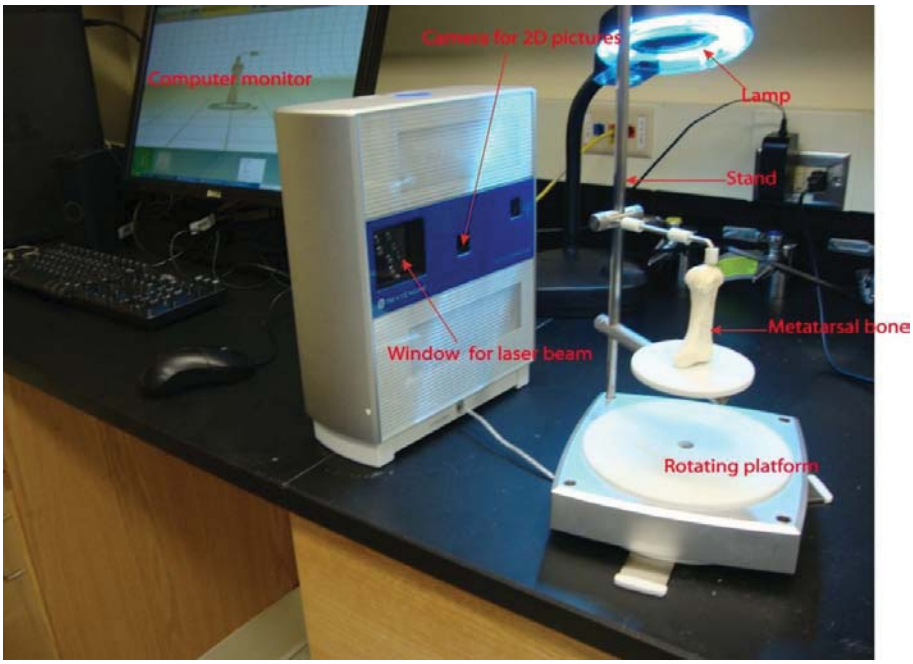


Figure A- 1: Set up for scanning bones with the laser scanner.

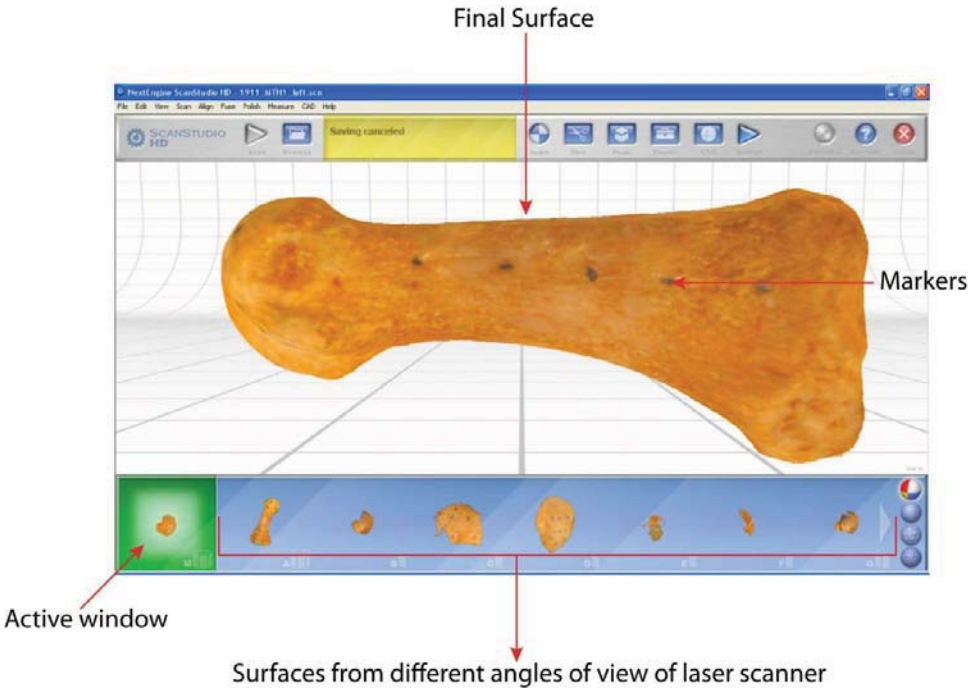


Figure A- 2: Metatarsal surface created in scan studio (Resolution during acquisition was 400 dots per square inch).

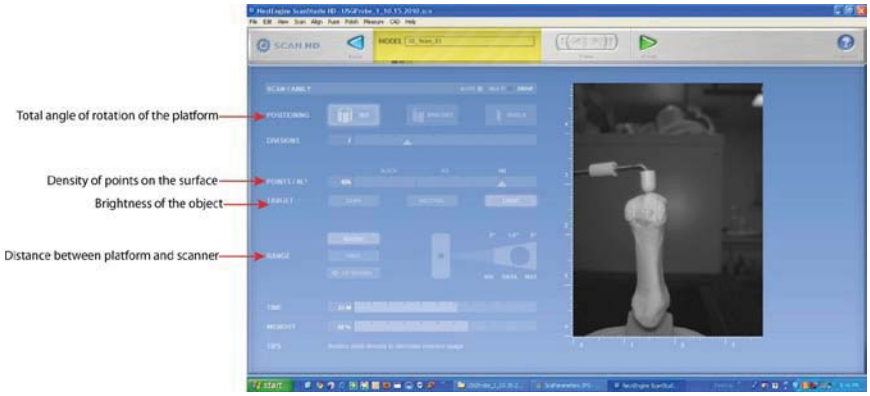


Figure A- 3: Parameter set-up for scanning the surface of osteological specimens

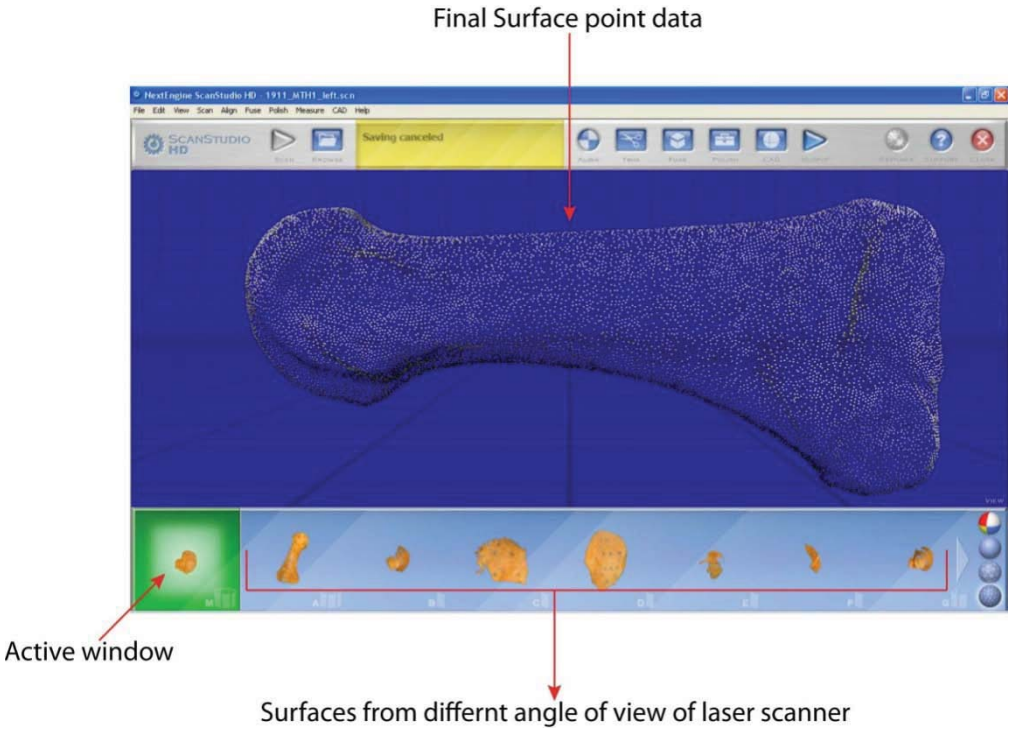


Figure A- 4: Metatarsal surface shown as point data

*Principles of laser scanner*:

A laser scanner uses laser light to measure distances from the laser sensor to the object in a systematic pattern[81].

The 3D laser scanner used in the current work is a triangulation 3D laser scanner. Triangulation scanners shine a laser on the object and use a camera to look for the location of the laser dot. The distance of the surface from the laser source determines the location of the laser dot in the camera's field of view. This technique is called triangulation because the laser source, the camera and the laser dot form a triangle (Figure A-5).

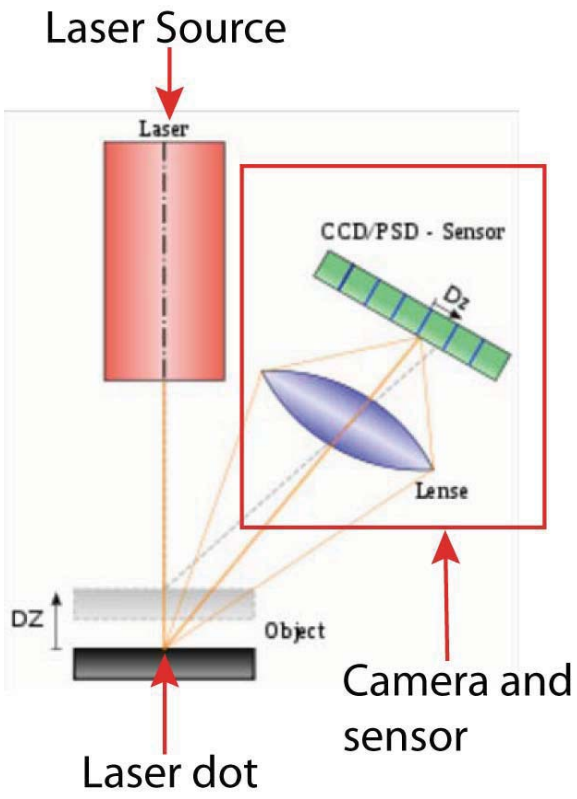


Figure A- 5: Triangulation laser.
Source: http://en.wikipedia.org/wiki/File:Laserprofilometer_EN.svg

Since the distance between the camera and the laser emitter and the angle of the laser source corner are known, the angle of the camera corner is determined by looking at the location of the laser dot in the camera's field of view. This information determines the shape and size of the triangle and gives the location of the laser dot corner of the triangle. In the NextEngine scanner a laser stripe instead of a single laser dot is swept across the object to expedite the acquisition process.

# Appendix B: Magnetic Resonance Imaging and Turbo Spin Echo sequence

MRI basic principles: Magnetic resonance imaging[82] (MRI) is a medical imaging technique used to visualize the detailed internal structures of human body. MRI uses the property of nuclear magnetic resonance of nuclei of atoms inside the body to create images. An MRI machine uses a strong magnetic field to align the magnetization of some of atoms (mainly hydrogen) in the body, and radio frequency to systematically alter the orientation of this magnetization. This causes the nuclei of atoms to produce a rotating magnetic field which is detected by the receiver embedded in the scanner. This information on the rotating magnetic field is recorded to construct the images. The 3-D spatial information of the image is obtained by providing magnetic field gradients in each direction.

Obtaining an MR Imaging Signal: The human body is composed largely of water molecules and each molecule has two hydrogen nuclei or protons. Inside the strong magnetic field of the MRI scanner the magnetic moments of these protons change from their resting states and align with the direction of the magnetic field which creates a 'net magnetization vector' along the magnetic field. A radio frequency transmitter, which is briefly turned on, produces a further varying electromagnetic field. The photons of this field have a resonance frequency which is absorbed by the protons and the photons flip the spin of the aligned protons of the body. The radio frequency transmitter is then turned off, which causes the protons to revert back to the original lower-energy spin-down state

and the magnitude of magnetization decays. The difference in the energy is released as a photon, and the released photons are received by the signal detector in the scanner.

Turbo spin echo: Turbo spin echo (TSE) is technique in which multiple radio frequency (RF) pulses, which cause a flip angle of 180º of the net magnetization vector, are used to continually refocus the decaying magnetization (Figure B-1). In this way, multiple MRI signals may be recorded from each excitation pulse. In the current study the repetition time (TR) and were 1500 millisecond and 51 millisecond respectively.

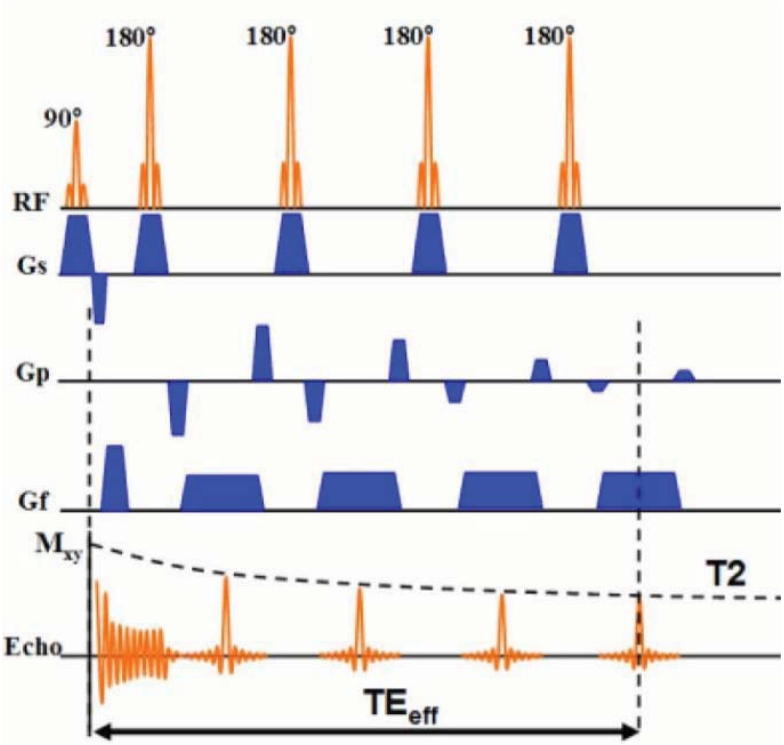


Figure B- 2: Turbo spine echo pulse; RF= radio frequency, Gs: Slice selection gradient; Gp: Phase encoding gradient; Gf: Frequency encoding gradient; Mz: Magnitude of the magnetization of the protons; TE: Echo time which represents the time between the 90 degree pulse and the peak of the echo signal; T2: The time constant of the magnetization decay. Source: http://www.revisemri.com/questions/pulse_sequences/tse

# Appendix C: Delaunay Triangulation

For a set P of points in the plane, a Delaunay triangulation[68] is a triangulation DT (P) such that no point in P is inside the circumcircle of any triangle in DT (P) (FigureC-1). A Delaunay triangle minimizes the angles of all the triangles in the triangulation. By considering a circumscribed sphere, the concept of Delaunay triangulation is extended to three and higher dimensions. In the current study Delaunay triangulation in two and three dimensions were used. The Delaunay triangulation was invented by Boris Delaunay in 1943.

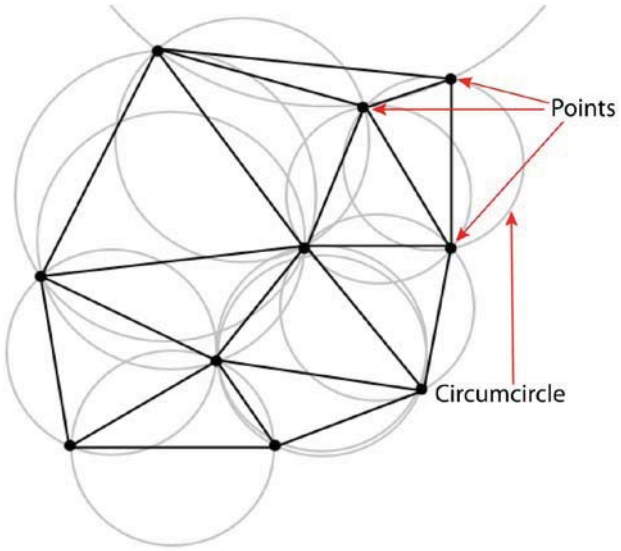


Figure C-1: A Delaunay triangulation in plane shown with circumcircle Source:http://upload.wikimedia.org/wikipedia/commons/c/c9/Delaunay_circumcircles.png

# Appendix D: Canny edge detection algorithm

Edge detection algorithms are used to reduce the amount of data in an image while preserving its structural properties. The Canny[66], which is one of the several edge detection algorithms, has following steps:

1. Smoothing: To prevent noise being detected as an edge, smoothing is done with Gaussian filter.

2. Finding the gradient: The edges where the grayscale intensity of the image changes the most are located and this is determined by gradients of the image. Gradients at each pixel are determined by applying the Sobel-operator. The edge strength is determined as the Euclidean distance of the gradient. At this stage the edges are a wide band of pixels.

3. Non-maximum suppression: The purpose of this step is to convert the band of pixels in the image to “sharp” edges. This is done by preserving all local maxima in the gradient image and deleting everything else.

4. Double thresholding: The edge pixels remaining after non-maximum suppression are designated with their strength and double thresholding is used to select strong edge pixels. Edge pixels stronger than the high threshold are marked as strong; edge pixels weaker than the low threshold are deleted and edge pixels between the two thresholds are marked as weak.

5. Edge detection by hysteresis: The strong edges are designated as ‘certain edges’ and immediately included in the final edge. Weak edges are included if and only if they are connected to certain edges. Those edges which are not connected to a certain edge are suppressed.

# Appendix E: MATLAB Codes

1. Iterative closest point algorithm:

This algorithm takes two surface data and align them.

```
function [f ] = AlignmentWithMyLSQ(x,data2send)
%'data2send' is a data structure.  data2send.TemplateData contains the
%template data. 'data2send.datap' contains the template data.
% x : the variables for optimization which contains the three angles of
% rotation and three coordinate values for translation.
 [distance_obtained ]= FindingMinDistanceDataToTemplate(x,data2send); %
FindingMinDistanceDataToTemplate function is called. This function sends the distances
from two surfaces for each point.
f=sum(distance_obtained.^2);  % total sum of the distances squares.
function [distance_obtained ]= FindingMinDistanceDataToTemplate(x,data2send)
datap1=data2send.datap; % Target data
%% Rotation angles:
theta1=x(1);% angle around z-axis in global axes in degree
theta2=x(2);% angle around y-axis in global axes in degree
theta3=x(3);% angle around x-axis in global axes in degree
%% Generating rotation matrix
R1 = [cosd(theta1) sind(theta1) 0; -sind(theta1) cosd(theta1) 0;0 0 1];
R2 = [cosd(theta2)  0 sind(theta2);0 1 0 ; -sind(theta2)  0 cosd(theta2)];
R3 = [1 0 0 ;  0  cosd(theta3) sind(theta3);  0 -sind(theta3) cosd(theta3)];
```

```
R=R1*R2*R3;
 %% Rotating and translating data.
ThisMatrix=[];
for i=1:length(datap1)
ThisMatrix(:,i) = R*datap1(i,:)' + [x(4) x(5) x(6)]';
end
ThisData=ThisMatrix';
%% Calculating distance of template from bone data points
distance_obtained=[];
%% Distaqnce from template  to  target  data.
for i=1:length(data2send.TemplateData(:,1))
   distance_obtained(i,:)=min(sqrt((data2send.TemplateData(i,1)- ThisData(:,1)).^2 +
(data2send.TemplateData(i,2)- ThisData(:,2)).^2 + (data2send.TemplateData(i,3)-
ThisData(:,3)).^2));
end
```

2.  Find  complete articular surface of MTH1:

This algorithm find the anterior articular surface of MTH1.

```
% data2send.data: metatarsal surface data
   %% I.Removing points posterior to the centroid of data.
   %% II. Find centroid.
   DataCentroid=mean(data2send.data);
   % Removing points beyond centroid.
```

```
[IndexID]=find(data2send.data(:,1)>= DataCentroid(1));
data2send.datap=data2send.data(IndexID,:);
DataCentroid=mean(data2send.datap);
% Removing points beyond centroid.
[IndexID]=find(data2send.datap(:,1)>= DataCentroid(1));
data2send.datap=data2send.datap(IndexID,:);
%% III. Finding the line around which cutting plane will rotate.
% Finding  index number of point with highest z-value.
[Top TopID]=max(data2send.datap(:,3));
% Finding index number of point with lowest y-value.
[Bottom BottomID]=min(data2send.datap(:,3));
% Finding index of point with largest y-value
[RightExtrm RightExtrmID]=max(data2send.datap(:,2));
%Finding index of point with lowest y-value.
[LeftExtrm LeftExtrmID]=min(data2send.datap(:,2));

% Choosing topmost point as posterior point
PosteriorPointID=TopID;
% Find point in midway of top and bottom point.
BetwTopBottom=(data2send.datap(TopID,:)+data2send.datap(BottomID,:))/2;
% Left point on the required line.
FirstPoint=[BetwTopBottom(1),LeftExtrm,BetwTopBottom(3)];
% Right point on the required line.
```

```
    SecondPoint=[BetwTopBottom(1),RightExtrm,BetwTopBottom(3)];
    % Point which will rotate to make rotating planes.

ThirdPoint=[data2send.datap(PosteriorPointID,1),data2send.datap(TopID,2),data2send.d
atap(TopID,3)];
    % Point in the middle of right and left point.
    MidPoint=(FirstPoint + SecondPoint)/2 ;
    planes=[];
    k=1;
    Section=[];
    %% IV. Cutting the planes in this for loop and obtaining the points in the plane and
finding their projections on the plane.
    for ii=1:length(angles)
        theta1=0;
        theta2=angles(ii);
        theta3=0;
        R1 = [cosd(theta1) sind(theta1) 0; -sind(theta1) cosd(theta1) 0;0 0 1];
        R2 = [cosd(theta2)  0 sind(theta2);0 1 0 ; -sind(theta2)  0 cosd(theta2)];
        R3 = [1 0 0 ;  0  cosd(theta3) sind(theta3);  0 -sind(theta3) cosd(theta3)];
        R=R1*R2*R3;
        MovingPoint = R*ThirdPoint';
        plane=createPlane(FirstPoint,MidPoint,MovingPoint');
        %  Making new coordinate system on the plane
```

```
        % Midpoint as Anterior.
        Anterior=MidPoint;
        % xaxis from midpoint to the First point.
        xaxis=(FirstPoint-MidPoint)./sqrt(sum((FirstPoint-MidPoint).^2));
        % Z axis as normal to the plane.
        zaxis = planeNormal(plane);
        % y axis as line perpendicular to the X-Z plane.
        yaxis=cross(xaxis,zaxis);
        % Creating Unit vector in the direction of each of the axis.
X_new_vector_unit=xaxis;Y_new_vector_unit=yaxis/sqrt(sum(yaxis.^2));Z_new_vector
_unit=zaxis/sqrt(sum(zaxis.^2));
        % Rotation matrix for finding the coordinates of the projected
        % points when the axes are made for each plane.
        rotation_matrix= [X_new_vector_unit;Y_new_vector_unit;Z_new_vector_unit];
        %          Thus, making a
        %          coordinate system based on the mid point, first point and the normal
        %          to the plane. Let us say it 'COORDINATE SYSTEM BY PLANE'.
        l=1;ll=0;
        Section(k).plane=plane; % corresponding plane of the section
        for j=1:length(data2send.datap) % Here we are taking single point at a time.
           d = abs(distancePointPlane(data2send.datap(j,:), plane)); % distance of this point
from the plane
           %        Projecting the points on respective plane
```

```
projectiononplane=projPointOnPlane(data2send.datap(j,:), plane); % this point projection on the current plane
if(abs(d)<=0.385/3) %% Threshold of the distance of the point from the plane to be included in the section.
% Finding the coordinate values  of pojections based on 'COORDINATE SYSTEM BY PLANE'.
translated_data = projectiononplane - Anterior;
transformeddatap= (rotation_matrix)*translated_data';
transformeddatap=transformeddatap'; %Value of the point with respect to 'COORDINATE SYSTEM BY PLANE'.
% Next step,  we are doing to avoid points which are intersected by plane below the X-axis on the plane.
%              so that we do not get points from lower surface while
%              intersecting points on the upper surface.
if(transformeddatap(2)>0)
   Section(k).transformeddatap(l,:)=transformeddatap; % Final value of the points with respect to 'COORDINATE SYSTEM BY PLANE' which we take in a given section.
   Section(k).projectiononplane(l,:)=projectiononplane; % data projected on this plane.
   Section(k).datap(l,:)=data2send.datap(j,:); % values from the original data which constitue the section.
```

```
                l=l+1;
            end
        end
    end
    k=k+1;
end
h1=figure;
hold on
plot3(data2send.datap1(:,1),data2send.datap1(:,2),data2send.datap1(:,3),'.r');
k=1;
%% V.Finding the articulating part of anterior surface i.e. removingdatapoints from side of sections.
% fraction to remove from sides ( after some trial and error we found this value).
FractionToRemove=1/7; % Fraction to remove from sides.
FractionRight=1/7; % FractionRight=Fraction which the right side will increase in every iteration
% Section1 : contains the articulating part of anterior surface.
Section1=[];
% Displaying sections in the bone.
for iii=1:length(Section)
    test=isempty(Section(iii).datap);
    if(test~=1)
```

```
        if(iii<=ExtraAngle+10) % When the rotating plane is from -10 degree to +10
degree.
             miny=(1-FractionRight)*max(Section(iii).datap(:,2))+ FractionToRemove*
min(Section(iii).datap(:,2));
            maxy=FractionToRemove*min(Section(iii).datap(:,2))+ (1-
FractionToRemove)* max(Section(iii).datap(:,2));
            indexgreaterthany=find(Section(iii).datap(:,2)> miny);
            indexlessthany=find(Section(iii).datap(:,2)< maxy);
            indexgreaterthanx=find(Section(iii).datap(:,1)> DataCentroid(1));
            intersecty=intersect(indexlessthany,indexgreaterthany);
            indextofit=intersect(intersecty,indexgreaterthanx);
             Section1(k).datap=Section(iii).datap(indextofit,:);
            Section1(k).transformeddatap=Section(iii).transformeddatap(indextofit,:);
            Section1(k).plane=Section(iii).plane;
            Section1(k).projectiononplane=Section(iii).projectiononplane;
           plot3(Section1(k).datap(:,1),Section1(k).datap(:,2),Section1(k).datap(:,3),'.g');
            k=k+1;
            hold on
            FractionRight=(FractionRight+ 1/(ExtraAngle+10));
            FractionRight1=FractionRight;
             else
            miny=FractionToRemove*max(Section(iii).datap(:,2))+ (1-
FractionToRemove)* min(Section(iii).datap(:,2));
```

```
            midx=(max(Section(iii).datap(:,1))+min(Section(iii).datap(:,1)))/2;
            maxy=FractionToRemove*min(Section(iii).datap(:,2))+ (1-
FractionToRemove)* max(Section(iii).datap(:,2));
            indexgreaterthany=find(Section(iii).datap(:,2)> miny);
            indexlessthany=find(Section(iii).datap(:,2)<maxy);
            indexgreaterthanx=find(Section(iii).datap(:,1)> DataCentroid(1));
            intersecty=intersect(indexlessthany,indexgreaterthany);
            indextofit=intersect(intersecty,indexgreaterthanx);
            Section1(k).datap=Section(iii).datap(indextofit,:);
            Section1(k).transformeddatap=Section(iii).transformeddatap(indextofit,:);
            Section1(k).plane=Section(iii).plane;
            Section1(k).projectiononplane=Section(iii).projectiononplane;
          plot3(Section1(k).datap(:,1),Section1(k).datap(:,2),Section1(k).datap(:,3),'.g');
            k=k+1;
            hold on
          end
       end
   end
```

3. Checking threshold of the slices of the cutting planes:

This algorithm fit a curve to the slices obtained with rotating cutting planes on MTH1 and found the root mean square error for the middle one third of the slices.

```
thresholds=0.25:0.2*50/100:1; % Threshold to be checked
for thres_ind=1:length(thresholds)

   %% Fitting curve to these sections of articulating surface.
   k=1;
   % error_vals: rms error for each of the section.
   error_vals=[];
   % difference: difference between fitted curve and data points at each
   % of the data point.
   THRESHOLD=thresholds(thres_ind);
   % patch1: this contains the required pathc which will be articulating
   % with only phalanx.
   patch1=[];
   l=1;ll=[];
   for iv=1:length(Section1)
      test=isempty(Section1(iv).transformeddatap);
      if(test~=1)
         % Fitting curve to each section
         x=Section1(iv).transformeddatap(:,1);
         y=Section1(iv).transformeddatap(:,2);
         if(length(Section1(iv).transformeddatap(:,2))>=3)
            p = polyfit(x,y,2); % polynomial coefficient
```

```
f = polyval(p,x); % Value of y-coordinate with the polynomial and x-coordinate values

difference(k).diff=(y-f).^2; % differerence square for the the actual y-coordinate and the polynomial values
differenceLength=length(difference(k).diff); % length of the difference vector
%% Checking the RMS  in the middle third of the section.
lowerboundindex=int32(differenceLength/3);
upperboundindex=2*lowerboundindex;

Middle3rdRMS=sqrt(sum(difference(k).diff(lowerboundindex+1:upperboundindex)));
%% Checking if the two consecutive slice has RMS more than threshold.
if(Middle3rdRMS<=  THRESHOLD)
   patch1(l).points=Section1(iv).datap;
   l=l+1;
   ll=[ll,1];
else ll=[ll,0];
end
if(length(ll)>=2)
   if((ll(end-1)==0) && (ll(end)==0))
      break;
   elseif(ll(end-1)==0 && (ll(end)~=0))
      patch(l).points=Section1(iv-1).datap;
```

```
            patch1(l+1).points=Section1(iv).datap;
            l=l+2;
        end
    end
    h3=figure;
    plot(x,y,'o',x,f,'*')
    saveas(h3,['section1No' num2str(iv) 'fit2'],'fig')
    close all
    clear h3
    h6=figure;
    hist(difference(k).diff);
    saveas(h6,['section1No' num2str(iv) 'DiffHist2'],'fig')
    rms_error=sqrt(sum((y-f).^2))/length(y);
    error_vals=[error_vals,rms_error];
    k=k+1;
    close all;
    clear h6
  end
 end
end
```

3. Best fit ellipsoid:

```
function [f ] = FindEllipsoidWithMyLSQ(x,data2send)
%'data2send' is a data structure.  'data2send.datap' contains the bone data.
data2send.size_which contains the size of the matrix used to create ellipsoid with matlab
function ellipsoid().
% x : the variables for optimization which contains the three angles of
% rotation , three semi-axes lengths and three coordinate values for center of ellipsoid.
 [distance_obtained ]= FindingMinDistanceDataToEllipsoid(x,data2send); % calling
function FindingMinDistanceDataToEllipsoid which calculates the distances from the
surface of bone data points to the surface of ellipsoid.
f=sum(distance_obtained.^2); % total sum of the distances squares
 function [distance_obtained ]= FindingMinDistanceDataToEllipsoid(x,data2send)
 n=data2send.size_matrix; % extracting the size of matrix to be used for creating ellipsoid
datap=data2send.datap;
theta1=x(7);% angle around z-axis in global axes in radians
theta2=x(8);% angle around y-axis in global axes in radians
theta3=x(9);% angle around x-axis in global axes
%generating rotation matrix
R1 = [cosd(theta1) sind(theta1) 0; -sind(theta1) cosd(theta1) 0;0 0 1];
R2 = [cosd(theta2)  0 sind(theta2);0 1 0 ; -sind(theta2)  0 cosd(theta2)];
R3 = [1 0 0 ;  0  cosd(theta3) sind(theta3);  0 -sind(theta3) cosd(theta3)];
R=R1*R2*R3;
```

```
[x1 y1 z1] = ellipsoid(x(1),x(2),x(3),abs(x(4)),abs(x(5)),abs(x(6)),n);% Generate ellipsoid
without rotation as per the matlab ellipsoid function.
x1=reshape(x1,length(x1)*length(x1),1);%make the data mesh into linear data points.
y1=reshape(y1,length(y1)*length(y1),1);%make the data mesh into linear data points.
z1=reshape(z1,length(z1)*length(z1),1);%make the data mesh into linear data points.
temp_ellipsoid_datap_1=[ x1 y1 z1] ; %data2send.ImplantStem;%temporary ellipsoid
linear data points without rotation.
% Rotating the data points of temporary ellipsoid
for i=1:length(temp_ellipsoid_datap_1)
E_matrix(:,i) = R*temp_ellipsoid_datap_1(i,:)';
end
temp_ellipsoid_datap=E_matrix';%%temporary ellipsoid linear data points with rotation.
 %finding distances between the given data points and the point on the surface of
%the temporary ellipsoid.Which I suppose to be the distance which has minimum
%numerical value.
for i=1:length(datap(:,1))
    distance_obtained(i,:)=min(sqrt((datap(i,1)- temp_ellipsoid_datap(:,1)).^2 +
(datap(i,2)- temp_ellipsoid_datap(:,2)).^2 + (datap(i,3)- temp_ellipsoid_datap(:,3)).^2));
end
```

4. Edge walking algorithm:

This algorithm find all the pixels in the geodesic path between two given pixels on an edge.

```
function [f ] = AlignmentWithMyLSQ(x,data2send)
%'data2send' is a data structure.  data2send.TemplateData contains the
%template data. 'data2send.datap' contains the template data.
% x : the variables for optimization which contains the three angles of
% rotation and three coordinate values for translation.
 [distance_obtained ]= FindingMinDistanceDataToTemplate(x,data2send); %
FindingMinDistanceDataToTemplate function is called. This function sends the distances
from two surfaces for each point.
f=sum(distance_obtained.^2);  % total sum of the distances squares.
function [distance_obtained ]= FindingMinDistanceDataToTemplate(x,data2send)
datap1=data2send.datap; % Target data
%% Rotation angles:
theta1=x(1);% angle around z-axis in global axes in degree
theta2=x(2);% angle around y-axis in global axes in degree
theta3=x(3);% angle around x-axis in global axes in degree
%% Generating rotation matrix
R1 = [cosd(theta1) sind(theta1) 0; -sind(theta1) cosd(theta1) 0;0 0 1];
R2 = [cosd(theta2)  0 sind(theta2);0 1 0 ; -sind(theta2)  0 cosd(theta2)];
R3 = [1 0 0 ;  0  cosd(theta3) sind(theta3);  0 -sind(theta3) cosd(theta3)];
R=R1*R2*R3;
```

```
%% Rotating and translating data.
ThisMatrix=[];
for i=1:length(datap1)
ThisMatrix(:,i) = R*datap1(i,:)' + [x(4) x(5) x(6)]';
end
ThisData=ThisMatrix';

%% Calculating distance of template from bone data points
distance_obtained=[];
%% Distaqnce from template  to  target  data.
for i=1:length(data2send.TemplateData(:,1))
   distance_obtained(i,:)=min(sqrt((data2send.TemplateData(i,1)- ThisData(:,1)).^2 +
(data2send.TemplateData(i,2)- ThisData(:,2)).^2 + (data2send.TemplateData(i,3)-
ThisData(:,3)).^2));
end
```

5. Edge growing algorithm:

```
   %%  Loading the image files
   if kk<10
      II=rgb2gray(imread([directoryname1 '\' '2dseq0000.000' num2str(kk) '.tif']));
   elseif kk<100
      II=rgb2gray(imread([directoryname1 '\' '2dseq0000.00' num2str(kk) '.tif']));
   else
```

```
    II=rgb2gray(imread([directoryname1 '\' '2dseq0000.0' num2str(kk) '.tif']));
  end
 % Outer border of the cartilage:
  Edge193_Partial= Edge_Partial;
  % Transpose image
  I=II';
  imshow(II); hold on



  %% Translating the edge points reference frame to the centroid of edges:
  % Best fit circle to the outer border
  [xc,yc,R,a] = circfit(Edge193_Partial(:,1),Edge193_Partial(:,2));
  % Center of the circle.
  CentroidEdge=[xc,yc];
  % Converting the outer border pixel coordinates from cartesian to polar
  TranslatedEdges=[Edge193_Partial(:,1)-CentroidEdge(1) ,Edge193_Partial(:,2)-
CentroidEdge(2)];
  TranslatedEdgesCentroid=mean(TranslatedEdges);


  TranslatedEdges2Polar=ones(length(TranslatedEdges),2);
  for ii=1:length(TranslatedEdges)
```

```
    [TranslatedEdges2Polar(ii,1)
TranslatedEdges2Polar(ii,2)]=cart2pol(TranslatedEdges(ii,1),TranslatedEdges(ii,2));
  end
  clear i ii
   I1Indices=[]; % Stores the cartilage pixels
  DepthFromEachEdgePoint=[]; % The depth of pixel at each of the outer pixel of outer
border

  for i=1:length(TranslatedEdges2Polar)
     if kk<247
     k=5; % The intensity value examination starts after leaving 5 pixels and 20 pixels
depending upon the proximity of the image to the anterior most slice of image. This value
was chosen after various trial and error.
     elseif kk==255
        k=5;
     else k=20;
     end
% Adding the first few pixels ( 5 and 20 here) in the cartilage region.
     for m=1:k
        [X1,Y1] = pol2cart(TranslatedEdges2Polar(i,1),TranslatedEdges2Polar(i,2)-m-1);
        x=int32(X1+CentroidEdge(1));y=int32(Y1+CentroidEdge(2));
        I1Indices=[I1Indices;[x,y]];
        plot(I1Indices(:,1),I1Indices(:,2),'.m');
```

```
    shg
    if m==1
        DepthFromEachEdgePoint(i).OuterEnd=[x,y];
    end
    m=m+1;

end

[X1,Y1] = pol2cart(TranslatedEdges2Polar(i,1),TranslatedEdges2Polar(i,2)-k-1);
x=int32(X1+CentroidEdge(1));y=int32(Y1+CentroidEdge(2));
count=1;
%% Checking the further pixels for intensity value
if kk<247
    while(I(x,y)>=20 && I(x,y)<220)

        I1Indices=[I1Indices;[x,y]];
        k=k+1;
        [X1,Y1] = pol2cart(TranslatedEdges2Polar(i,1),TranslatedEdges2Polar(i,2)-k);

        x=int32(X1+CentroidEdge(1));y=int32(Y1+CentroidEdge(2));
        TerminalPointTowardCenter(i,:)=[x,y];
            plot(x,y,'.m')
            shg
```

```
        count=count+1;

    end
    DepthFromEachEdgePoint(i).legnth=count-1;

    DepthFromEachEdgePoint(i).InnerEnd=[x,y];
else

    while(abs(int32(X1))>=2 || abs(int32(Y1))>=2)

        I1Indices=[I1Indices;[x,y]];
        k=k+1;
        [X1,Y1] = pol2cart(TranslatedEdges2Polar(i,1),TranslatedEdges2Polar(i,2)-k);

        x=int32(X1+CentroidEdge(1));
        y=int32(Y1+CentroidEdge(2));
        TerminalPointTowardCenter(i,:)=[x,y];
              plot(x,y,'.m')
              shg
        count=count+1;
    end
    DepthFromEachEdgePoint(i).legnth=count-1;
    DepthFromEachEdgePoint(i).InnerEnd=[x,y];
```

```
        end

      end

    end
```

# References

1. Klenerman et al.. Foot and its disorder its diorders. Blackwell Scientific Publications. 1976;(2):19.

2. Williams et al.. Gray's Anatomy 37th edition. Churchill Livingstone, Edinburggh,. 1989;1598.

3. Shereff MJ et al. Kinematics of the first metatarsophalangeal joint. The Journal of bone and joint surgery.. 1986;68(68):392-8.

4. Stokes IA, Hutton WC, Stott JR, Lowe LW. Forces under the hallux valgus foot before and after surgery. Clin Orthop Relat Res. 1979;(142):64-72.

5. Lawrence RC, Felson DT, Helmick CG, Arnold LM, Choi H, Deyo RA et al. Estimates of the prevalence of arthritis and other rheumatic conditions in the United States. Part II. Arthritis Rheum. 2008;58(1):26-35.

6. Moskowitz RW. The Burden of Osteoarthritis Clinical and Quality of Life Issues. Am J Manag Care. 2009;15(8):223-9.

7. Arden N, Nevitt MC. Osteoarthritis: epidemiology. Best Pract Res Clin Rheumatol. 2006;20(1):3-25.

8. Menz HB, Munteanu SE, Landorf KB, Zammit GV, Cicuttini FM. Radiographic evaluation of foot osteoarthritis: sensitivity of radiographic variables and relationship to symptoms.

Osteoarthritis Cartilage. 2009;17(3):298-303.

9. Roddy E, Zhang W, Doherty M. Prevalence and associations of hallux valgus in a primary care population. Arthritis Rheum. 2008;59(6):857-62.

10. Scott DL, Wolfe F, Huizinga TWJ. Rheumatoid arthritis. Lancet. 2010;376(9746):1094-108.

11. Schlesinger N. Diagnosis of Gout Clinical Laboratory and radiologic findings. Am J Manag Care. 2005;11(15):443-50.

12. Bal A, Aydog E, Aydog ST, Cakci A. Foot deformities in rheumatoid arthritis and relevance of foot function index. Clin Rheumatol. 2006;25(5):671-5.

13. Badlissi F, Dunn JE, Link CL, Keysor JJ, McKinlay JB, Felson DT. Foot musculoskeletal disorders, pain, and foot-related functional limitation in older persons. J Am Geriatr Soc. 2005;53(6):1029-33.

14. Coughlin MJ, Shurnas PS. Hallux rigidus. Grading and long-term results of operative treatment. J Bone Joint Surg Am. 2003;85-A(11):2072-88.

15. Dhukaram V, Hullin MG, Senthil Kumar C. The Mitchell and Scarf osteotomies for hallux valgus correction: a retrospective, comparative analysis using plantar pressures. J Foot Ankle Surg. 2006;45(6):400-9.

16. Schneider W et al. Chevron osteotomy in hallux valgus. The Journal of Bonea and Joint Surgery. 2004;86:1016-20.

17. Berg RP, Olsthoorn PGM, Pöll RG. Scarf osteotomy in hallux valgus: a review of 72 cases. Acta Orthop Belg. 2007;73(2):219-23.

18. Schenk S, Meizer R, Kramer R, Aigner N, Landsiedl F, Steinboeck G. Resection arthroplasty with and without capsular interposition for treatment of severe hallux rigidus. Int Orthop. 2009;33(1):145-50.

19. Fadel GE et al. Implant arthroplasty of the hallux metatarsophalangeal joint. The Foot. 2002;12:1-9.

20. DeHeer PA et al. The case against first metatarsal phalangeal joint implant arthroplasty. Clin Podiatr Med Surg. 2006;23:709-23.

21. Salonga CC, Novicki DC, Pressman MM, Malay DS. A Retrospective Cohort Study of the BioPro(R) Hemiarthroplasty Prosthesis. J Foot Ankle Surg. 2010;

22. Hasselman CT et al. Resurfacing of the first metatarsal head in the treatment of hallux rigidus. Techniques in Foot & Ankle Surgery. 2008;7(1):31-40.

23. Hutton WC, Dhanendran M. The mechanics of normal and hallux valgus feet--a quantitative study. Clin Orthop Relat Res. 1981;(157):7-13.

24. Cavanagh PR, Rodgers MM, Iiboshi A. Pressure distribution under symptom-free feet during barefoot standing. Foot Ankle. 1987;7(5):262-76.

25. Mann RA, Thompson FM. Arthrodesis of the first metatarsophalangeal joint for hallux valgus in rheumatoid arthritis. J Bone Joint Surg Am. 1984;66(5):687-92.

26. Coughlin MJ, Mann RA. Arthrodesis of the first metatarsophalangeal joint as salvage for the failed Keller procedure. J Bone Joint Surg Am. 1987;69(1):68-75.

27. Schneider W, Knahr K. Keller procedure and chevron osteotomy in hallux valgus: five-year results of different surgical philosophies in comparable collectives. Foot Ankle Int. 2002;23(4):321-9.

28. Harisboure A, Joveniaux P, Madi K, Dehoux E. The Valenti technique in the treatment of hallux rigidus. Orthopaedics & traumatology, surgery & research : OTSR. 2009;95(3):202-9.

29. Trnka HJ, Hofstaetter SG, Hofstaetter JG, Gruber F, Adams SB, Easley ME. Intermediate-term results of the Ludloff osteotomy in one hundred and eleven feet. J Bone Joint Surg Am. 2008;90(3):531-9.

30. Raikin SM, Ahmad J, Pour AE, Abidi N. Comparison of arthrodesis and metallic hemiarthroplasty of the hallux metatarsophalangeal joint. J Bone Joint Surg Am. 2007;89(9):1979-85.

31. Shi K, Hayashida K, Owaki H, Kawai H. Replacement of the first metatarsophalangeal joint with a Swanson implant accompanied by open-wedge osteotomy of the first metatarsal bone for hallux valgus in rheumatoid arthritis. Mod Rheumatol. 2007;17(2):110-4.

32. Hanyu T, Yamazaki H, Ishikawa H, Arai K, Tohyama CT, Nakazono K et al. Flexible hinge

toe implant arthroplasty for rheumatoid arthritis of the first metatarsophalangeal joint: long-term results. J Orthop Sci. 2001;6(2):141-7.

33. Olms K, Dietze A. Replacement arthroplasty for hallux rigidus. 21 patients with a 2-year follow-up. Int Orthop. 1999;23(4):240-3.

34. Osteomed. Bio-Action Great Toe Implant [Internet]. 2009 [cited 2009]. Available from: http://www.osteomedcorp.com/Products/Extremity/BioAction.html

35. Implants International. Arthroplasty [Internet]. 2009 [cited 2009]. Available from: http://www.implantsinternational.com/docs/Arthroplasty/Roto-Glide%20Brochure.pdf

36. Werner A, Lechniak Z, Skalski K, Kdzior K. Design and manufacture of anatomical hip joint endoprostheses using CAD/CAM systems. Journal of Materials Processing Technology. 2000;107(1-3):181-6.

37. Mahfouz MR, Merkl BC, Fatah EEA, Booth R, Argenson JN. Automatic methods for characterization of sexual dimorphism of adult femora: distal femur. Comput Methods Biomech Biomed Engin. 2007;10(6):447-56.

38. Brownhill J, King G, Johnson J. Morphologic analysis of the distal humerus with special interest in elbow implant sizing and alignment. J Shoulder Elbow Surg. 2007;16(3 Suppl):S126-32.

39. Brownhill J, Mozzon J, Ferreira L, Johnson J, King G. Morphologic analysis of the proximal ulna with special interest in elbow implant sizing and alignment. J Shoulder Elbow Surg.

2009;18(1):27-32.

40. Besl PJ, McKay ND. A Method for Registration of 3-D Shapes. IEEE PAMI. 1992;14(2):239-56.

41. Simpson DJ, Gray H, D'Lima D, Murray DW, Gill HS. The effect of bearing congruency, thickness and alignment on the stresses in unicompartmental knee replacements. "Clin Biomech (Bristol. 2008;23(9):1148-57.

42. Ferrari J, Hopkinson DA, Linney AD. Size and shape differences between male and female foot bones: is the female foot predisposed to hallux abducto valgus deformity? J Am Podiatr Med Assoc. 2004;94(5):434-52.

43. Cwikla et al.. Morphological considerations of the first metatarsophalangeal joint. J Foot Surg. 1992;31(1):3-9.

44. Muehleman C, Kuettner K. Distribution of cartilage thickness on the head of the human first metatarsal bone. J Anat. 2000;197(04):687-91.

45. Buckwalter. Articular Cartilage and osteoarthirtis. . 2005;

46. Liu. Biomechanical Topography of Human Articular Cartilage in the First Metatarsophalangeal Joint. . 1998;

47. MullerGerbl. The thickness of the calcified layer of articular cartilage a funciton of the load supported. . 1987;:103-11.

48. Akiyama K, Sakai T, Koyanagi J, Murase T, Yoshikawa H, Sugamoto K. Three-dimensional distribution of articular cartilage thickness in the elderly cadaveric acetabulum: a new method using three-dimensional digitizer and CT. Osteoarthritis Cartilage. 2010;18(6):795-802.

49. Shepherd D, Seedhom B. Thickness of human articular cartilage in joints of the lower limb. Ann Rheum Dis. 1999;58(1):27-34.

50. Jurvelin J. Comparison of optical, needle probe and ultrasonic techniques for the measurement of articular cartilage thickness. J Biomech. 1995;28(2):231-5.

51. Abraham A, Goff I, Pearce M, Francis R, Birrell F. Reliability and validity of ultrasound imaging of features of knee osteoarthritis in the community. BMC Musculoskelet Disord. 2011;12(1):70.

52. Spannow AH, Pfeiffer-Jensen M, Andersen NT, Herlin T, Stenbog E. Ultrasonographic measurements of joint cartilage thickness in healthy children: age- and sex-related standard reference values. J Rheumatol. 2010;37(12):2595-601.

53. Stok KS, Müller R. Morphometric characterization of murine articular cartilage--novel application of confocal laser scanning microscopy. Microsc Res Tech. 2009;72(9):650-8.

54. Pastoureau P, Hunziker E, Pelletier JP. Cartilage, bone and synovial histomorphometry in animal models of osteoarthritis. Osteoarthritis Cartilage. 2010;18 Suppl 3:S106-12.

55. Wyler A, Bousson V, Bergot C, Polivka M, Leveque E, Vicaut E et al. Hyaline cartilage thickness in radiographically normal cadaveric hips: comparison of spiral CT arthrographic and

macroscopic measurements. Radiology. 2007;242(2):441-9.

56. Williams TG, Holmes AP, Bowes M, Vincent G, Hutchinson CE, Waterton JC et al. Measurement and visualisation of focal cartilage thickness change by MRI in a study of knee osteoarthritis using a novel image analysis tool. Br J Radiol. 2010;83(995):940-8.

57. Trinh N, Lester J, Fleming B, Tung G, Kimia B. Accurate measurement of cartilage morphology using a 3D laser scanner. Computer Vision Approaches to Medical Image Analysis. 2006;:37-48.

58. Eckstein F, Gavazzeni A, Sittek H, Haubner M, Lösch A, Milz S et al. Determination of knee joint cartilage thickness using three-dimensional magnetic resonance chondro-crassometry (3D MR-CCM). Magnetic Resonance in Medicine. 1996;36(2):256-65.

59. Frobell RB, Nevitt MC, Hudelmaier M, Wirth W, Wyman BT, Benichou O et al. Femorotibial subchondral bone area and regional cartilage thickness: A cross-sectional description in healthy reference cases and various radiographic stages of osteoarthritis in 1,003 knees from the Osteoarthritis Initiative. Arthritis Care & Research. 2010;62(11):1612-23.

60. Naish J, Xanthopoulos E, Hutchinson C, Waterton J, Taylor C. MR measurement of articular cartilage thickness distribution in the hip. Osteoarthritis Cartilage. 2006;14(10):967-73.

61. Cheng Y, Wang S, Yamazaki T, Zhao J, Nakajima Y, Tamura S. Hip cartilage thickness measurement accuracy improvement. Comput Med Imaging Graph. 2007;31(8):643-55.

62. Streekstra_2007_Model-based cartilage thickness measurement in the submillimeter range.

Phys. 2007;34(9):3562-70.

63. Stokes IA, Hutton WC, Stott JR. Forces acting on the metatarsals during normal walking. J Anat. 1979;129(Pt 3):579-90.

64. Bansal P, Stewart R, Entezari V, Snyder B, Grinstaff M. Contrast agent electrostatic attraction rather than repulsion to glycosaminoglycans affords a greater contrast uptake ratio and improved quantitative CT imaging in cartilage. Osteoarthritis Cartilage. 2011;

65. Pham D, Xu C, Prince J. Current Methods in Medical Image Segmentation 1. Annu Rev Biomed Eng. 2000;2(1):315-37.

66. Canny. A computational approach to edge detection. IEEE Trans Pattern Anal Mach Intell. 1986.

67. Asano et al.. Walkign on an arrangement topologically. ACM. 1991;297-306.

68. de Berg et al.. Computational Geometry: Algorithms and Applications. Springer-Verlag. 2008;:191-218.

69. Adams R, Bischof L. Seeded region growing. Pattern Analysis and Machine Intelligence, IEEE Transactions on. 1994;16(6):641-7.

70. Taubin G. A signal processing approach to fair surface design. Proceedings of the 22nd annual conference on Computer graphics and interactive techniques; 1995. p. 351-58.

71. Womack W, Ayturk UM, Puttlitz CM. Cartilage thickness distribution affects computational

model predictions of cervical spine facet contact parameters. J Biomech Eng. 2011;133(1):011009.

72. Flavin R, Halpin T, O'Sullivan R, FitzPatrick D, Ivankovic A, Stephens M. A finite-element analysis study of the metatarsophalangeal joint of the hallux rigidus. Journal of Bone and Joint Surgery-British Volume. 2008;90(10):1334.

73. Liu. Human articular cartilage biomechanics of the second metatarsal intermediate cuneiform joint. . 1997;36(5)

74. Marai. A kinematics-based method for generating cartilage maps and deformations in the multi-articulating wrist joint from CT images. . 2006;18:1-4244.

75. Glisson M. Comparison of X-rays and magnetic resonance imaging in the definition of tibiofemoral joint osteoarthritis. Radiography. 2000;6(3):205-9.

76. Boileau P, Walch G. The three-dimensional geometry of the proximal humerus: implications for surgical technique and prosthetic design. Journal of Bone and Joint Surgery-British Volume. 1997;79(5):857.

77. Zhang Y, Hamza A. Vertex-Based Anisotropic Smoothing of 3D Mesh Data. Electrical and Computer Engineering, 2006. CCECE'06. Canadian Conference on; 2006. p. 202-05.

78. Larsson S, Elloy M, Hansson L. Fixation of unstable trochanteric hip fractures: a cadaver study comparing three different devices. Acta Orthop. 1988;59(6):658-63.

79. Srinivas C. Toward the development of virtual surgical tools to aid orthopaedic FE analyses. Journal on advances in signal processing. 2010;2010:1902931-7.

80. Budhabhatti SP, Erdemir A, Petre M, Sferra J, Donley B, Cavanagh PR. Finite element modeling of the first ray of the foot: a tool for the design of interventions. (1). J Biomech Eng. 2007;129(5):750-6.

81. Terrestrial laser scanning--new perspectives in 3D surveying. International archives of photogrammetry, remote sensing and spatial information sciences. 2004;36(Part 8)

82. Hendee W, Morgan C. Magnetic resonance imaging. Part I--physical principles. West J Med. 1984;141(4):491-500.

# Copyright permissions

**A. Kumar**

**From:** Martin Pressman [pressmandpm@gmail.com]
**Sent:** Monday, July 11, 2011 4:18 AM
**To:** A. Kumar
**Subject:** Re: Permission to use figures from manuscripts

Dear Dr. Kumar,
You have my permission to use Fig. 1 in your thesis. You are in the land of MTPJ arthrodesis...implants for first Mtpj arthritis are heresy in Seattle, Regards M. Pressman

Sent from my iPad

On Jul 10, 2011, at 10:56 PM, "A. Kumar" <kumara4@u.washington.edu> wrote:

> Dear Dr. Martin,
>
> I am in the process of writing my thesis. I hope you would permit me to use the following figure from your article:
>
> FIGURE. 1
>
> From 'A Retrospective Cohort Study of the BioPro Hemiarthroplasty Prosthesis' The Journal of Foot & Ankle Surgery xxx (2010) 1–9
>
> Looking forward to your reply.
>
> Regards,
>
> Atul
>
> MBBS,MMST,PhD (Candidate)
>
> Visiting Scientist
>
> Department of Orthopedics and Sports Medicine
>
> University of Washington
>
> BB 1002

1

# PERMISSION LICENSE AGREEMENT

P2969.JBJSInc.JBJS Am.Raikin.1744.University of Washington.Kumara

JBJSInc.JBJS Am.Raikin.1744

7/13/2011

Atul Kumara

INVOICE ATTACHED

University of Washington
BB 1002
1959 NE Pacific St.
Seatltle, WA USA

Dear Kumara,

Thank you for your interest in JBJS [Am] material. Please note: This permission does not apply to any figure or other material that is credited to any source other than JBJS. It is your responsibility to validate that the material is in fact owned by JBJS. If material within JBJS material is credited to another source (in a figure legend, for example) then any permission extended by JBJS is invalid. We encourage you to view the actual material at www.ejbjs.org or a library or other source. Information provided by third parties as to credits that may or may not be associated with the material may be unreliable.

We are pleased to grant you non-exclusive, nontransferable permission, limited to the format described below, and provided you meet the criteria below. Such permission is for one-time use and does not include permission for future editions, revisions, additional printings, updates, ancillaries, customized forms, any electronic forms, Braille editions, translations or promotional pieces unless otherwise specified below. We must be contacted for permission each time such use is planned. This permission does not include the right to modify the material. Use of the material must not imply any endorsement by the copyright owner. This permission is not valid for the use of JBJS logos or other collateral material.

Abstracts or collections of abstracts and all translations must be approved by publisher's agent in advance, and in the case of translations, before printing. No financial liability for the project will devolve upon JBJS, Inc. or on Rockwater, Inc.. All expenses for translation, validation of translation accuracy, publication costs and reproduction costs are the sole responsibility of the foreign language sponsor. The new work must be reprinted and delivered as a stand-alone piece and may not be integrated or bound with other material. JBJS does not supply photos or artwork; these may be downloaded from the JBJS website, scanned, or (if available) obtained from the author of the article.

**PERMISSION IS VALID FOR THE FOLLOWING MATERIAL ONLY:**

**Fig 13**

Journal of Bone and Joint Surgery Amercian, , 2008, 90, , Comparison of Arthrodesis and Metallic Hemi-arthroplasty of the Hallux Metatarsophalangeal Joint Surgical Technique, Raikin, 171-180

**IN THE FOLLOWING WORK ONLY:**

electronic and/or print copies of PHD Thesis

CREDIT LINE(S) must be published next to any figure, and/or if permission is granted for electronic form, visible at the same time as the content republished with a hyperlink to the publisher's home page.

WITH PAYMENT OF PERMISSIONS FEE. License, once paid, is good for one year from your anticipated publication date unless otherwise specified above. Failure to pay the fee(s) or to follow instructions here upon use of the work as described here, will result in automatic termination of the license or permission granted. All information is required. Payment should be made to Rockwater, Inc. by check or credit card, via mail

Please contact Beth Ann Rocheleau at jbjs@rockwaterinc.com or 1-803-359-4578 with questions.

**A. Kumar**

**From:** Wolters Kluwer Rights and Permissions [journalpermissions@lww.com]
**Sent:** Tuesday, July 12, 2011 8:50 AM
**To:** A. Kumar
**Subject:** Permission to use figures from manuscripts [Incident: 110711-001016]

Recently you requested personal assistance from our on-line support center. Below is a summary of your request and our response.

If this issue is not resolved to your satisfaction, you may reopen it within the next 14 days.

Thank you for allowing us to be of service to you.

To access your question from our support site, click here.

**Subject**

Permission to use figures from manuscripts

**Discussion Thread**

**Response Via Email (Laura Lee)** 07/12/2011 11:50 AM

Permission is granted provided a prominent credit line is placed stating the original source and copyright year, Lippincott Williams & Wilkins.

**Customer By Email (A. Kumar)** 07/11/2011 05:13 PM

Hi there,

I am in the process of writing my thesis. I hope you would permit me to use the following figures from your article:

FIGURE. 1 and 20
From 'Resurfacing of the First Metatarsal Head in the
Treatment of Hallux Rigidus' Techniques in Foot & Ankle Surgery 7(1):31-40, 2008

I have got the permission from the author of the article (Please see below).

Looking forward to your reply.

Regards,
Atul

From: Hasselman, Carl [mailto:HasselmanCT@upmc.edu]
Sent: Monday, July 11, 2011 3:28 AM
To: A. Kumar
Subject: RE: Permission to use figures from manuscripts

You do have my permission to use the figures from this manuscript. However, I think you also need permission

from the publisher of the article which is Lippincott.

From: A. Kumar [mailto:kumara4@u.washington.edu]
Sent: Sunday, July 10, 2011 10:59 PM
To: Hasselman, Carl
Subject: Permission to use figures from manuscripts

Dear Dr. Hasselman,

I am in the process of writing my thesis. I hope you would permit me to use the following figures from your article:

FIGURE. 1 and 20
From 'Resurfacing of the First Metatarsal Head in the
Treatment of Hallux Rigidus' Techniques in Foot & Ankle Surgery 7(1):31-40, 2008

Looking forward to your reply.

Regards,
Atul

MBBS,MMST,PhD (Candidate)
Visiting Scientist
Department of Orthopedics and Sports Medicine
University of Washington
BB 1002
1959 NE Pacific St.
Seattle WA 98195

**Question Reference #110711-001016**

**Date Created:** 07/11/2011 05:13 PM
**Last Updated:** 07/12/2011 11:50 AM
**Status:** Solved
**Account Number:**
**Society List:** None
**Society Membership:** No

[---001:001847:50811---]

**ELSEVIER LICENSE**
**TERMS AND CONDITIONS**

Jul 18, 2011

This is a License Agreement between Atul Kumar ("You") and Elsevier ("Elsevier") provided by Copyright Clearance Center ("CCC"). The license consists of your order details, the terms and conditions provided by Elsevier, and the payment terms and conditions.

**All payments must be made in full to CCC. For payment instructions, please see information listed at the bottom of this form.**

| | |
|---|---|
| Supplier | Elsevier Limited<br>The Boulevard,Langford Lane<br>Kidlington,Oxford,OX5 1GB,UK |
| Registered Company Number | 1982084 |
| Customer name | Atul Kumar |
| Customer address | 6425 65th Ave NE<br>Seattle, WA 98115 |
| License number | 2712050559386 |
| License date | Jul 18, 2011 |
| Licensed content publisher | Elsevier |
| Licensed content publication | The Journal of Foot and Ankle Surgery |
| Licensed content title | A Retrospective Cohort Study of the BioPro® Hemiarthroplasty Prosthesis |
| Licensed content author | Christine C. Salonga, David C. Novicki, Martin M. Pressman, D. Scot Malay |
| Licensed content date | July-August 2010 |
| Licensed content volume number | 49 |
| Licensed content issue number | 4 |
| Number of pages | 9 |
| Start Page | 331 |
| End Page | 339 |
| Type of Use | reuse in a thesis/dissertation |
| Portion | figures/tables/illustrations |
| Number of figures/tables /illustrations | 1 |
| Format | print |
| Are you the author of this Elsevier article? | No |
| Will you be translating? | No |
| Order reference number | |

licensing transaction, (ii) these terms and conditions and (iii) CCC's Billing and Payment terms and conditions.

8. License Contingent Upon Payment: While you may exercise the rights licensed immediately upon issuance of the license at the end of the licensing process for the transaction, provided that you have disclosed complete and accurate details of your proposed use, no license is finally effective unless and until full payment is received from you (either by publisher or by CCC) as provided in CCC's Billing and Payment terms and conditions. If full payment is not received on a timely basis, then any license preliminarily granted shall be deemed automatically revoked and shall be void as if never granted. Further, in the event that you breach any of these terms and conditions or any of CCC's Billing and Payment terms and conditions, the license is automatically revoked and shall be void as if never granted. Use of materials as described in a revoked license, as well as any use of the materials beyond the scope of an unrevoked license, may constitute copyright infringement and publisher reserves the right to take any and all action to protect its copyright in the materials.

9. Warranties: Publisher makes no representations or warranties with respect to the licensed material.

10. Indemnity: You hereby indemnify and agree to hold harmless publisher and CCC, and their respective officers, directors, employees and agents, from and against any and all claims arising out of your use of the licensed material other than as specifically authorized pursuant to this license.

11. No Transfer of License: This license is personal to you and may not be sublicensed, assigned, or transferred by you to any other person without publisher's written permission.

12. No Amendment Except in Writing: This license may not be amended except in a writing signed by both parties (or, in the case of publisher, by CCC on publisher's behalf).

13. Objection to Contrary Terms: Publisher hereby objects to any terms contained in any purchase order, acknowledgment, check endorsement or other writing prepared by you, which terms are inconsistent with these terms and conditions or CCC's Billing and Payment terms and conditions. These terms and conditions, together with CCC's Billing and Payment terms and conditions (which are incorporated herein), comprise the entire agreement between you and publisher (and CCC) concerning this licensing transaction. In the event of any conflict between your obligations established by these terms and conditions and those established by CCC's Billing and Payment terms and conditions, these terms and conditions shall control.

14. Revocation: Elsevier or Copyright Clearance Center may deny the permissions described in this License at their sole discretion, for any reason or no reason, with a full refund payable to you. Notice of such denial will be made using the contact information provided by you. Failure to receive such notice will not alter or invalidate the denial. In no event will Elsevier or Copyright Clearance Center be responsible or liable for any costs, expenses or damage incurred by you as a result of a denial of your permission request, other than a refund of the amount(s) paid by you to Elsevier and/or Copyright Clearance Center for denied permissions.

**LIMITED LICENSE**

The following terms and conditions apply only to specific license types:

15. **Translation**: This permission is granted for non-exclusive world **English** rights only unless your license was granted for translation rights. If you licensed translation rights you may only translate this content into the languages you requested. A professional translator must perform all translations and reproduce the content word for word preserving the integrity of the article. If this license is to re-use 1 or 2 figures then permission is granted for non-exclusive world rights in all languages.

16. **Website**: The following terms and conditions apply to electronic reserve and author websites:
**Electronic reserve**: If licensed material is to be posted to website, the web site is to be password-protected and made available only to bona fide students registered on a relevant course if:
This license was made in connection with a course,
This permission is granted for 1 year only. You may obtain a license for future website posting,
All content posted to the web site must maintain the copyright information line on the bottom of each image,
A hyper-text must be included to the Homepage of the journal from which you are licensing at http://www.sciencedirect.com/science/journal/xxxxx or the Elsevier homepage for books at http://www.elsevier.com , and
Central Storage: This license does not include permission for a scanned version of the material to be stored in a central repository such as that provided by Heron/XanEdu.

17. **Author website** for journals with the following additional clauses:

All content posted to the web site must maintain the copyright information line on the bottom of each image, and
he permission granted is limited to the personal version of your paper. You are not allowed to download and post the published electronic version of your article (whether PDF or HTML, proof or final version), nor may you scan the printed edition to create an electronic version,
A hyper-text must be included to the Homepage of the journal from which you are licensing at http://www.sciencedirect.com/science/journal/xxxxx , As part of our normal production process, you will receive an e-mail notice when your article appears on Elsevier's online service ScienceDirect (www.sciencedirect.com). That e-mail will include the article's Digital Object Identifier (DOI). This number provides the electronic link to the published article and should be included in the posting of your personal version. We ask that you wait until you receive this e-mail and have the DOI to do any posting.
Central Storage: This license does not include permission for a scanned version of the material to be stored in a central repository such as that provided by Heron/XanEdu.

18. **Author website** for books with the following additional clauses:
Authors are permitted to place a brief summary of their work online only.
A hyper-text must be included to the Elsevier homepage at http://www.elsevier.com

All content posted to the web site must maintain the copyright information line on the bottom of each image
You are not allowed to download and post the published electronic version of your chapter,

nor may you scan the printed edition to create an electronic version.
Central Storage: This license does not include permission for a scanned version of the material to be stored in a central repository such as that provided by Heron/XanEdu.

19. **Website** (regular and for author): A hyper-text must be included to the Homepage of the journal from which you are licensing at http://www.sciencedirect.com/science/journal/xxxxx. or for books to the Elsevier homepage at http://www.elsevier.com

20. **Thesis/Dissertation**: If your license is for use in a thesis/dissertation your thesis may be submitted to your institution in either print or electronic form. Should your thesis be published commercially, please reapply for permission. These requirements include permission for the Library and Archives of Canada to supply single copies, on demand, of the complete thesis and include permission for UMI to supply single copies, on demand, of the complete thesis. Should your thesis be published commercially, please reapply for permission.

21. **Other Conditions**:

v1.6

**Gratis licenses (referencing $0 in the Total field) are free. Please retain this printable license for your reference. No payment is required.**

**If you would like to pay for this license now, please remit this license along with your payment made payable to "COPYRIGHT CLEARANCE CENTER" otherwise you will be invoiced within 48 hours of the license date. Payment should be in the form of a check or money order referencing your account number and this invoice number RLNK11022357.**
**Once you receive your invoice for this order, you may pay your invoice by credit card. Please follow instructions provided at that time.**

**Make Payment To:**
**Copyright Clearance Center**
**Dept 001**
**P.O. Box 843006**
**Boston, MA 02284-3006**

**For suggestions or comments regarding this order, contact Rightslink Customer Support: customercare@copyright.com or +1-877-622-5543 (toll free in the US) or +1-978-646-2777.**

| | |
|---|---|
| Title of your thesis/dissertation | DESIGN OF AN IMPLANT FOR FIRST METATARSOPHALANGEAL JOINT HEMIARTHROPLASTY |
| Expected completion date | Jul 2011 |
| Estimated size (number of pages) | 120 |
| Elsevier VAT number | GB 494 6272 12 |
| Permissions price | 0.00 USD |
| VAT/Local Sales Tax | 0.0 USD / 0.0 GBP |
| Total | 0.00 USD |
| Terms and Conditions | |

## INTRODUCTION

1. The publisher for this copyrighted material is Elsevier. By clicking "accept" in connection with completing this licensing transaction, you agree that the following terms and conditions apply to this transaction (along with the Billing and Payment terms and conditions established by Copyright Clearance Center, Inc. ("CCC"), at the time that you opened your Rightslink account and that are available at any time at http://myaccount.copyright.com).

## GENERAL TERMS

2. Elsevier hereby grants you permission to reproduce the aforementioned material subject to the terms and conditions indicated.

3. Acknowledgement: If any part of the material to be used (for example, figures) has appeared in our publication with credit or acknowledgement to another source, permission must also be sought from that source. If such permission is not obtained then that material may not be included in your publication/copies. Suitable acknowledgement to the source must be made, either as a footnote or in a reference list at the end of your publication, as follows:

"Reprinted from Publication title, Vol /edition number, Author(s), Title of article / title of chapter, Pages No., Copyright (Year), with permission from Elsevier [OR APPLICABLE SOCIETY COPYRIGHT OWNER]." Also Lancet special credit - "Reprinted from The Lancet, Vol. number, Author(s), Title of article, Pages No., Copyright (Year), with permission from Elsevier."

4. Reproduction of this material is confined to the purpose and/or media for which permission is hereby given.

5. Altering/Modifying Material: Not Permitted. However figures and illustrations may be altered/adapted minimally to serve your work. Any other abbreviations, additions, deletions and/or any other alterations shall be made only with prior written authorization of Elsevier Ltd. (Please contact Elsevier at permissions@elsevier.com)

6. If the permission fee for the requested use of our material is waived in this instance, please be advised that your future requests for Elsevier materials may attract a fee.

7. Reservation of Rights: Publisher reserves all rights not specifically granted in the combination of (i) the license details provided by you and accepted in the course of this

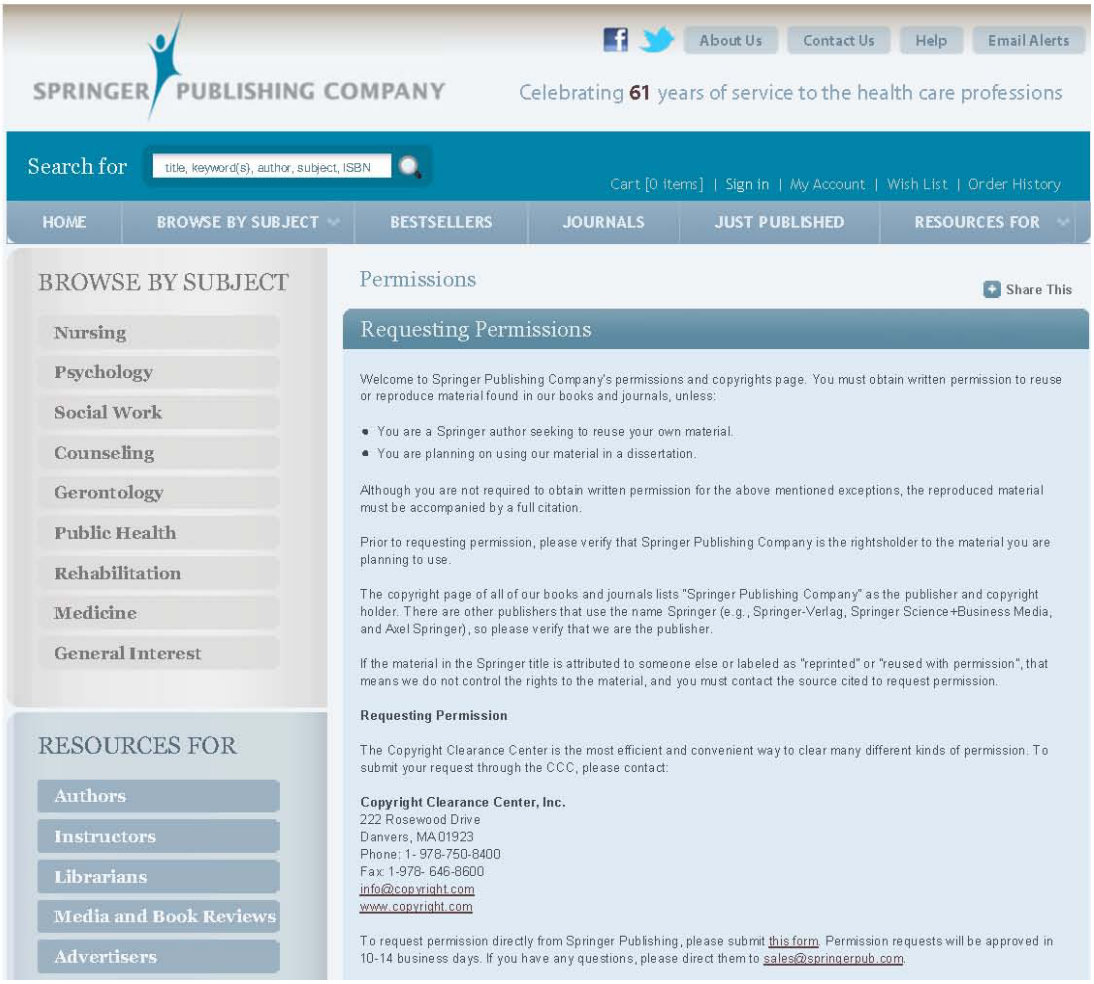
SPRINGER PUBLISHING COMPANY
About Us
Contact Us
Help
Email Alerts
Celebrating 61 years of service to the health care professions
Search for
title, keyword(s), author, subject, ISBN
Cart [0 items] | Sign In | My Account | Wish List | Order History
HOME
BROWSE BY SUBJECT
BESTSELLERS
JOURNALS
JUST PUBLISHED
RESOURCES FOR
BROWSE BY SUBJECT
Nursing
Psychology
Social Work
Counseling
Gerontology
Public Health
Rehabilitation
Medicine
General Interest
RESOURCES FOR
Authors
Instructors
Librarians
Media and Book Reviews
Advertisers
Permissions
Share This
Requesting Permissions
Welcome to Springer Publishing Company's permissions and copyrights page. You must obtain written permission to reuse or reproduce material found in our books and journals, unless:
You are a Springer author seeking to reuse your own material.
You are planning on using our material in a dissertation.
Although you are not required to obtain written permission for the above mentioned exceptions, the reproduced material must be accompanied by a full citation.
Prior to requesting permission, please verify that Springer Publishing Company is the rightsholder to the material you are planning to use.
The copyright page of all of our books and journals lists "Springer Publishing Company" as the publisher and copyright holder. There are other publishers that use the name Springer (e.g., Springer-Verlag, Springer Science+Business Media, and Axel Springer), so please verify that we are the publisher.
If the material in the Springer title is attributed to someone else or labeled as "reprinted" or "reused with permission", that means we do not control the rights to the material, and you must contact the source cited to request permission.
Requesting Permission
The Copyright Clearance Center is the most efficient and convenient way to clear many different kinds of permission. To submit your request through the CCC, please contact:
Copyright Clearance Center, Inc.
222 Rosewood Drive
Danvers, MA 01923
Phone: 1- 978-750-8400
Fax: 1-978- 646-8600
info@copyright.com
www.copyright.com
To request permission directly from Springer Publishing, please submit this form. Permission requests will be approved in 10-14 business days. If you have any questions, please direct them to sales@springerpub.com.

atul kumar <sharmaatul11@gmail.com>

# Re: Permission to use figures from manuscripts

**Andreas Dietze <adietze@online.no>** **Tue, Jul 19, 2011 at 12:14 AM**
To: Atul Kumar <sharmaatul11@gmail.com>

Hello again

you get the permition to use the pictures in you thesis. I would appreciate to recieve a copy of your thesis since I'm intresseted in that field.
Good luck and all the best
Dr.med.Andreas Dietze, PhD
Dep. orthopedic surgery
Head of the departmet
Vestfold county hospital
3103 Toensberg
Norway

> From: Atul Kumar [sharmaatul11@gmail.com]
> Sent: 2011-07-18 23:02:05 MEST
> To: Andreas Dietze [adietze@online.no]
> Subject: Re: Permission to use figures from manuscripts
>
> Dear Dr. Andreas,
>
> Please reply at your earliest possible convenience.
>
> Regards,
> Atul
>
>
>
> On Thu, Jul 14, 2011 at 6:17 PM, Atul Kumar <sharmaatul11@gmail.com> wrote:
>
> > Thanks for your reply.
> >
> > The context is to give introduction about different kinds of available for
> > first metatarsophalangeal arthroplasty.
> > I am planning to cite the source just below the figure. Please suggest if
> > want it in some other way.
> >
> > Regards,
> > Atul
> >
> >
> >
> > On Tue, Jul 12, 2011 at 2:32 AM, Andreas Dietze <adietze@online.no> wrote:
> >
> >> Dear dr Kumar,
> >> I would appreciate to know the context in which you are intending to use
> >> the figures and how you are planning the citation.
> >> Regards
> >> Andreas Dietze
> >> On 11.07.2011, at 04:44, A. Kumar wrote:

> >>
> >> ** **
> >> Dear Dr. Andreas,****
> >> ** **
> >> I am in the process of writing my thesis. I hope you would permit me to
> >> use the following figures from your article:****
> >> ** **
> >> Figure1 and Figure 2****
> >> From ?Replacement arthroplasty for hallux rigidus****
> >> 21 patients with a 2-year follow-up.? International Orthopaedics (SICOT)
> >> (1999) 23:240?243****
> >> ** **
> >> Looking forward to your reply.****
> >> ** **
> >> Regards,****
> >> Atul****
> >> ** **
> >> MBBS,MMST,PhD (Candidate)****
> >> Visiting Scientist****
> >> Department of Orthopedics and Sports Medicine****
> >> University of Washington****
> >> BB 1002****
> >> 1959 NE Pacific St.****
> >> Seattle WA 98195****
> >> ** **
> >>
> >>
> >>
> >

**A. Kumar**

**From:** Steven Raikin [steven.raikin@rothmaninstitute.com]
**Sent:** Monday, July 11, 2011 4:50 PM
**To:** A. Kumar
**Subject:** RE: Permission to use figures from manuscripts

The journal maintains copyright for all images.
Please contact JBJS for permission requests.

**Steven M. Raikin, M.D.**
Director: Orthopaedic Foot and Ankle Service
Rothman Institute
Associate Professor Orthopaedic Surgery
Jefferson Medical College

---

**From:** A. Kumar [mailto:kumara4@u.washington.edu]
**Sent:** Sun 7/10/2011 10:34 PM
**To:** Steven Raikin
**Subject:** Permission to use figures from manuscripts

Dear Dr. Steven,

I am in the process of writing my thesis. I hope you would permit me to use the following figure from your article:

FIG. 13
From ' Comparison of Arthrodesis and Metallic Hemi-arthroplasty of the Hallux Metatarsophalangeal Joint. Surgical Technique.' J Bone Joint Surg Am. 2008;90:171-180. doi:10.2106/JBJS.H.00368

Looking forward to your reply.

Regards,
Atul

MBBS,MMST,PhD (Candidate)
Visiting Scientist
Department of Orthopedics and Sports Medicine
University of Washington
BB 1002
1959 NE Pacific St.
Seattle WA 98195

**A. Kumar**

**From:** Hasselman, Carl [HasselmanCT@upmc.edu]
**Sent:** Monday, July 11, 2011 3:28 AM
**To:** A. Kumar
**Subject:** RE: Permission to use figures from manuscripts

You do have my permission to use the figures from this manuscript. However, I think you also need permission from the publisher of the article which is Lippincott.

---

**From:** A. Kumar [mailto:kumara4@u.washington.edu]
**Sent:** Sunday, July 10, 2011 10:59 PM
**To:** Hasselman, Carl
**Subject:** Permission to use figures from manuscripts

Dear Dr. Hasselman,

I am in the process of writing my thesis. I hope you would permit me to use the following figures from your article:

FIGURE. 1 and 20
From 'Resurfacing of the First Metatarsal Head in the
Treatment of Hallux Rigidus' Techniques in Foot & Ankle Surgery 7(1):31–40, 2008

Looking forward to your reply.

Regards,
Atul

MBBS,MMST,PhD (Candidate)
Visiting Scientist
Department of Orthopedics and Sports Medicine
University of Washington
BB 1002
1959 NE Pacific St.
Seattle WA 98195

1